Title
Identification and Optogenetic Perturbation of Subsets of preBï¿½tC Neurons in vivo

Author
Sherman, David

Publication Date
2014

Peer reviewed|Thesis/dissertation

UNIVERSITY OF CALIFORNIA

Los Angeles

Identification and Optogenetic Perturbation of Subsets of preBötC Neurons *in vivo*

A dissertation submitted in partial satisfaction of the

Requirements for the degree Doctor of Philosophy

in Neurobiology

by

David Sherman

2014

ABSTRACT OF THE DISSERTATION

Identification and Optogenetic Perturbation of Subsets of preBötC Neurons *in vivo*

By

David Sherman

Doctor of Philosophy in Neurobiology

University of California, Los Angeles, 2014

Professor Jack Feldman, Chair

Inhibitory neurons are a substantial component of the rhythmic preBötzinger Complex (preBötC) microcircuit, a node in the ventrolateral medulla critical for generating eupneic breathing in mammals. The role of glycinergic preBötC neurons in generating and modulating respiratory rhythm in spontaneously breathing anesthetized or awake mice was investigated by optogenetically-targeted excitation or inhibition. Channelrhodopsin-2 (ChR2) or Archaerhodopsin (Arch) were expressed in glycinergic neurons by injecting *AAV2/1-Ef1α-DIO-ChR2-eYFP* or *AAV2/1-flex-CBA-Arch-GFP*, respectively, into the preBötC of GlyT2-Cre mice. In spontaneously breathing mice, inspiratory-phase bilateral laser photostimulation of ChR2-expressing preBötC glycinergic neurons decreased tidal volume and shortened inspiratory duration, whereas expiratory-phase stimulation delayed the onset of the next inspiration. Prolonged stimulation produced apneas lasting as long as the light pulse (> 20s). Equivalent protocols producing photoinhibition of Arch-expressing glycinergic neurons during inspiration

increased tidal volume without altering inspiratory duration, whereas expiratory-phase stimulation shortened the latency until the onset of the next inspiration. During Breuer-Hering lung inflation reflex-induced apneas, prolonged photoinhibition restored rhythmic breathing. We conclude that glycinergic preBötC neurons modulate the pattern of inspiratory motor output and are important for production of reflex apneas. However, while modulatory, these neurons are not necessary for rhythmogenesis in intact (awake or anesthetized) mice. We also identified a novel marker, *reelin*, of excitatory preBötC neuronal subpopulations and assessed its anatomical and functional implications for preBötC neuroanatomy.

The dissertation of David Sherman is approved.

Nicholas Brecha

Peyman Golshani

Thomas Otis

Jack Feldman, Committee Chair

University of California, Los Angeles

2014

DEDICATION

Malleis Milito

TABLE OF CONTENTS

LIST OF FIGURES

LIST OF TABLES

ABBREVIATION

AAV2/1	adeno-associated virus 2 serotype 1
AlstR	allatostatin receptor
Arch	archaerhodopsin
BötC	Bötzinger Complex
ChAT	Choline Acetyltransferase
ChR2	channelrhodopsin-2
CPAP	continuous positive airway pressure
cVRG	caudal subregion of the ventral respiratory group
DIO	double inverted open reading frame
FLEX	flip excision switch
eYFP	enhanced yellow fluorescent protein
GFP	green fluorescent protein
GlyT2	glycine transporter 2
IRES	internal ribosome entry site
ir	immunoreactive
NeuN	neuronal nuclei
NK1R	neurokinin 1 receptor
NTS	nucleus tractus solitarius
pFRG/RTN	parafacial respiratory group/retrotrapezoid nucleus
preBötC	preBötzinger Complex
rVRG	rostral subregion of the ventral respiratory group
SST	somatostatin
TH	tyrosine hydroxylase

VRG	ventral respiratory group

ACKNOWLEDGEMENTS

I'd like to thank my mentor, Jack Feldman, for training me into the research equivalent of Navy SEAL. He has held me and my research to incredibly high standards, provided me with financial support, and given me unfettered access to cutting-edge resources and equipment that have made my dissertation work possible. I'd also like to thank him for entertaining and encouraging my every research folly, including my wild idea to move the lab into using mice and harnessing all of the molecular biology advantages that they afford.

I'd like to take thank Dr. Nicholas Brecha and Dr. Thomas Otis for taking me under their wing and looking after me in my time at UCLA, and I'd like to thank Dr. Peyman Golshani for serving on my committee and providing helpful guidance along the way.

I'd like to thank Jason Worrell for pushing me when I needed to be pushed, pulling me when I needed to be pulled, and carrying me in between.

VITA

2007	A.B., Biology (Mind, Brain, Behavior Track) Harvard College
2008-present	Graduate Student Researcher Department of Neurobiology University of California, Los Angeles
2010-2012	T32 Neural Microcircuits Predoctoral Fellowship
2013	Dissertation Year Fellowship, Graduate Division, UCLA

Publications and Presentations

D. Sherman, J.W. Worrell, Y. Cui, and J.L. Feldman. Optogenetic perturbation of glycinergic preBötC neurons modulates inspiratory pattern. In preparation.

W. Tan, D. Sherman, J. Turesson, X.M. Shao, W.A. Janczewski, and J.L. Feldman. Reelin demarcates a subset of pre-Bötzinger complex neurons in adult rat. *J. Comp. Neurol.* 2011; 520(3): 606-619. PMCID: PMC3751584.

P. Fuller, D. Sherman, N.P. Pederson, C.B. Saper, J. Lu. Reassessment of the structural basis of the ascending arousal system. *J. Comp. Neurol.* 2011; 519(5): 933-56. PMCID: PMC3119596.

D.A. Wood, N. Patterson, P. Fuller, D. Sherman, C.B. Saper, J. Lu. Genetic dissection of neural circuitry underlying REM sleep behavior disorder (RBD). *Soc. Neurosci. Abs.*, 736.28; 2007.

J. Lu, D. Sherman, M. Devor, C.B. Saper. A putative flip-flop switch for control of REM sleep. *Nature* 2006; 441: 589-94. PMID: 16688184.

CHAPTER I

Introduction

INTRODUCTION

The preBötzinger Complex (preBötC)[1, 2] is a heterogeneous population of excitatory and inhibitory neurons in the ventrolateral medulla[3, 4] first identified in 1991 as a site important for respiratory rhythmogenesis[1]. Subsequently, a growing body of evidence from *in vitro* and *in vivo* studies has highlighted its essential role in generating respiratory rhythm[1, 2, 5, 6]. The preBötC contains rhythmically active, i.e., phasic, neurons whose burst firing drive bulbospinal premotor neurons that project to motoneurons innervating inspiratory pump muscles, especially the diaphragm and external intercostal muscles[1]. Most preBötC neurons express persistent Na^+ current (I_{NaP}) and Ca^{2+}-activated nonspecific and voltage-insensitive cation current (I_{CAN})[7-9] that modulate excitability and burst firing properties[10, 11]. These neurons must act in concert to generate a wide range of breathing patterns suited to meet a variety of metabolic, physiological, and physical demands. During even modest increases in movement such as walking, human O_2 consumption more than triples from its baseline levels; sustained, powerful movements from larger muscles, such as those produced in fleeing predators or chasing prey, produce even larger increases in O_2 consumption[5]. With limited reserves of O_2 in blood (~4 min at normal metabolic rates), the need for continuous breathing is clear, as is the need for rapid responses to changing environments and demands.

The role of the preBötC as a dominant rhythm generator is shown in several experiments, indicating both its necessity and its sufficiency in generating rhythmic breathing:

1) Respiratory rhythm persists in thin brainstem slices containing the preBötC, indicating that some basic kernel for rhythmogenesis is preserved in this preparation, despite most respiratory compartments aside from the preBötC having been eliminated[1].

(2) Near complete lesion of a subset of preBötC neurons expressing the neurokinin-1 receptor (NK1R) using the neurotoxin Substance P-conjugated saporin yields a pathological, ataxic breathing pattern in the adult rats[12].

(3) Silencing a subset of glutamatergic neurons within the preBötC — those expressing the neuropeptide somatostatin (SST) — produces a persistent apnea in conscious adult rats xthat is not rescued through voluntary effort despite considerable distress and hypoxia[2]. The SST neurons were hyperpolarized for prolonged periods of time by virally introducing the Drosophila allatostatin receptor (AlstR)[13, 14] into the neurons and then, after appropriate time to allow for protein expression, activating the receptor to open a hyperpolarizing K^+ channel through intracerebellomedullary cistern (*i.c.c.*) administration of its agonist, allatostatin.

(4) *In vitro* experiments using holographic photolysis, a technique of directing three-dimensional patterned light to uncage a molecularly-caged glutamate in a spatially and temporally restricted manner, to activate small numbers of preBötC neurons show that the activation of as few as 4-9 preBötC neurons is sufficient to trigger an ectopic burst of preBötC neuronal activity and respiratory motor output[15]. This reveals that quite small numbers of preBötC neurons are capable of instigating a full burst of activity from the entire preBötC.

These experiments begin to probe what is necessary for a respiratory rhythm to persist by selectively perturbing preBötC neuronal activity. The future direction of this field is the continued categorization and subdivision of neuron types and cataloging of their functional contributions to the preBötC microcircuit. Periodic advances in technology bring ever finer resolution to this process. Far more progress has been made in defining subtypes of excitatory preBötC neurons. Yet, the preBötC contains a substantial population of glycinergic neurons (~50% of all inspiratory-modulated preBötC neurons)[4, 16] intermingled with the glutamatergic, i.e., excitatory, neurons. At present, very little is known about their projections or their

contribution to rhythm generation. Glycinergic neurotransmission is considered to be important in a wide range of rhythmogenic processes[17-19], although within the respiratory network, the blockade of inhibitory neurotransmitters, i.e. GABA and glycine, *in vitro* or *in vivo* does not abolish the respiratory rhythm[20, 21]. Several models of rhythm generation propose that inhibition plays a dominant role in the generation of respiratory rhythm[22, 23], but evidence in support of this idea is lacking and recently published work indicates that in vivo this is not the case[20]. These models rely heavily on reciprocal inhibitory connections between the preBötC and other compartments of the respiratory network, such as the BötC and pFRG, and while these connections are likely present, there is no evidence to suggest that these interactions are obligatory for rhythmogenesis in the intact animal[20].

Although the preBötC has been extensively studied, most physiological studies of preBötC neurons have not explicitly determined whether they are excitatory or inhibitory; surprisingly, until recently, the neuronal data was typically interpreted as if all recorded neurons were excitatory. This has left an enormous shortfall in our understanding of the neuron subtypes that comprise the preBötC and the respiratory network in its entirety. It is of fundamental importance in the pursuit of the mechanism of rhythmogenesis to identify the subsets of neurons that make up the preBötC, their role in generating the respiratory rhythm, and the manner in which they interact with one another in their various functions. This is critical information in trying to understand how disordered breathing emerges from a once functioning circuit in a wide range of disease states and to develop new therapies to rebalance the network. Sleep disordered breathing emerges in the progression of a range of neurodegenerative conditions, including Parkinson's disease[24, 25], multiple systems atrophy (MSA)[26, 27], and amyotrophic lateral sclerosis (ALS)[28, 29]. There are even substantial losses of $NK1R^+$ neurons in the preBötC of advanced PD and MSA patients. In many neurodegenerative disorders, as well as in the

general elderly population, central respiratory arrest is hypothesized as a cause of death, resulting from a progressive loss of preBötC neurons.

Yet, until 1999, there were no molecular signatures identified for the preBötC despite its importance to respiration and its link to many degenerative health conditions. At that time, Gray and colleagues identified the NK1 receptor as the first molecular marker of the preBötC[30, 31] and further research found another preBötC subpopulation that expresses the neuropeptide, somatostatin, which partially overlaps with NK1R-expressing subset[3]. And most recently, the transcription factor, developing brain homeobox protein 1 or *dbx1*, has been found to be fate-determinant transcription factor in the developmental lineage of excitatory preBötC neurons[32, 33]. As *dbx1* neurons encompass all excitatory neurons, all SST^+ preBötC neurons and all $NK1R^+$ preBötC neurons are *dbx1* neurons but the converse is not true. In the first study presented in this dissertation, we identify a novel marker of preBötC neurons, the signaling protein reelin, and assess how it fits in with our current understanding of delineated cell types. These steps towards further delineating preBötC cell types and defining their functional roles are important advances towards fully understanding the machinery that underpins rhythmogenesis in the preBötC, but may also impact and inform the study of other rhythmic circuits and behaviors, such as locomotion.

Much of the difficulty in studying the role of inhibition in the respiratory network arises from the anatomy of the ventral respiratory column and the challenges of specifically targeting its subcompartments. The preBötC lies within a rostral-caudal column running caudally from the facial nucleus; immediately rostral is the Bötzinger Complex (BötC) which contains expiratory-phased glycinergic neurons and immediately caudal is the rostral ventral respiratory group (rVRG), which contains bulbospinal premotoneurons that transmit inspiratory drive to phrenic motoneurons. The Bötzinger Complex makes monosynaptic projections to preBötC, inspiratory premotoneurons in the rVRG, and phrenic motor neurons that project to the diaphragm[34-36].

Another important respiratory area, sitting just ventrolateral to facial nucleus, is the parafacial respiratory group (pFRG), which is thought to be an oscillator for driving active expiration via rhythmic contraction of the abdominal muscles[37]. The connections of the pFRG are not presently known, although many models of its function do hypothesize that it is coupled with the preBötC, in what is known as the "dual oscillator hypothesis"[38, 39]. In addition to these respiratory areas, the respiratory network is surrounded by a wide variety of non-respiratory neuron types, including C1 adrenergic neurons, cardiovagal motor neurons, and GABAergic interneurons[40-43]. The heterogeneity of the preBötC and its surrounding respiratory and non-respiratory areas requires quite precise neuronal targeting.

In order to successfully dissect the preBötC microcircuit, it is necessary to employ techniques that are both temporally-precise and cell-specific, allowing for exquisite control in turning subsets of neurons "on" or "off" and observing any changes produced in breathing. Francis Crick once argued this point, that "to understand a complex biological system one must be able to interfere with it both precisely and delicately"[44]. Methods of targeting preBötC neurons until recently could not achieve this level of sophistication. Substance P-conjugated saporin lesions of the preBötC, described above, achieve cell-specificity but are irreversible, and most pharmacological methods prior to this could not achieve much specificity at all, except where receptor expression was restricted in some manner, i.e., NK1 receptors on a subset of excitatory preBötC neurons. Recent advances in molecular biology, virology, and mouse genetics have brought an unprecedented ability to target proteins to certain cell types. In 2008, Tan et al. successfully restricted expression of the Drosophila allatostatin receptor (AlstR) to only SST preBötC neurons in adult rats and used this cell-specific expression to silence these neurons by applying its agonist, allatostatin (AL)[2]. This was achieved by designing an AAV2 vector to express AlstR under the SST promoter, achieving expression only where this promoter is active, i.e., in SST-expressing neurons. Where cell-specific promoters are not readily

available, specificity has been introduced and capitalized on by distinguishing neurons by their projection targets. This can accomplished by combining retrograde tracing with wheat germ agglutinin conjugated to cre recombinase (WGA-cre) and cre-dependent expression of experimentally useful proteins, i.e., ChR2, Arch, AlstR.

As techniques employed for studying neural microcircuits come to rely more and more on genetics and more elaborate intersectional strategies, there is a growing imperative to define neurons according to the promoters that set them apart from their neighboring neurons. With the knowledge that SST expression in the ventrolateral medulla is localized uniquely to a subset of preBötC neurons in the rat, this promoter could be appropriated and used to introduce novel proteins that could be used to manipulate neuronal function and alter the microcircuit. Gene-based strategies are largely the means by which cell-specificity is achieved *in vivo*.

Until quite recently, most experimental approaches to study populations of neurons were characterized by some form of latency to action. Pharmacological manipulation can produce long-lasting effects, but with significant time delays in the onset of action due to the need for the drug to diffuse and bind receptors. In many modalities, the behavioral time scale is so slow that these delays are not meaningful; a drug taking 30 seconds to diffuse into the brain tissue after microinjection does not impact the study of circadian rhythm or anything on a similar time scale. However, this speed is not ideal when studying the respiratory cycle, since an adult mouse breathes nearly 3 times per second. Moreover, the respiratory network contains many compensatory mechanisms, so gradual or prolonged alterations of the network may allow for shifts in activity to compensate for changes in network excitability. Thus, the time scale of breathing requires quick onset perturbations.

The advent of optogenetics[45, 46], whereby light-activated ion channels, known collectively as opsins, are introduced into specific neurons and used as experimental tools to probe neuronal function *in vivo*, has solved both issues of cellular and temporal specificity. Opsin

proteins can be introduced into neurons either through viral vector microinjection or mouse transgene expression[46]. With this technique, cell specificity is achieved with genetic techniques, as in prior studies[2], although the use of more sophisticated intersectional strategies, such as cre-dependent expression cassettes, has vastly refined the process of targeting protein expression to the correct neurons. However, where optogenetics profoundly alters the research landscape is in its ability to produce millisecond time scale perturbations in *in vivo* microcircuits. In terms of studying respiration, this speed allows for the study of neurons on a cycle by cycle basis without time for the network to compensate for any induced changes. There are many forms of opsins, each possessing unique channel properties and photocurrents, but the most popular in research at present are Channelrhodopsin-2 (ChR2) and Halorhodopsin or Archaerhodopsin (Arch)[47, 48]. ChR2 is a transmembrane nonselective cation channel activated by blue light (473 nm), producing membrane depolarization[48, 49], while Arch is a hyperpolarizing proton pump activated by orange light (540 nm)[47]. When introduced into neurons in an intact animal, ChR2 or Arch allow precise targeting and a means to reliably and repeatedly test gain-of-function and loss-of-function in the microcircuit at millisecond time scales.

Loss of function studies targeting $NK1R^+$ or SST^+ neurons generated ataxic breathing patterns and apneas, respectively. Other subsets of neurons may exert more nuanced and modulatory effects on respiratory rhythmogenesis and perturbations from their endogenous activity may result in subtler changes, requiring careful attention to a variety of respiratory parameters. Since breathing can persist after blockade of inhibitory neurotransmitters in intact rats[20], we would expect to find a modulatory role for the substantial population of inhibitory preBötC neurons. In the second study presented in this dissertation, we test the role of inhibitory preBötC neurons in both gain-of-function and loss-of-function experiments performed in intact mice with ChR2 and Arch, respectively. These neurons are anatomically defined by the expression of the glycine transporter 2 (GlyT2) protein in preBötC, which is a unique marker for

glycinergic neurons[50], and through the use of the GlyT2 promoter, we were able to restrict opsin expression to glycinergic preBötC neurons. We then chronically implanted fiber optics targeting the preBötC and studied the effect of perturbing the endogenous activity of these neurons on respiration by delivering light bilaterally into the brain.

CHAPTER II

Reelin Demarcates a Subset of PreBötzinger Complex Neurons in Adult Rat

Published in final edited form as:

Tan W, **Sherman D**, Turesson J, Shao XM, Janczewski WA, Feldman JL

Reelin demarcates a subset of pre-Bötzinger complex neurons in adult rat.

J Comp Neurol. Feb 15, 2012; 520(3): 606–619.

doi: 10.1002/cne.22753

For these experiments, I performed:

Reelin Histology

Retrograde Tracing from Spinal Cord

Plethysmograph Recordings

Imaging

INTRODUCTION

The pre-Bötzinger complex (preBötC) in the ventrolateral medulla is the hypothesized kernel for generating the normal inspiratory-dominated respiratory rhythm in vivo and its *in vitro* equivalent[1, 30, 39, 51], containing many different respiratory neuron types with distinctive respiratory-modulated discharge patterns[52, 53]. The preBötC and its immediate surrounding area contain neurons presumptively unrelated to generation or modulation of respiratory pattern, such as C1 adrenergic neurons and cardiovagal motor neurons[40-43]. Given its heterogeneity, clearly defined criteria for identifying neurons making up the preBötC are essential for determining their roles in respiratory motor patterning. Two molecules that identify overlapping subpopulations of glutamatergic preBötC neurons, demarcated by expression of NK1R and/or SST have been useful in this regard: 1) Lesioning NK1R-expressing preBötC neurons abolishes normal breathing in adult rats[51]; 2) acute silencing of SST-expressing preBötC neurons produces prolonged apnea that can result in asphyxia[2]. The transcription factor dbx1 is critical for proper development of glutamatergic preBötC neurons[32, 33]. However, each of these markers has limitations. In the preBötC, NK1R immunoreactivity (-ir) is localized predominantly in neuronal processes and not somata, SST expression decreases significantly during aging[54-56], and dbx1 is expressed only prenatally in progenitor neurons[32, 33].

Here, we sought to identify additional markers to complement and extend the utility of NK1R, SST, and dbx1, which could be helpful in revealing the function and structure of preBötC neuronal microcircuitry underlying respiratory rhythm and pattern generation. To this end, we constructed and screened a subtractive cDNA library from preBötC inspiratory neurons and neighboring nucleus ambiguous (NA) motoneurons and identified one molecule, reelin, as a strong candidate for being a useful marker. Reelin was expressed in the preBötC and in more caudal inspiratory bulbospinal ventral respiratory group (ibsVRG) premotoneurons, which were clearly distinguishable by differences in their somatic diameters.

We then studied adult mice lacking the reelin protein (Reeler) to screen for respiratory deficits. These mice exhibited abnormal responses to hypoxia, suggesting that reelin may have a functional post-developmental role in breathing.

RESULTS

Construction and screening of a preBötC inspiratory neuron subtractive cDNA library

The preBötC contains respiratory-related neurons with several distinct activity patterns, including inspiratory and expiratory[52, 53]. Individual preBötC neurons from neonatal mice were whole-cell patched from the rostral slice surface (Figure 2-1A,C), and hypoglossal nerve activity was measured via a suction electrode (Figure 2-1A,B). The intraneuronal components of preBötC inspiratory neurons (n = 12) and of nucleus ambiguous (NA) motoneurons (n = 10) were aspirated into patch electrodes (Figure 2-1B,C) and processed to construct a subtractive cDNA library (see Materials and Methods). Forty-nine candidate genes with greatly enhanced expression in the preBötC compared with NA were obtained. Twelve of these candidates were expressed sequence tags (ESTs) belonging to unknown genes (data not shown); the rest were known or predicted genes that belong to several categories, including kinases, GTPases, transcriptional factors, Ca^{2+}-binding proteins, membrane proteins, and cytoskeleton-related proteins (Table 1).

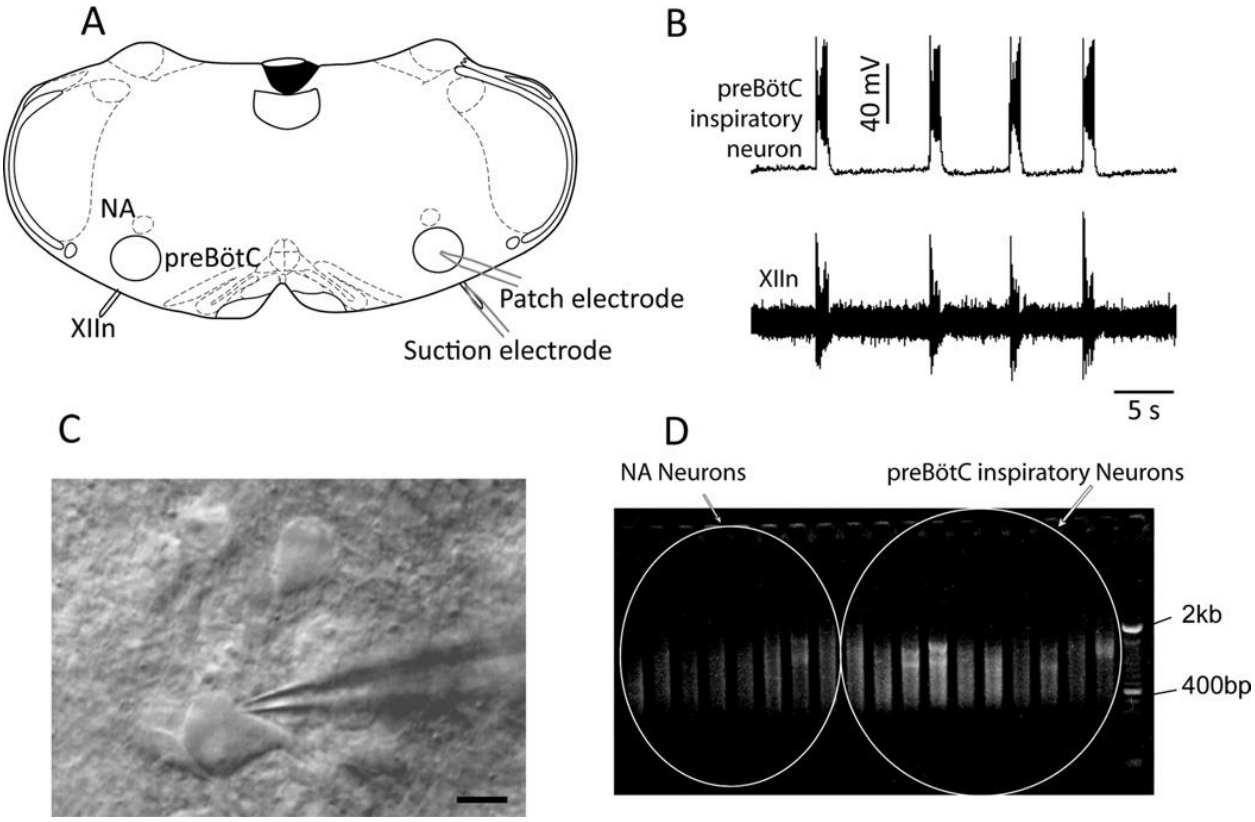

Figure 2-1 RNA isolation and cDNA amplification from single inspiratory preBötC neurons. **A**: Outline of mouse medullary slice showing experimental setup. **B**: Typical inspiratory preBötC neuron identified by a burst of activity concurrent XII nerve output. **C**: Patch/intracellular RNA aspirating electrode on inspiratory neuron viewed under infrared illumination. **D**: cDNA amplification from single neurons. Each lane represents cDNA enriched from a single preBötC inspiratory or NA neuron. NA, nucleus ambiguus; preBötC, pre-Bötzinger complex; XII, hypoglossal nucleus; XIIn, hypoglossal nerve. Scale bar = 10 μm.

Table 1. List of partial candidate genes that were screened from subtractive cDNA library of single inspiratory preBötC neuron

Gene name	Gene ID from Gene Bank
Abelson helper integration site (Ahi1) gene	gi|33392716|gb|BC055400.1|
Activin receptor A, type 1 (Acvr1)	gi|40254648|ref|NM_007394.2|
Agrin (Agrn)	gi|42490750|ref|NM_021604.2|
Armadillo repeat gene deleted in velo-cardio-facial syndrome (Arvcf)	gi|40254128|ref|NM_033474.2|
BM-009 homolog	gi|26344414|dbj|AK075613.1|
BM88, function unknown, or 1500001H12 gene	gi|31981113|ref|NM_021316.2|
BarH-like 1 (Drosophila) Barhl1	gi|255958264|ref|NM_019446.4|
Calcium modulating ligand (Caml)	gi|6671661|ref|NM_007596.1|
Corticotropin releasing hormone (crh)	gi|45429989|ref|NM_205769.1|
Cyclin-dependent kinase 4 (Cdk4)	gi|31560614|ref|NM_009870.2|
Estrogen related receptor gamma (Esrrg)	gi|52345417|ref|NM_011935.2|
Exocyst complex component 7	gi|74150201|dbj|AK140450.1|
Glioma tumor suppressor candidate region gene 2	gi|74199027|dbj|AK151836.1|
Riken cDNA 2900016C05 gene	gi|12850934|dbj|AK013532.1|
G protein-coupled receptor associated sorting protein 1 (Gprasp1)	gi|53729356|ref|NM_026081.5|
G protein-coupled receptor associated sorting protein 2 (Gprasp2), Predicted	gi|26081919|dbj|AK030638.1|
Hematopoietic signal peptide-containing membrane domain-containing 1	gi|54125558|gb|AY761098.1|
Hypothetical Integrin A (or I)domain structure containing protein	gi|38174365|gb|BC061211.1|
Integral membrane protein 2B	gi|74207160|dbj|AK151889.1|
Kin of IRRE like 3 (Drosophila), KIRRE, NEPH1	gi|38648724|gb|BC063072.1|
Latexin	gi|31980631|ref|NM_016753.2|
Membrane-associated ring finger (C3HC4) 4	gi|113865912|ref|NM_001045533.1|
Member T2 (Rhot2), Ras family	gi|34328359|ref|NM_145999.2|

Neuronal protein 3.1	gi|32451790|gb|BC054762.1|
Nulp1, bHLH family	gi|11036455|gb|U94988.1|MMU94988
PKI gamma	gi|20071652|gb|BC026550.1|
Progesterone receptor membrane component 1	gi|74198077|dbj|AK159599.1|
RAB4A, ras family	gi|74202132|dbj|AK136566.1|
Rho GDP dissociation inhibitor (GDI) alpha	gi|74217975|dbj|AK170718.1|
Reelin	gi|117320553|ref|NM_011261.2|
Riken cDNA 2900016C05 gene	gi|12850934|dbj|AK013532.1|
S100 calcium binding protein A10 (S100a10)	gi|113930762|dbj|NM_009112.2|
Solute carrier family 6 member 5 (Slc6a5)	gi|225579048|dbj|NM_001146013.1|
Tubulin tyrosine ligase-like family, member 6 (Ttll6)	gi|282847335|dbj|NM_172799.4|
Very KIND protein	gi|74181190|dbj|AK147335.1|
Visinin-like 1 (Vsnl1), (Vsnl1), (NVL- 1) (NVP-1) (HLP3)	gi|67514555|ref|NM_012038.3|
Zinc finger, DHHC domain containing 2 (Zdhhc2)	gi|31341589|ref|NM_178395.2|

Expression patterns of candidate genes in preBötC

The expression patterns of adult rat preBötC gene candidates were confirmed by immunohistochemistry when an antibody was available or by in situ hybridization (in adult mice). Some candidates did not show detectable expression levels in the brainstem (data not shown) by either technique. Some other candidates showed ubiquitous expression throughout the brainstem in adult mice, e.g., visinin-like 1, a calcium sensor protein (data not shown), whereas others exhibited high levels of expression restricted to various brainstem nuclei including the preBötC in adult mice. 1) The progesterone receptor membrane component 1 (PRMC1) gene was highly expressed in the vestibular nucleus, solitary tract, and inferior olive, with more moderate expression in the preBötC (Figure 2-2, top). The presence of PRMC1 in the preBötC indicates that some hormones may directly modulate breathing. 2) The Abelson helper integration site (Ahi1) gene was highly expressed in the vestibular nucleus and solitary tract and at moderate levels in the preBötC (Figure 2-2, middle). Mutations in Ahi1 cause Joubert syndrome, an autosomal recessive disorder with hypotonia, ataxia, developmental delay, oculomotor apraxia, and neonatal breathing abnormalities[57, 58]. The expression of Ahi1 in pre-BötC may underlie these breathing abnormalities. 3) Latexin, an endogenous carboxypeptidase inhibitor, was expressed in the hypoglossal, facial, ambiguus nuclei, and Bötzinger complex (BötC), with a few scattered neurons in the rostral preBötC (Figure 2-2, bottom). 4) A novel exon of cAMP-dependent protein kinase inhibitor (PKI) gamma was also expressed in the preBötC. This 158-bp exon was the first exon and separated by 44-kbp intron 1 from exon 2 (data not shown). Here, we focus on reelin, which was highly expressed in a subset of preBötC neurons but in few other structures in the brainstem.

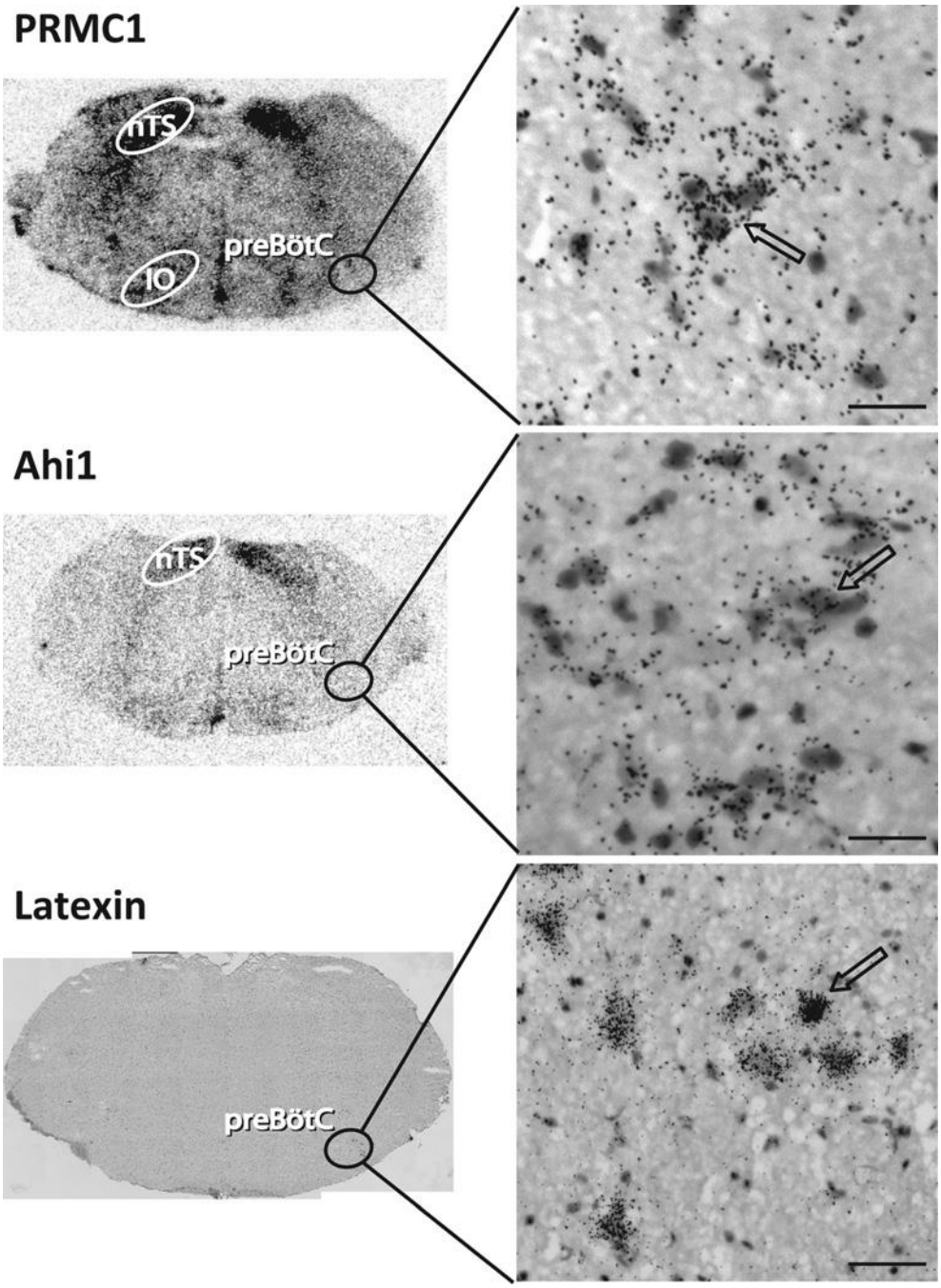

Figure 2-2 Medullary expression pattern of PRMC1, Ahi1, and Latexin genes in preBötC using 35S-radiolabeled RNA probes in brightfield photomicrographs. **Top**: PRMC1 is highly expressed in nucleus of the solitary tract (NTS), inferior olive (IO), and preBötC. **Middle**: Ahi1 is highly expressed in NTS and in preBötC. **Bottom**: Latexin is expressed in rostral preBötC and BötC (not shown). Counterstain: hemotoxylin-eosin. Left: Low-magnification of transverse medullary

slice; right: high-magnification depicting preBötC. The arrows indicate labeled neurons. Scale bars = 30 μm.

Reelin expression profile in the rat brainstem

Reelin is a secreted glycoprotein that plays an important role in corticogenesis and neuronal positioning during their development[59-62]. In the medulla, *reelin* neurons were located in adult rats in four regions related to brainstem control of breathing (Figure 2-3): i) preBötC extending caudally into the ibsVRG; ii) a diffuse area dorsal to the facial nucleus which we designate as the dorsal facial group (DFG); iii) a region containing premotoneurons projecting to hypoglossal motoneurons which we designate as the parahypoglossal group (PHG)[54], and; iv) pontine respiratory group

The reelin antibody labeled neuronal somata but not processes in the brainstem. Reelin neurons were concentrated below the caudal NA compact division and about 500 μm from the caudal edge of the facial nucleus (Bregma −11.7 mm) in the ventrolateral medulla, i.e., pre-BötC (Figure 2-3A–C). Reelin neurons extended more caudally from preBötC to the rostral VRG, which contains bulbospinal inspiratory premotor neurons. NA motoneurons did not show any expression of reelin, which is expected from results of the subtractive hybridization using cDNAs from NA single cell as control. There were a few reelin-expressing neurons in the BötC between Bregma levels −11.8 and −12.3 mm (Figures 1-3A, 1-5A). The number of reelin neurons gradually increased along the rostral-caudal axis in the ventrolateral medulla between Bregma levels −11.8 to −12.8 mm. The peak distribution of reelin neurons in the ventrolateral medulla was between Bregma levels −12.8 and −13.0 mm, 1.1 mm from the caudal edge of the facial nucleus (Bregma −11.7 mm), after which the number of reelin neurons decreased along the longitude axis of the ventrolateral medulla (Figure 2-5A). Ninety percent of reelin neurons were concentrated between Bregma levels −12.3 and −13.6 mm. The number of reelin neurons in the pre- BötC and VRG decreased slightly in 24-week-old rats in comparison with 2- and 8-week-old rats (Figure 2-5A).

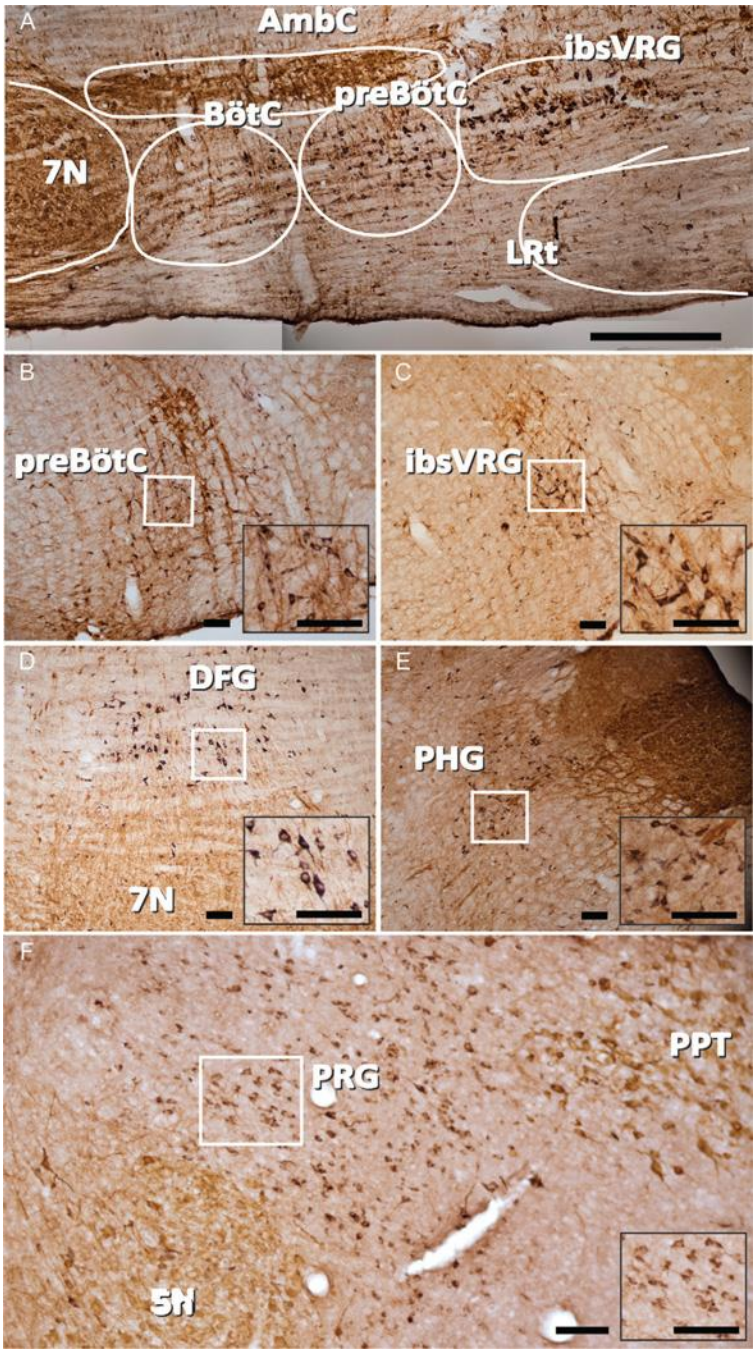

Figure 2-3 Reelin expression in preBötC, ibsVRG, DFG, PHG, and PRG. **A**: Sagittal mosaic image of ventral respiratory column depicting reelin (black) and ChAT (brown) immunoreactivity. Double labeling with ChAT was used to reveal the motor neurons in the sections. **B**: Reelin neurons in preBötC in coronal section. **C**: Reelin neurons in ibsVRG in coronal section. **D**: Reelin neurons in PHG in coronal section. **E**: Sagittal view of the DFG. **F**: Sagittal view of the

PRG depicting a band of reelin neurons between the trigeminal nucleus and the pedunculopontine tegmentum. **Insets** represent higher magnification of reelin-ir neurons from the boxed areas in each panel. BötC, Bötzinger complex; ibsVRG, inspiratory bulbospinal ventral respiratory group; 5N, trigeminal nucleus; 7N, seventh nucleus; DFG, dorsal to facial nucleus group; PRG, pontine respiratory group; PHG, parahypoglossal group; PPT, pedunculopontine tegmentum. Scale bars = 500 μm in A; 100 μm in B–F.

NK1R and SST immunoreactivities define subpopulations of preBötC neurons[3, 30, 51]. We next investigated whether these two molecules were coexpressed in reelin neurons. In the ventrolateral medulla, the majority of NK1R (84.0% ± 7.4%, n = 4; Figure 2-4A–C) and SST neurons (84.9% ±6.1%, n = 4; Figure 2-4D–F) coexpressed reelin, but not the converse. This result suggests that reelin neurons encompass a larger population of preBötC neurons than NK1R and SST neurons. There was no overlap between TH neurons and reelin neurons (Figure 2-4G–H), showing that these neurons are not catecholaminergic.

Reelin neurons were also found in the parahypoglossal group (PHG; Figure 2-3D), a region innervated by preBötC neurons[54] that is thought to contain hypoglossal premotor neurons. The expression of reelin in PHG neurons was highest in young rats (~8 weeks old), but it was barely detectable in older rats (24 weeks old; data not shown).

Reelin neurons were found in a diffuse area dorsal to the facial nucleus, which we refer to as *DFG* (Figure 2-3E). These reelin neurons were concentrated in an area ~200–300 µm above the dorsal boundary of the facial nucleus (RC 1.1 mm, DV 0.6 mm, ML 0.5 mm), between Bregma levels −10.4 and −11.7 mm. More rostrally, we observed a band of reelin neurons that extended in sagittal sections from the dorsal boundary of the trigeminal nucleus dorsally and rostrally to the caudal boundary of the pedunculopontine tegmentum (PPT; Figure 2-3F). This band includes portions of the supratrigeminal nucleus, medial and lateral parabrachial nuclei, and Kölliker-Fuse, which comprise the pontine respiratory group (PRG). In addition to these respiratory areas, reelin neurons were found in the ventromedial medulla, an area containing many glutamatergic and GABAergic bulbospinal premotoneurons.

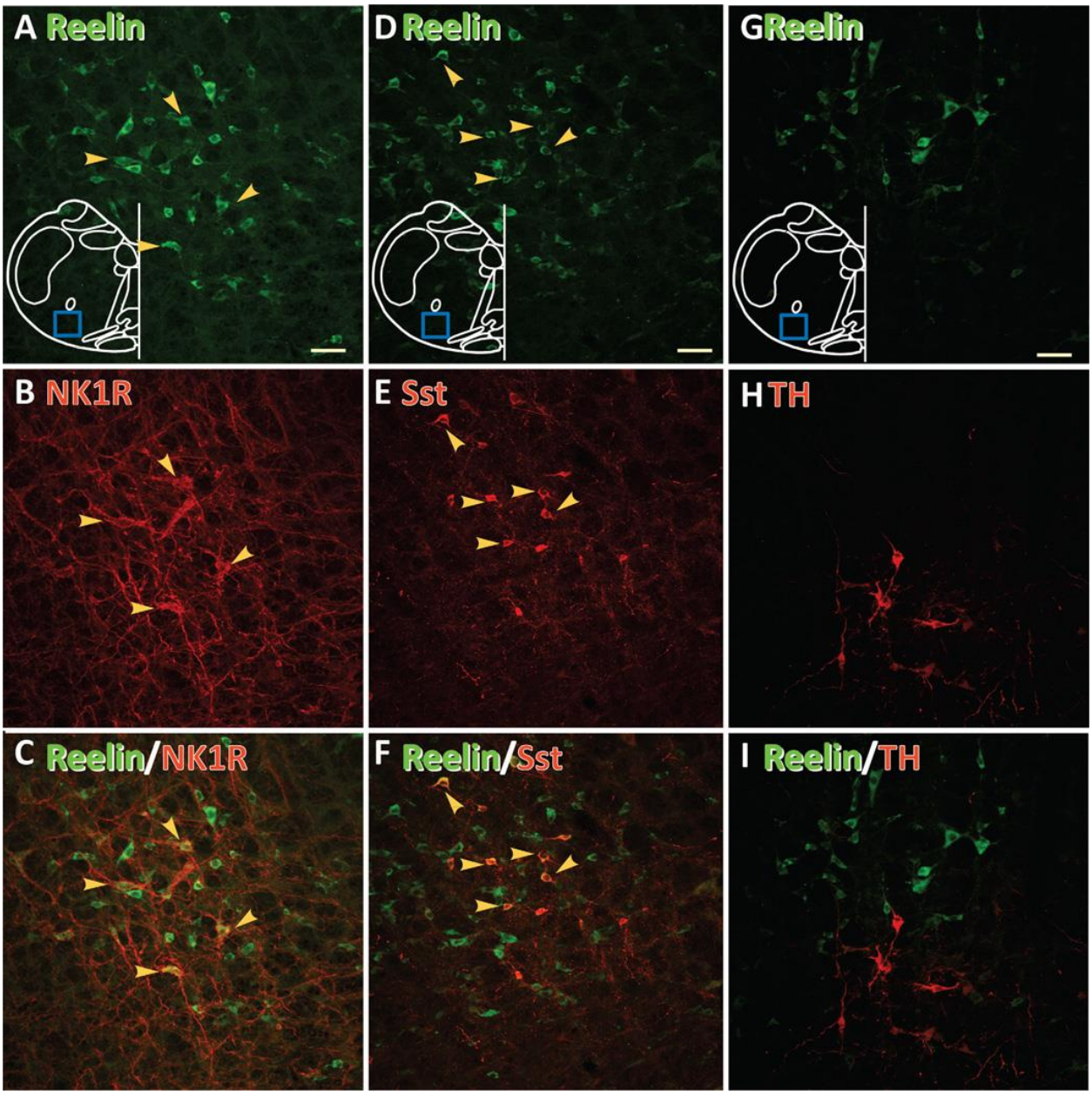

Figure 2-4 Pre-BötC reelin neurons coexpress NK1R and SST but not TH. **A,D,G**: Reelin neurons (green). The blue box represents the area including preBötC where image was acquired. **B**: NK1R neurons. **E**: SST neurons. **H**: TH neurons. **C,F,I**: Superimpositions. Neurons colocalizing two markers indicated by yellow arrows. NK1R, neurokinin 1 receptor; SST, somatostatin; TH, tyrosine hydroxylase. Scale bars = 50 μm.

Difference in soma size distinguishes preBötC from ibsVRG reelin neurons

Although there was a continuous column of reelin neurons extending caudally from the preBötC, we observed two distinct populations based on soma size, transitioning at Bregma level −12.8 mm, with the population with smaller somata more rostral. We hypothesized that the anatomic boundary between these populations was at the caudal preBötC border, with the more caudal population being the ibsVRG. To test this hypothesis, we injected the retrograde tracer FG into the C2–C4 spinal cord ventral horn. Seven days after injection, FG strongly labeled neurons in the VRG, defining a population of bulbospinal neurons caudal to the preBötC. Immunolabeling for reelin colabeled FG-positive neurons with an average soma diameter of 26.5 ± 3.7 µm based on immunofluorescent staining (n = 30) and of 27.1 ± 3.8 µm based on DAB staining (n = 135; Figure 2-5B). The more rostral preBötC reelin neurons (Figure 2-5C–G) had significantly smaller soma diameters based on DAB staining of 15.5 ± 2.4 µm (n = 130; P = 0.00002).

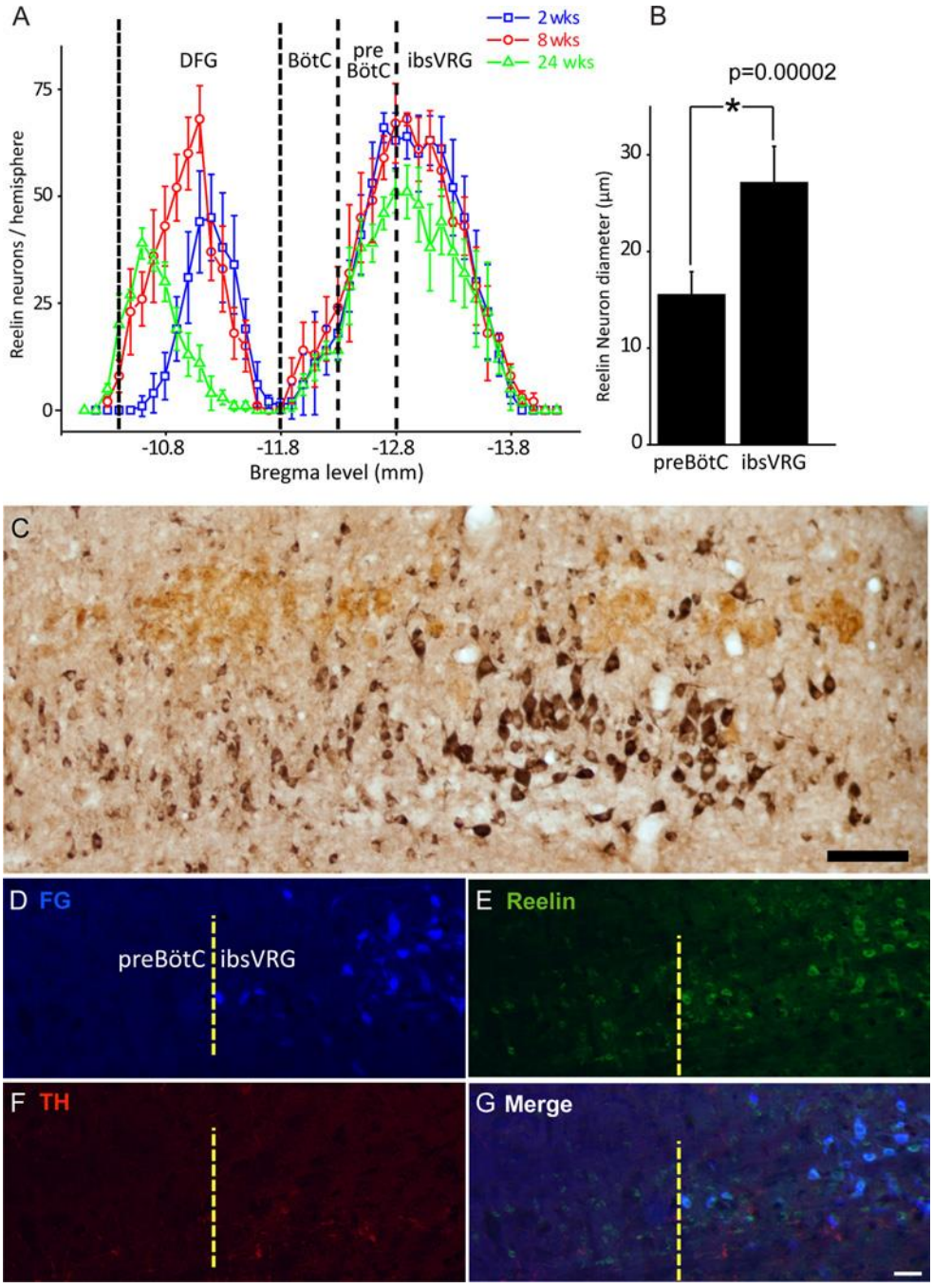

Figure 2-5 Distinctive reelin populations set the anatomic boundary of preBötC and ibsVRG. **A**: Reelin neuron rostrocaudal distribution in ventrolateral medulla at three different ages. One reelin neuron group resides in the region from Bregma levels −10.4 to −11.7 mm in DFG; another reelin neuron group located in preBötC and ibsVRG with peak cell numbers from Bregma levels −12.7 to −12.9 mm. Caudal edge of the facial nucleus: Bregma −11.7 mm. **B**:

Pre-BötC reelin neurons have significantly smaller soma diameter than those of ibsVRG (ANOVA, P = 0.00002). **C**: Sagittal view depicting preBötC and ibsVRG reelin populations, labeled for reelin (black) and ChAT (brown). Double label with ChAT was used to reveal the motor neurons in the sections. **D–G**: ibsVRG neurons retrogradely labeled from the C2–C4 level of the spinal cord with FG (D) were stained for reelin (E) and TH (F). G: Merge. Note that FG-positive cells in ibsVRG are colocalized with reelin but do not express TH. ChAT, choline acetyltransferase; FG, Fluorogold; ibsVRG, inspiratory bulbospinal ventral respiratory group; TH, tyrosine hydroxylase. Scale bars = 100 μm in C; 50 μm in G (applies to D–G).

Impaired response to respiratory challenges suggests a respiratory role for reelin in mouse

We examined whether the loss of reelin had any functional consequences for respiration. We chose to study Reeler transgenic mice[63], which lack functional reelin protein, as a broad screen of respiratory involvement of the reelin protein.

Reeler mice exhibited an impaired response to hypoxia, but responded to hypercapnia. Awake in room air at rest, f_I of Reeler mice was 154.7 ± 4.8 breaths/min and of their (control) littermates was 162.7 ± 5.1 breaths/min (n = 5; P = 0.03) (Figure 2-6). In response to hypercapnia (5% CO_2 −21% O_2−74% N_2), f_I in both groups of mice increased similarly: Reeler mice to 245.9 ± 45.0 breaths/min (n = 5; P = 0.002) and control mice to 269.7 ± 18.3 breaths/min (n = 5; P = 10^{-6}) (Figure 2-6); there was no difference between the groups (P = 0.31). In response to hypoxia (8% O_2–92%N_2), f_I did not change in Reeler mice (148.5 ± 23.6 breaths/min; n = 5; P = 0.50), whereas control mice had the classic robust increase (235.3 ± 25.5 breaths/min; P = 0.0002) (Figure 2-6).

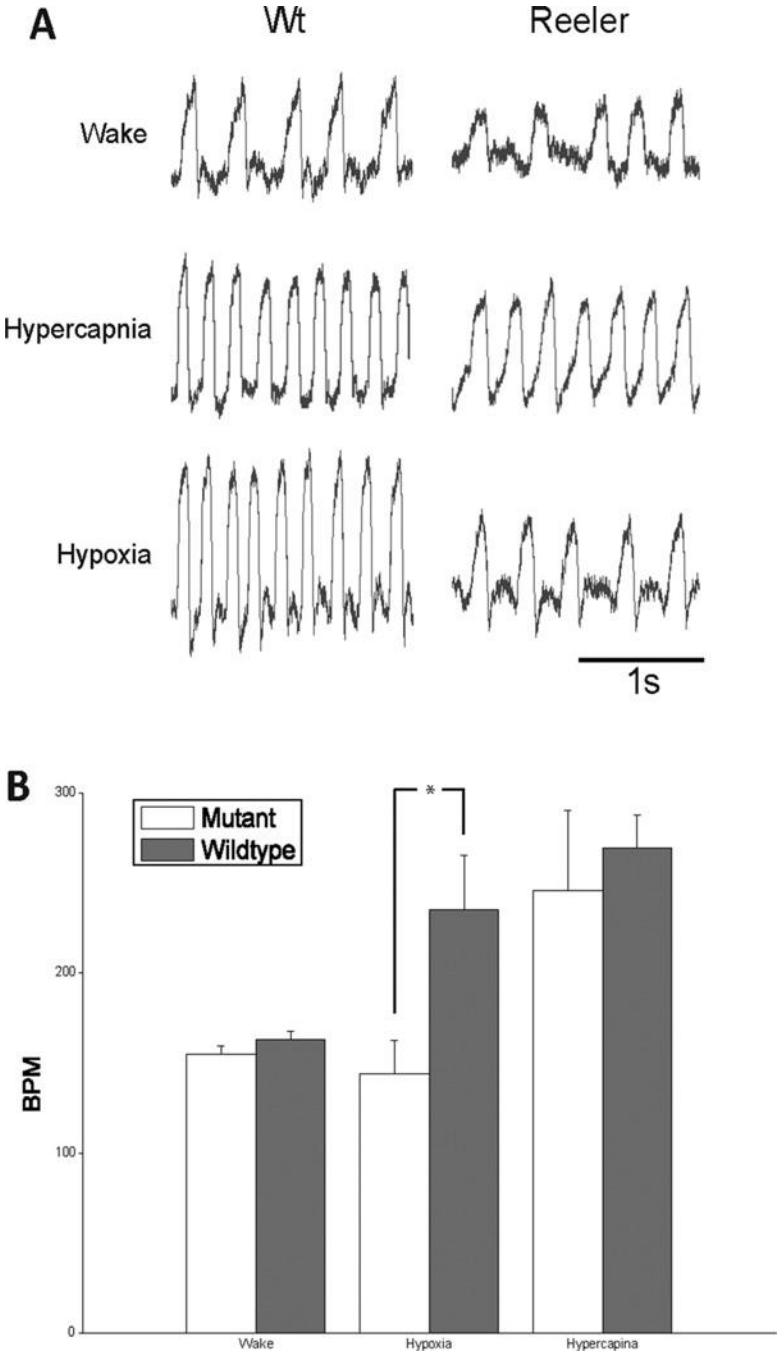

Figure 2-6 Reeler mouse shows impaired response to hypoxia but not hypercapnia. **A**: Plethysmographic record of breathing patterns during wakefulness and hypoxic and hypercapnic challenges from Reeler and littermate control mice. Amplitudes are not normalized. **B**: Quantitative analysis of breathing frequency from Reeler and littermate controls. Compared with littermates, Reeler mice had a significantly slower breathing frequency in

response to hypoxia (ANOVA, P = 0.0002), which was not signficiantly different from baseline (ANOVA, P = 0.501). Values are mean ± SD (n = 5 for each group). BPM, breaths per minute.

DISCUSSION

When studying a heterogeneous population of neurons, such as those comprising the preBötC, defining cell types according to their activity and gene and protein expression profiles is of considerable utility. Here we constructed a cDNA library for screening candidate genes from preBötC inspiratory neurons. In order to obtain genetic material from these neurons, we whole cell patched them and extracted the mRNA through the patch pipette. This ensured the purity of the genetic material, without contamination from neighboring cells or processes connecting onto the neuron. As mRNA obtained via patch electrode may only represent a portion of the total cellular mRNA of any neuron and since our goal was to identify candidate genes that we would subsequently verify with other techniques, we combined the extracted contents from 12 preBötC inspiratory neurons during the subtractive hybridization procedure. At this point, we did not differentiate between inspiratory-modulated glutamatergic and glycinergic neurons. We used exponential amplification to multiply the cDNAs. We obtained efficient amplification for the 3' portion of highly expressed genes from preBötC inspiratory neurons by using a single poly(dT)-tailed primer after tagging 3' ends of cDNAs by poly(dA). With this strategy, we successfully constructed a subtractive cDNA library from preBötC inspiratory neurons compared to NA motoneurons and obtained several molecular candidates (See Results). We focused on *reelin*, which was highly expressed in preBötC neurons and neighboring ibsVRG neurons and relatively few other areas in the brainstem.

Reelin is a secreted extracellular glycoprotein essential in prenatal development for neuronal migration and positioning[60, 64-67]. *Reelin* is also implicated in the modulation of synaptic plasticity, stimulation of synaptic terminal density and hypertrophy of dendritic spines, and enhancement of glutamate-evoked Ca^{2+} currents via NMDA receptor subunits in adult animals[68-75].

The expression level of *reelin* is altered in some neurological diseases, such as schizophrenia[74, 76-78], psychotic bipolar disorder[76, 79], and Alzheimer's disease[80, 81]. Two members of low density lipoprotein receptor gene family mediate *reelin* signaling pathway: apolipoprotein E receptor 2 (ApoER2) and very-low-density lipoprotein receptor (VLDLR)[74]. Many molecules are involved in the signaling cascade triggered by *reelin*, including SFK, Dab1, Lis1, PI3K, etc[74]. In particular, we found that *reelin* demarcates a subset of preBötC neurons that may set the caudal boundary between the preBötC and ibsVRG.

Reelin expression partially overlaps with two known markers for glutamatergic preBötC neurons: somatostatin and NK1 receptor. The extent of heterogeneity among preBötC neurons is currently unknown, and the distinction between neurons that express one, two, or all three of these markers is unclear. At present, we are unable to determine whether all preBötC *reelin* neurons are involved in respiration. However, strong colocalization with two other preBötC markers suggests that many of these neurons are critical to respiration. The addition of a third preBötC marker will afford researchers another level of resolution in trying to define structural and functional preBötC subunits.

We recently found that the PHG receives projections from preBötC SST neurons[54]. We hypothesize that this region contains premotor neurons to hypoglossal motoneurons and interneurons relaying signals from the preBötC to NTS. Interestingly, there were many *reelin* neurons in this region in young rats, but this *reelin* expression dramatically decreased in older rats. The reason for this age-related change in *reelin* expression and the function of *reelin* neurons in the PHG is presently unknown. We also found a group of *reelin* neurons residing dorsal to the facial nucleus that maintained *reelin* expression across age groups. Their anatomical connections and function, respiratory or otherwise, is also currently unidentified.

We found substanial numbers of *reelin* neurons in the pontine respiratory group, forming a band from the trigeminal motor nucleus sweeping dorsally and rostrally to the

pedunculopontine tegmentum. This group of neurons included portions of the supratrigeminal nucleus, medial and lateral parabrachial nuclei, and Kölliker-Fuse. The role of these reelin neurons is currently unknown, although these areas contain many respiratory-phased neurons with projections to medullary respiratory targets. In addition, this area receives dense projections from SST preBötC neurons.

Most of the areas containing *reelin* neurons outside of the preBötC are known or presumed to contain premotor neurons. The only non-respiratory area with identified *reelin* neurons was in the ventromedial medulla, which is also a site of non-respiratory bulbospinal neurons[82, 83].

The Reeler mouse was first described in 1951[63] and later the locus of the *reelin* gene was mapped and identified[60, 61]. Reeler mice have characteristic "reeling" movements and show many pathological brain structures, including inversion of cortical layers[62], decreased cerebellar size[84], and impaired dendrite outgrowth[85]. We found that the Reeler mouse had an impaired response to hypoxia compared to their littermates. Although the loss of *reelin* in these knockouts is complete and thus does not allow us to pinpoint the origin of any breathing deficit, these results are suggestive of a role for *reelin* in the development of circuits that modulate breathing in response to hypoxia or more directly in mediating the hypoxic response in adults rats. It is also worth noting that Reeler mice having a normal response to hypercapneic challenge would be consistent with the absence of *reelin labeling found within the RTN/pFRG as well as other chemosensitive areas.*

In summary, we successfully constructed a subtractive cDNA library from preBötC inspiratory neurons and determined that *reelin* clearly labels a subset. The anatomical boundary of the preBötC and ibsVRG is at the border of two *reelin* populations with distinct soma diameters. Mice lacking functional *reelin* protein exhibited abnormal responses to hypoxia, indicating a possible modulatory role for *reelin* in breathing in the adult.

CHAPTER III

Optogenetic Perturbation of Glycinergic preBötC Neurons Shapes Inspiratory Pattern

INTRODUCTION

Breathing in mammals is a complex behavior that must work (nearly) continuously from birth throughout life and can be rapidly modified to support a wide range of physiological and functional demands. The preBötC, in the ventrolateral medulla, is a critical locus for respiratory rhythmogenesis in the intact, eupneic mammal[2] and in reduced *en bloc* and slice preparations[1]. The preBötC contains intermingled heterogeneous populations of excitatory and inhibitory neurons[3, 4]. Excitatory preBötC neurons are critical components of the respiratory central pattern generator (CPG)[2, 32, 33, 86]; however, the role of inhibitory preBötC neurons is not well understood. Respiratory rhythm persists after bilateral blockade of fast inhibitory neurotransmitters in the preBötC in intact rats[20]. Since there is a substantial population of glycinergic preBötC neurons[4], many of which are phasically active during inspiration[16], we wanted to determine their contribution to breathing movements by examining the effects of direct, fast on/fast off, perturbation of their ongoing activity.

We utilized optogenetic tools to probe the functional contribution of glycinergic preBötC neurons to respiratory rhythm and pattern. By viral transfection resulting from localized virus injection, we expressed Channelrhodopsin-2 or Archaerhodopsin in glycinergic preBötC neurons of transgenic mice expressing Cre recombinase driven by the GlyT2 promoter. Since the GlyT2 promoter is specific to glycinergic neurons[50], this intersectional strategy allowed us to selectively activate and inhibit these glycinergic neurons in the intact, awake or anesthetized, mouse. We found that tuning glycinergic neuronal activity profoundly modulates the amplitude and timing of inspiratory motor output. We conclude that glycinergic preBötC neurons are important for modulation of respiratory pattern, are critical for production of reflex apneas, but are not necessary for rhythmogenesis *per se*.

RESULTS

Preliminary studies in transgenic mice

As an initial screen of the functional role of GlyT2 preBötC neurons, we crossed transgenic mice expressing Cre recombinase under the glycine transporter 2 (GlyT2) promoter (GlyT2-Cre) with another transgenic mouse line containing a floxed conditional expression cassette containing either ChR2-tdTomato or Arch-GFP in the Rosa26 locus (R26-floxed-ChR2 or R26-floxed-Arch). Resulting progeny positive for both alleles expressed ChR2 or Arch only in GlyT2 neurons (herein referred to GlyT2-ChR2 or GlyT2-Arch mice). To efficiently deliver light into the preBötC of these mice, we implanted optical cannulae bilaterally from a dorsal approach, about 200 – 400 µm above the preBötC (Figure 3-1). This was achieved by delivering a 1 s pulse train (100 ms pulses with a 50 ms interpulse interval) of blue light bilaterally into the preBötC. In GlyT2-ChR2 mice, there was a pronounced delay in the onset of the next breath when photostimulation was delivered during expiration (Figure 3-2); however, photostimulation during inspiration did not alter a breath once started. We found in these transgenic mice that the effect of photostimulation was finite; prolonged photostimulation delayed the onset of the next breath for a maximum of ~3 s before the next breath broke through despite continued photostimulation (Figure 3-3). In GlyT2-Arch mice, photoinhibition produced an increased breath amplitude and shortened the interval between breaths, resulting in an increased respiratory frequency (Figure 3-4). Since higher levels of protein expression are possible with viral vectors, we were keenly interested in moving to use viral delivery of opsins as a means of ensuring a maximal behavioral response. Viral injection also allows for further restriction of protein expression to a localized injection site within the preBötC as opposed to all glycinergic neurons in the brain, so we promptly turned our attention to viral delivery of opsin proteins as a more sophisticated means of addressing this problem.

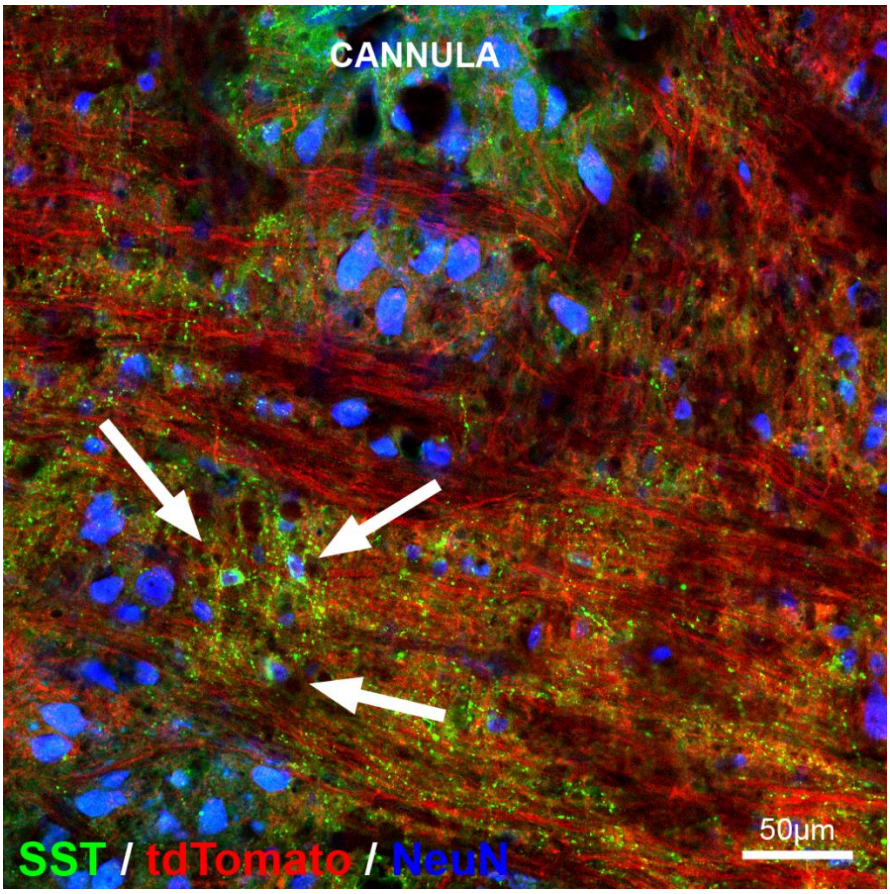

Figure 3-1 Cannulae implanted dorsal to preBötC for *in vivo* targeting of ChR2-expressing GlyT2 neurons within the preBötC in transgenic GlyT2-ChR2 mice. White arrows identify SST^{+} neurons (green). Scale bar: 50 µm.

a

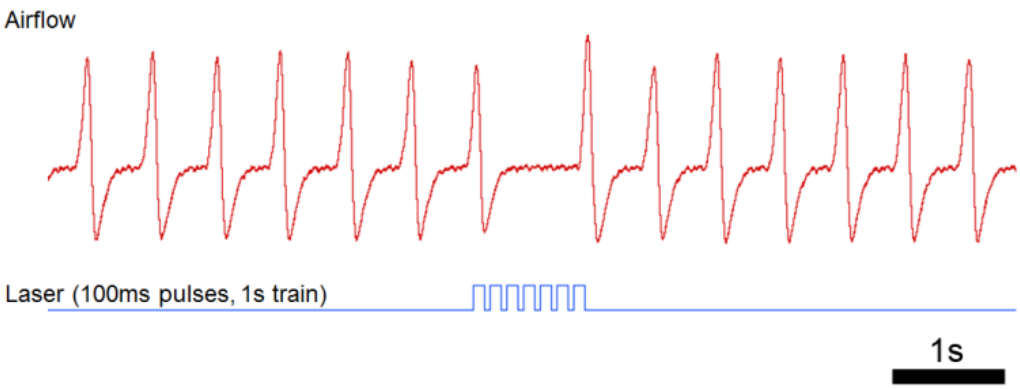

b

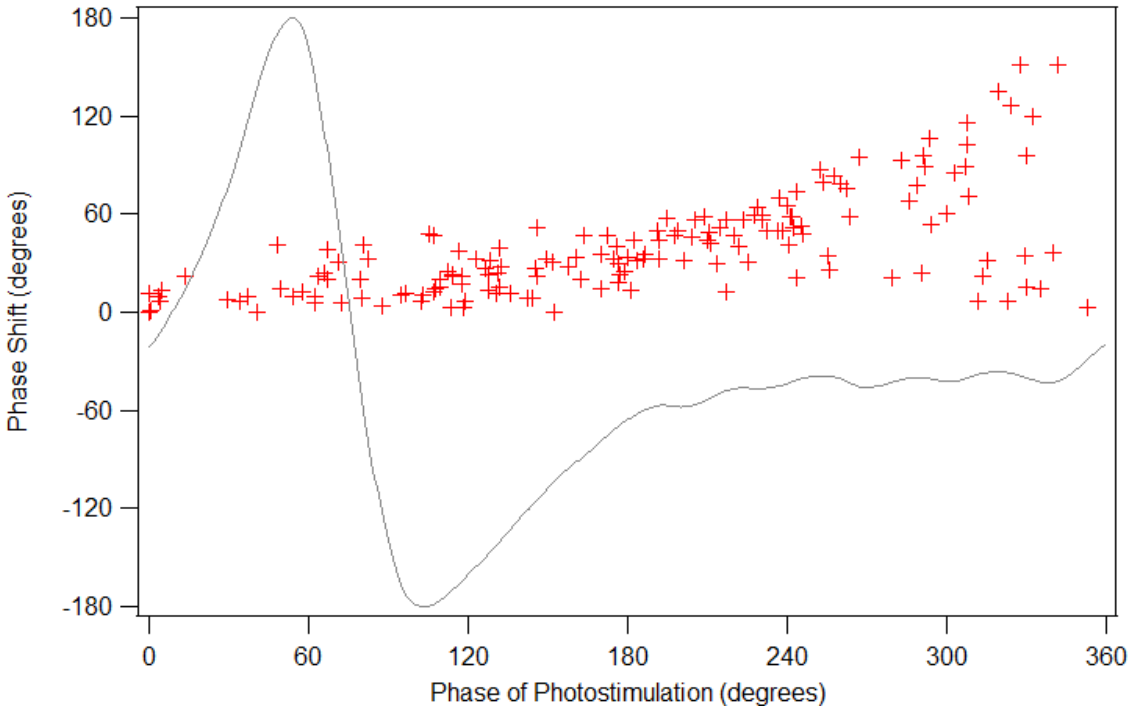

Figure 3-2 Photostimulation of ChR2-expressing neurons in the preBötC of transgenic GlyT2-ChR2 mice delays inspiration. (**a**) A 1 s pulse train (blue trace; 100 ms pulses with a 50 ms interpulse interval) of blue light (473 nm) produced a pause in breathing as shown on the airflow trace (red) of anesthetized GlyT2-ChR2 mice. Scale bar: 1 s. (**b)** Representative phase

response curve (see Methods) showing relationship between phase of photostimulation and the resulting shift in respiratory phase.

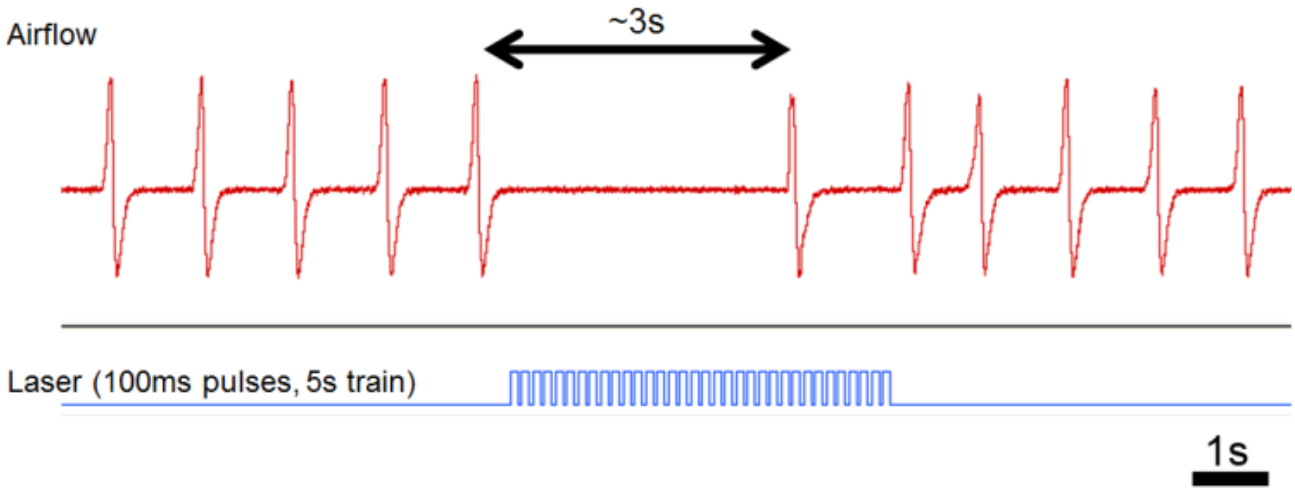

Figure 3-3 Prolonged photostimulation in transgenic GlyT2-ChR2 mice produces finite delay in breathing. A 5 s pulse train (blue trace; 100 ms with a 50 ms interpulse interval) delivered bilaterally into the preBötC of anesthetized GlyT2-ChR2 mice. Scale bar: 1 s.

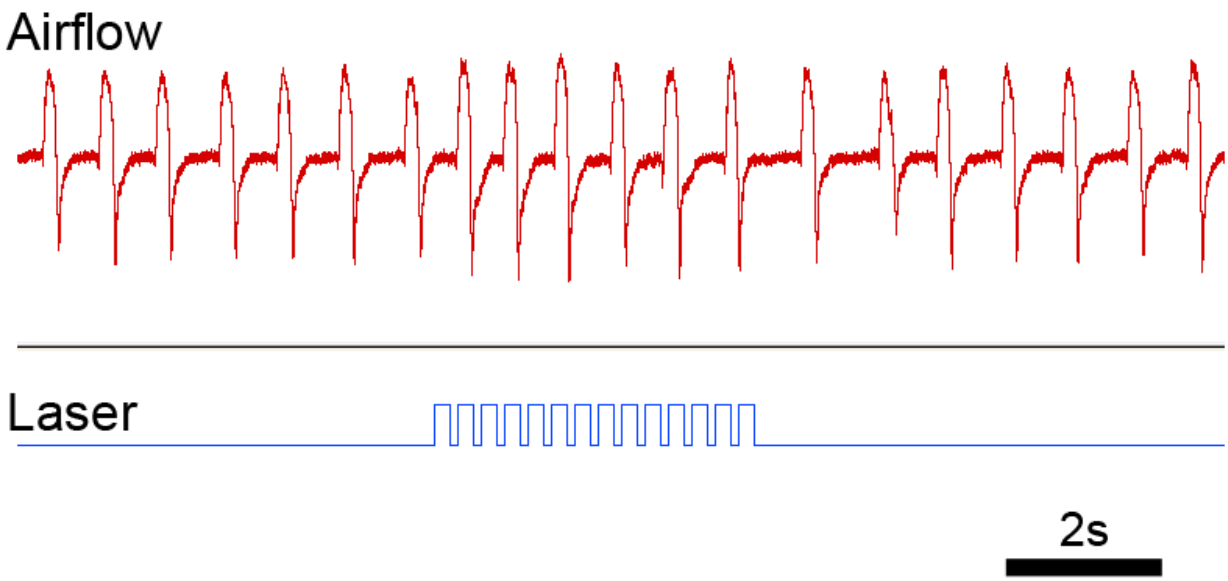

Figure 3-4 Photoinhibition of Arch-expressing neurons in the preBötC produced an increase in respiration in GlyT2-Arch mice. A 4 s pulse train (100 ms pulses with a 50 ms interpulse interval) of orange light (blue trace; 593 nm) was delivered bilaterally into the preBötC of GlyT2-Arch mice and changes in airflow (red) were recorded. Scale bar: 2 s.

Targeting opsin protein expression to glycinergic preBötC neurons

To further restrict ChR2 or Arch to glycinergic preBötC neurons, we used adeno-associated viruses (AAV2/1; Figure 3-5) encoding either ChR2-eYFP driven by the constitutive promoter Ef1α in a double floxed inverted open reading frame configuration (DIO-ChR2)[87] or Arch-GFP driven by the constitutive chicken β-actin (CBA) promoter in a FLEX switch (FLEX-Arch). We injected either virus bilaterally into the preBötC of GlyT2-Cre mice (Figure 3-6). These injections produced protein expression in preBötC neurons that was detectable *post hoc*. The peak density of transfected neurons was caudal to the facial nucleus (VII) by 750 – 900 µm in ChR2 experiments and 600 – 750 µm in Arch experiments and ventral to the compact nucleus ambiguus, which overlapped with the distribution of somatostatin (SST)-expressing preBötC neurons (Figure 3-7, 2-8). Within the preBötC, transfected neurons intermingled but rarely colocalized with SST immunoreactivity in either DIO-ChR2 (0.3 ± 0.6 out of 45.5 ± 13.4 SST^+ neurons; n = 3) or FLEX-Arch (2 ± 0 out of 36.3 ± 9.8 SST^+ neurons; n = 3) transfected mice (Figure 3-9). EYFP/GFP expression colocalized with glycine immunoreactivity in both sets of mice (Figure 3-10).

AAV2/1-Ef1α-DIO-ChR2-eYFP

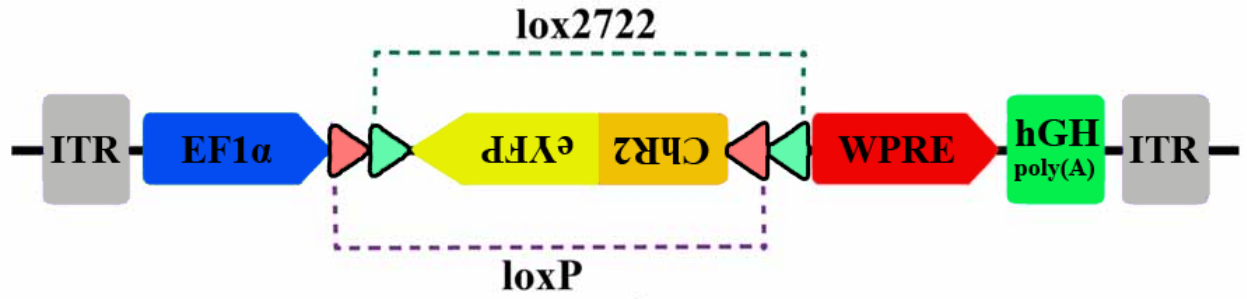

AAV2/1-flex-CBA-Arch-GFP

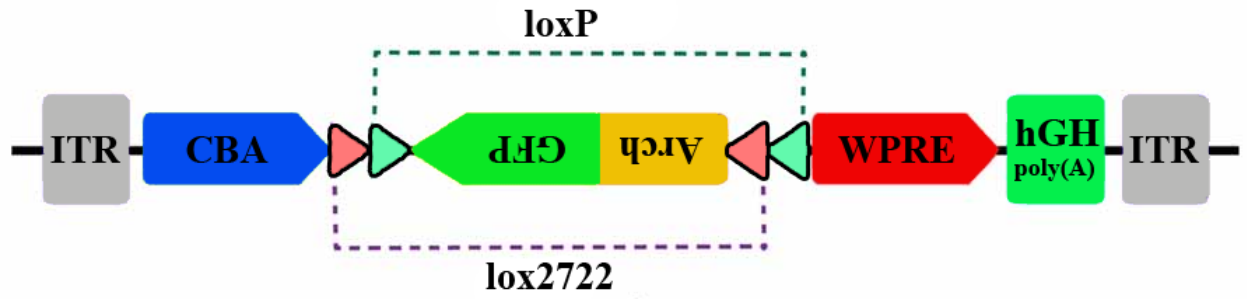

Figure 3-5 Gene constructs for cre-dependent expression of opsin proteins. Gene constructs containing ChR2-eYFP or Arch-GFP in cre-dependent expression cassettes.

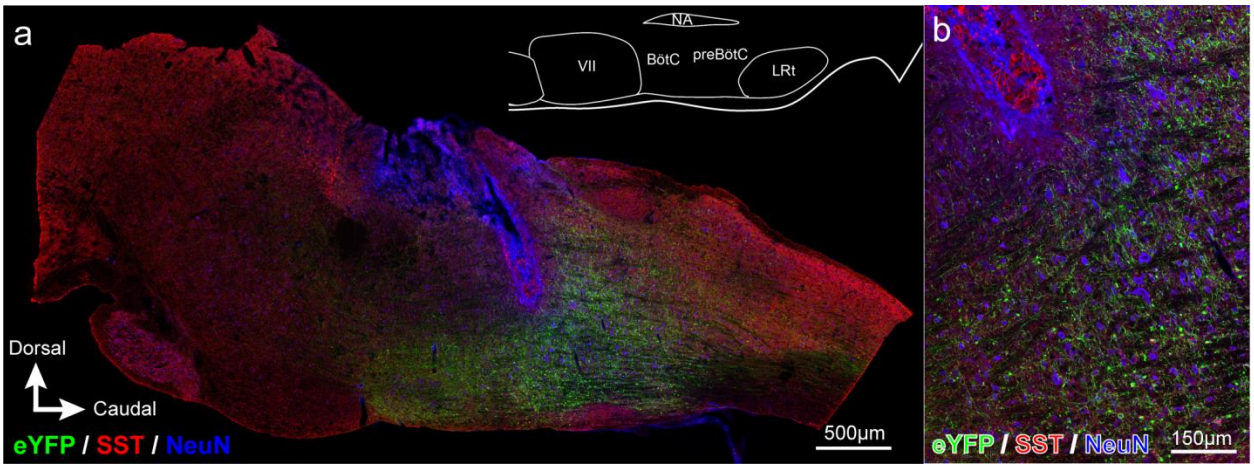

Figure 3-6 Cre-dependent ChR2 or Arch expression targeted to GlyT2 preBötC neurons. (**a**) Representative confocal mosaic micrograph of a sagittal brainstem section of a GlyT2-cre^{+} mouse showing eYFP^{+} and SST^{+} neurons after injection of AAV2/1-Ef1α-DIO-ChR2-eYFP into preBötC. Abbreviations: VII: facial nucleus, NA: nucleus ambiguus, BötC: Bötzinger Complex, LRt: lateral reticular nucleus. (**b**) High-magnification micrograph of section in (a) showing eYFP^{+} preBötC neurons intermingled with SST^{+} neurons.

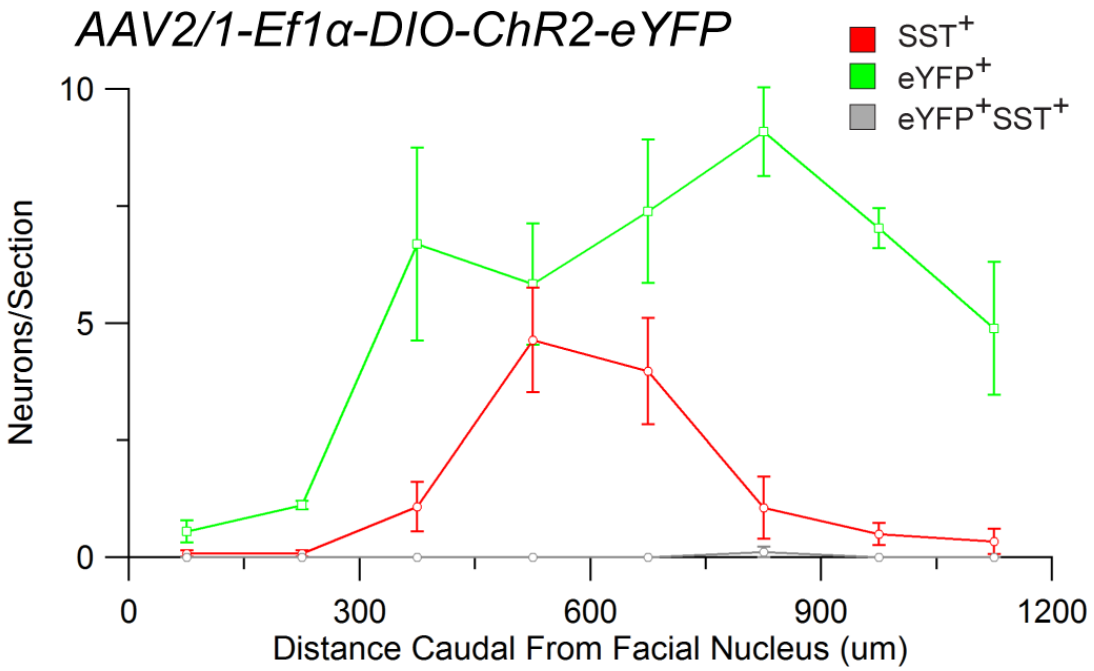

Figure 3-7 Distribution of GFP^+ (green) and SST-ir (red) neurons relative to the caudal boundary of the facial nucleus. GFP^+SST^+ (gray) indicates double-labeled neurons expressing both eYFP and SST. Error bars: mean ± s.e.m.

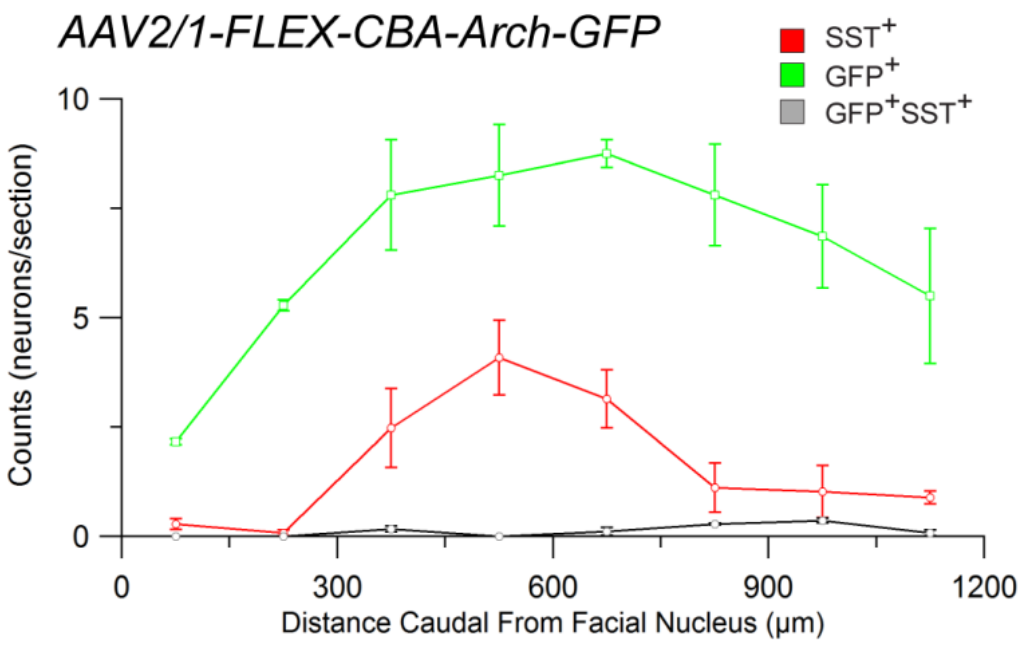

Figure 3-8 Distribution of GFP^+ (green) and SST-ir (red) neurons relative to the caudal boundary of the facial nucleus. GFP^+SST^+ (gray) indicates double-labeled neurons expressing both GFP and SST. Error bars: mean ± s.e.m.

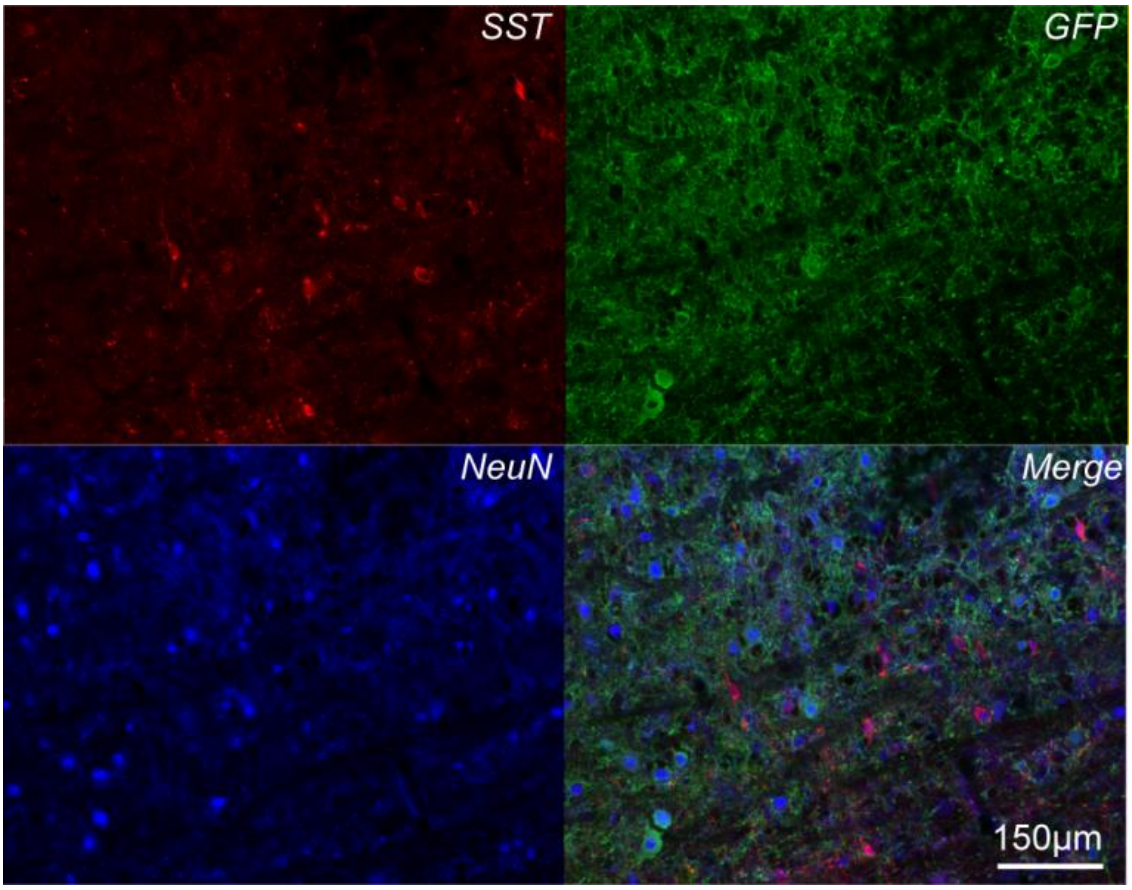

Figure 3-9 GlyT2 preBötC neurons intermingle with $SST^{+`}$ subpopulations. Representative single channel and overlay confocal micrographs showing $eYFP^{+}$ preBötC neurons (green) with SST (red) and NeuN (blue) immunoreactivity. Scale bar: 150 µm.

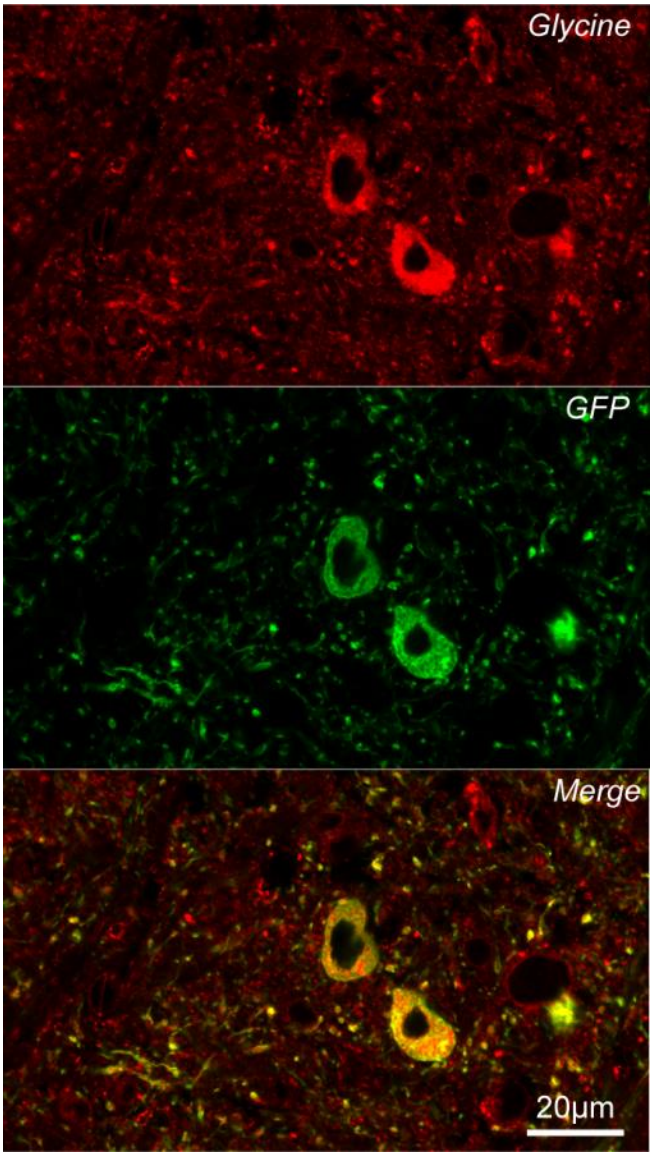

Figure 3-10 Glycine immunoreactivity colocalizes with transfected neurons. Single channel and overlay confocal micrographs showing GFP^+ preBötC neurons (green) with glycine immunoreactivity (red). Scale bar: 150 µm.

Short photostimulation of ChR2-transfected GlyT2 preBötC neurons depressed inspiratory motor output or lengthened expiratory duration in anesthetized mice

To efficiently deliver light into the preBötC, we implanted optical cannulae bilaterally from a dorsal approach, about 200 – 400 µm above the preBötC. In anesthetized Cre^{+} mice, brief bilateral photostimulation (100 ms pulse; 473 nm; Figure 3-11) of ChR2-transfected GlyT2 preBötC neurons generated respiratory phase-dependent changes in breathing (n = 5). We constructed phase response curves, using the breath prior to photostimulation as a reference for a 360° cycle (see Methods), to determine whether ChR2 activation affected respiratory cycle timing (Figure 3-12).

Stimulation during early inspiration (0° – 30°) resulted in premature burst termination (Figure 3-13), which is a breath of truncated peak inspiratory airflow (decreased to 56.4 ± 5.9% of control; $P = 10^{-10}$; Figure 3-14) and shortened inspiratory duration (decreased to 67.5 ± 5.4% of control; $P = 10^{-10}$; Figure 3-15). In contrast, stimulation during expiration (150° – 360°) delayed the onset of the subsequent inspiration (Figure 3-16), with the strongest effect during the late expiratory - often referred to as pre-inspiratory - phase (330° – 360°; Figure 3-12). Thus, stimulation during late expiration (330° – 360°) generated a 233.4 ± 19.5° shift ($P = 10^{-10}$), while stimulations falling earlier in expiration (150° – 180°) produced a smaller 93.6 ± 15.9° shift (P = 0.007; Figure 3-12). This phase shift was significant throughout much of expiration (150° – 360°). Following this phase shift, the next breath had no significant change in peak inspiratory airflow (101.0 ± 3.2% of control; P = 1; Figure 3-14) or inspiratory duration (104.2 ± 3.0% of control; P = 1; Figure 3-15).

Prolonged photostimulation of ChR2-transfected GlyT2 preBötC neurons produced apnea in anesthetized or awake mice

We wanted to determine how the respiratory network responded to longer activation of ChR2-expressing neurons. In anesthetized mice, a 1 s photostimulus pulse train (7x 100 ms pulses; n = 5) at any time during the respiratory cycle stopped breathing, i.e., produced an apnea, that continued until after the pulse train of light completed (Figure 3-17). We observed that the subsequent respiratory cycle began at a fairly constant delay after the pulse train turned off regardless of stimulus phase (300 – 862 ms, min – max; n = 3; Figure 3-18). In anesthetized mice breathing room air, prolonged stimulation (up to 20 s pulse trains; n = 3) produced an apnea that persisted until the pulse train ended (Figure 3-19). In awake, freely moving mice, the same 1 s pulse train produced consistent apneas (n = 5; Figure 3-20). When ventilation was increased in these mice with 5 min of either hypoxic (8% O_2; n = 5) or hypercapnic (5% CO_2; n = 5) inspired gas mixtures, ChR2 activation still produced apnea (Figure 3-20).

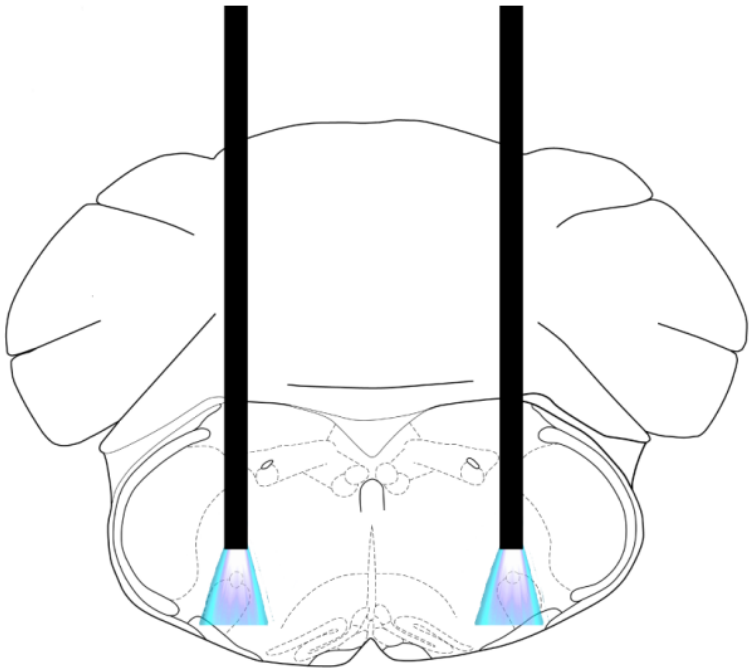

Figure 3-11 Schematic representation depicting bilateral placement of optical cannulae targeting preBötC for directing blue light (473 nm) into the brain.

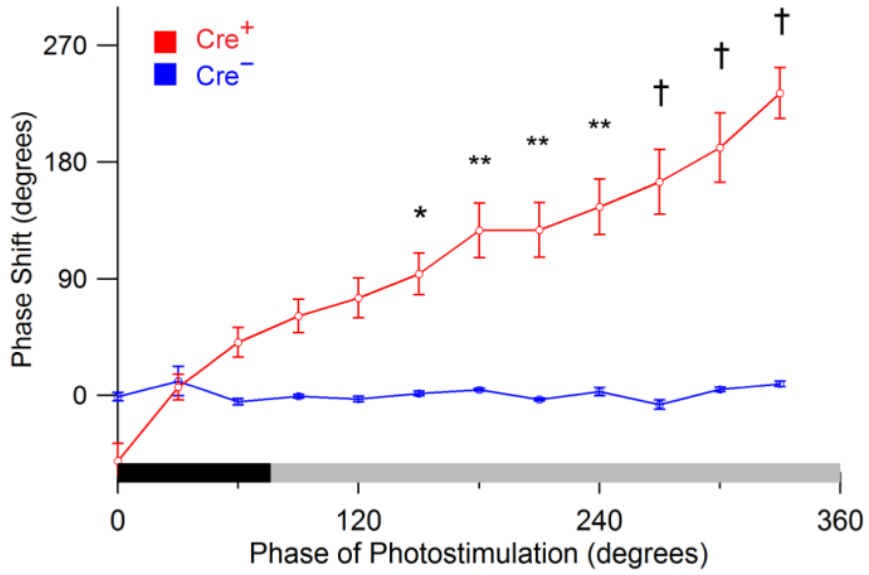

Figure 3-12 Phase response curve in response to brief photostimulation of ChR2-expressing GlyT2 preBötC neurons in GlyT2-cre^{+} and GlyT2-cre^{-}. A 100 ms pulse of blue light (473 nm) was delivered bilaterally into the preBötC and airflow was measured for light-induced shifts in breathing. Photostimulated cycles were compared to the previous (control) cycle. Respiratory phase is depicted on the x axis, with inspiration (black) defined from 0 to 71.8° and expiration (gray) defined from 71.8° to 360°. The dotted vertical line at 0° indicates onset of inspiration. Error bars, mean ± s.e.m. * $P < 0.05$; ** $P < 0.001$; † $P < 10^{-8}$.

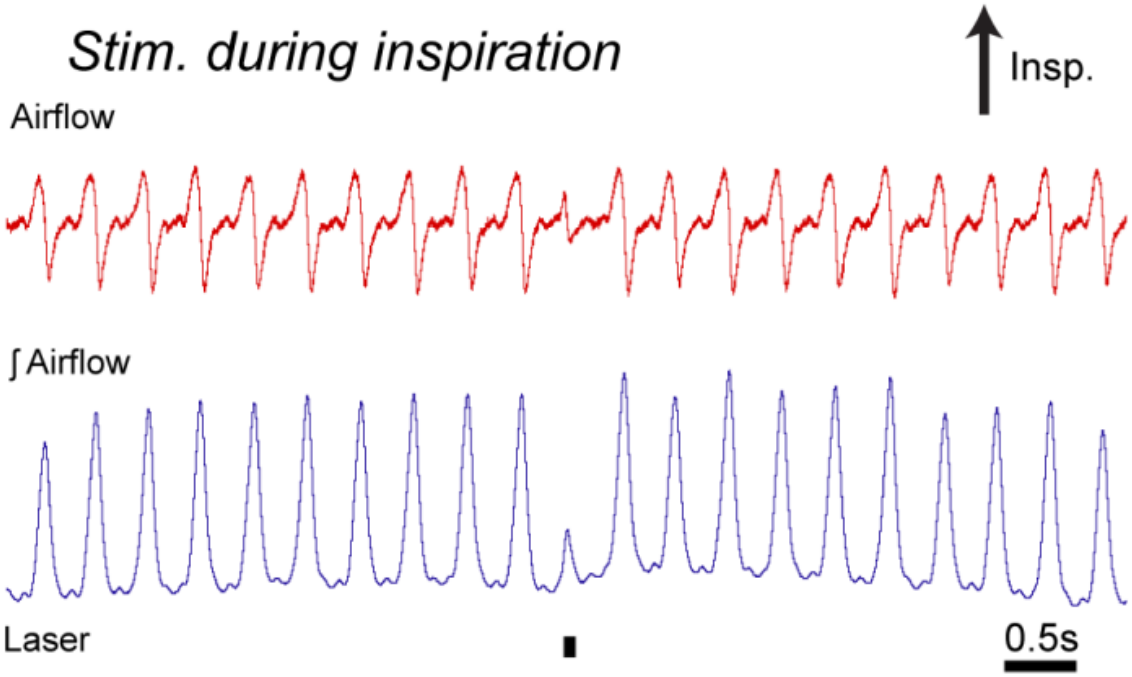

Figure 3-13 Brief photostimulation of ChR2-expressing GlyT2 preBötC neurons during inspiration prematurely terminates breaths. Representative airflow and tidal volume trace, with photostimulation indicated by the black line. Scale bar: 0.5 s.

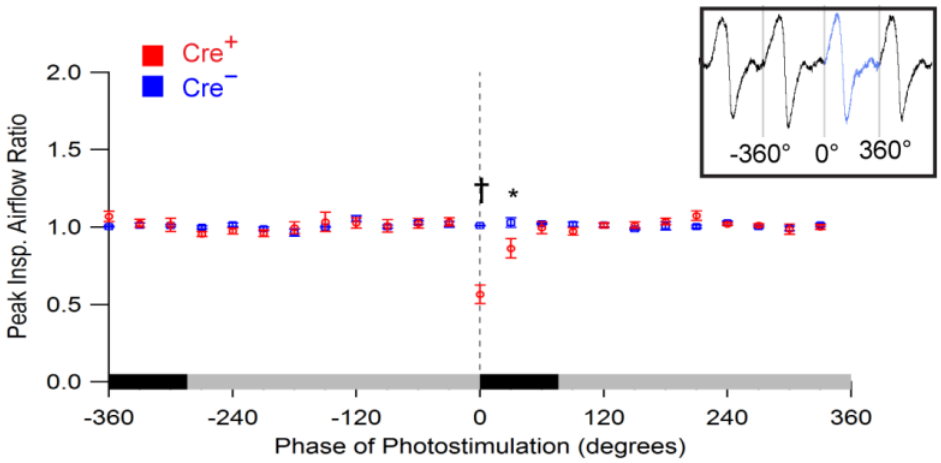

Figure 3-14 Comparison of photostimulated cycle to prior control cycle for ratio of peak inspiratory airflow in Cre^{+} and Cre^{-} anesthetized mice. Respiratory phase is depicted on the x axis, with inspiration (black) defined from 0 to 71.8° and expiration (gray) defined from 71.8° to 360°. The dotted vertical line at 0° indicates onset of inspiration. Error bars, mean ± s.e.m. * $P < 0.05$; ** $P < 0.001$; † $P < 10^{-8}$.

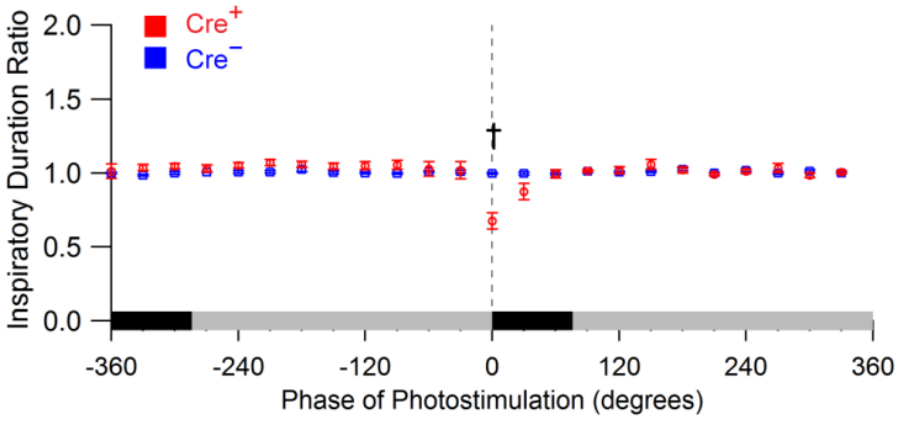

Figure 3-15 Comparison of photostimulated cycle to prior control cycle for ratio of inspiratory duration in Cre^+ and Cre^- anesthetized mice. Respiratory phase is depicted on the x axis, with inspiration (black) defined from 0 to 71.8° and expiration (gray) defined from 71.8° to 360°. The dotted vertical line at 0° indicates onset of inspiration. Error bars, mean ± s.e.m. * $P < 0.05$; ** $P < 0.001$; † $P < 10^{-8}$.

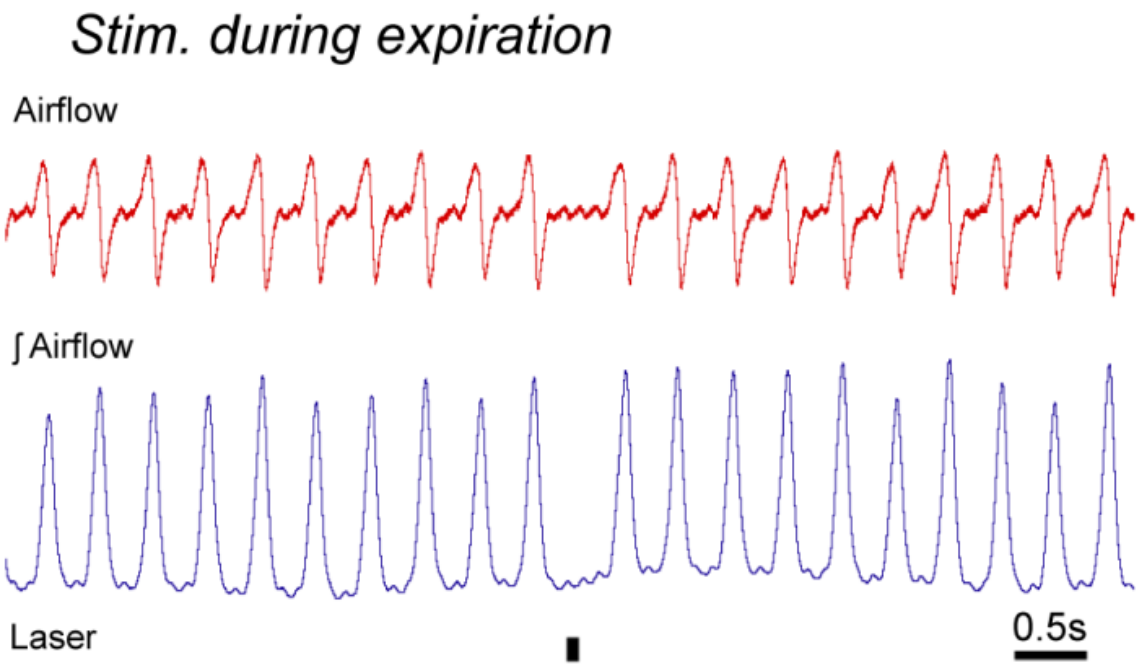

Figure 3-16 Brief photostimulation of ChR2-expressing GlyT2 preBötC neurons during expiration delays the onset of the next breath. Representative airflow and tidal volume trace showing characteristic delay in response to photostimulation delivered via optical cannulae into the preBötC of GlyT2-Cre^{+} mice. Scale bar: 0.5 s.

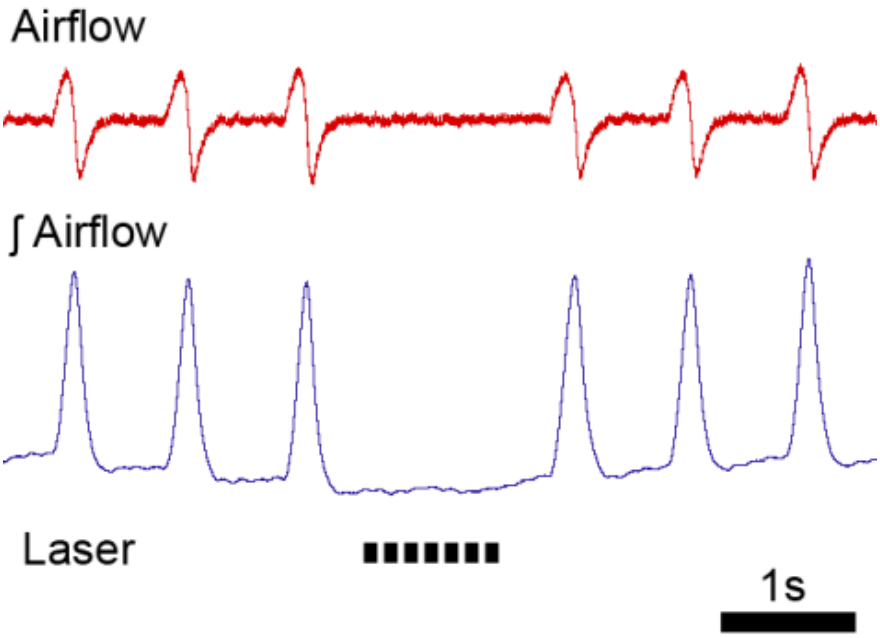

Figure 3-17 A 1s pulse train results in apnea. Laser pulses indicated with black lines. Scale bar: 1s.

a

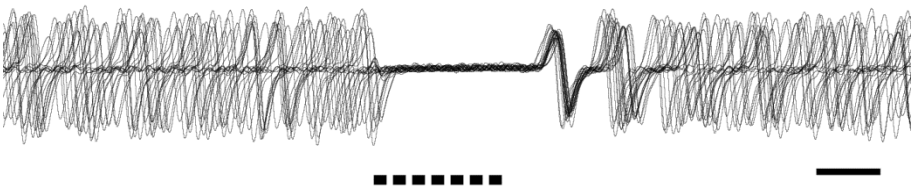

b

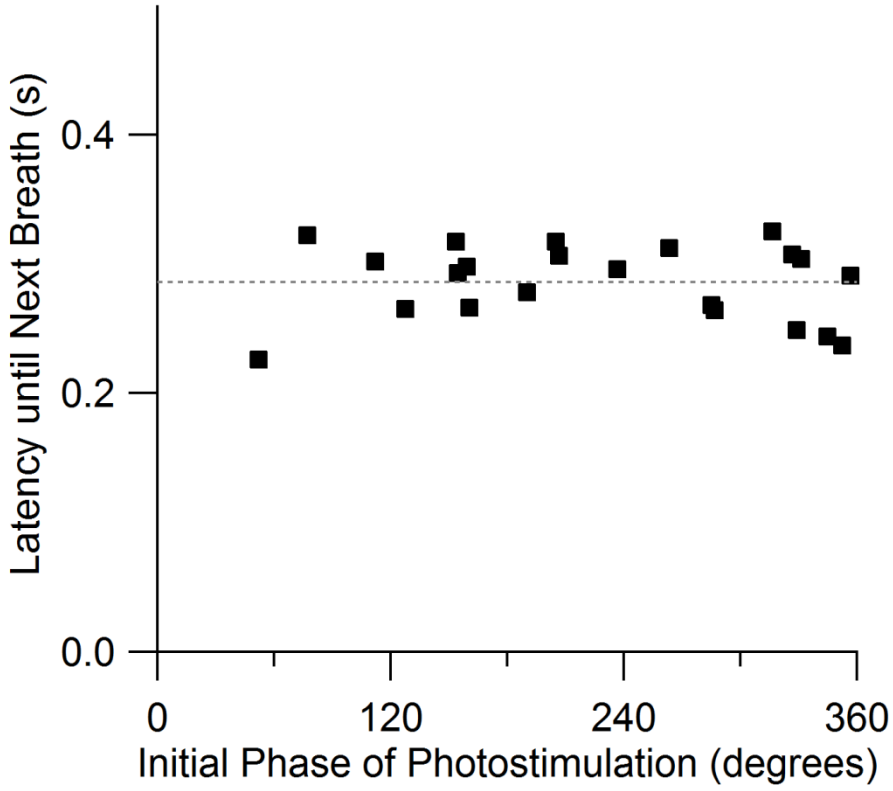

Figure 3-18 Respiratory cycle resets after photostimulation-induced apnea**. (a)** Overlay of airflow traces aligned to the laser onset (7x 100 ms pulses with a 50 ms interpulse interval) reveals that the next breath occurs at a fairly constant delay after the laser shuts off. Scale bar: 0.5 s. (**b**) Representative graph of this latency as a function of initial phase of photostimulation. Dotted line indicates mean latency.

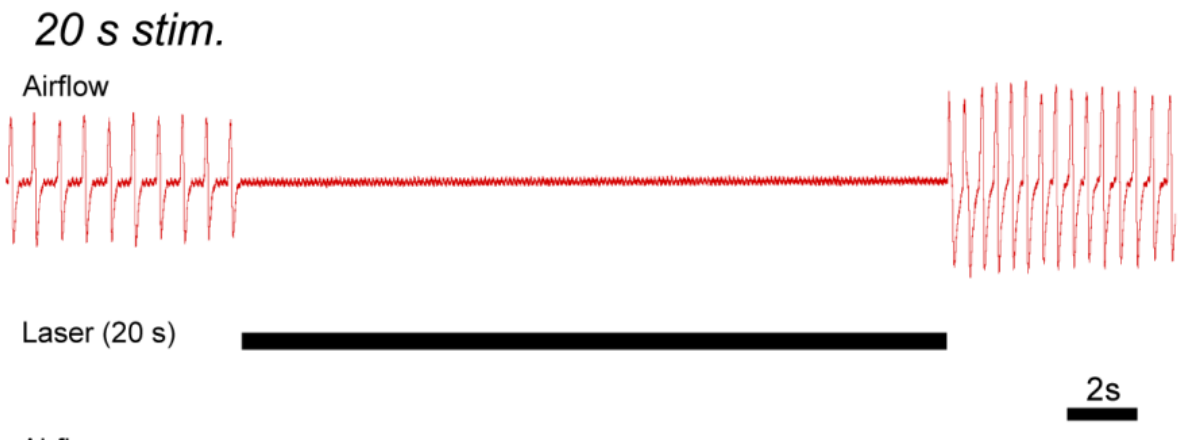

Figure 3-19 Prolonged photostimulation results in long-lasting apnea. Airflow trace during bilateral delivery of 20 s pulse trains of light (100 ms pulses, 50 ms interpulse delay) into mice expressing ChR2 in GlyT2 preBötC neurons. Scale bar: 2 s.

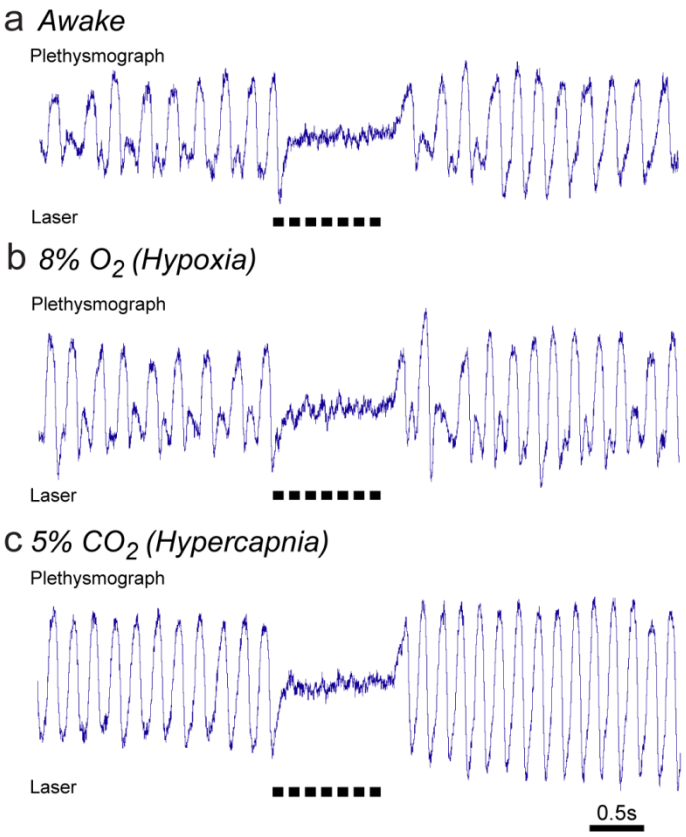

Figure 3-20 Photostimulation during awake, hypoxic, or hypercapnic states produces apnea**.** Awake, behaving mice in a plethysmograph chamber received a 1 s pulse train (100 ms pulses with a 50 ms interpulse interval). Scale bar: 0.5 s.

Photoinhibition of Arch-transfected GlyT2 preBötC neurons augments inspiration in anesthetized mice

We examined the effects on breathing resulting from hyperpolarizing GlyT2 preBötC neurons. In anesthetized mice, bilateral photoinhibition (100 ms pulse; 593 nm; Figure 3-21) of Arch-transfected GlyT2 preBötC neurons (n = 7) augmented inspiratory airflow when applied just prior to and during early inspiration (Figure 3-22) and shortened expiratory time when applied during expiration (Figure 3-23). Peak inspiratory airflow increased when photoinhibition was preinspiratory (240° – 360° of prior cycle) or early inspiratory (0 – 30°), with a maximal effect at 0 – 30° (159.0 ± 22.4% of control; $P = 10^{-7}$; Figure 3-24). Photoinhibition that was preinspiratory or inspiratory did not produce a significant change in inspiratory duration (103.0 ± 0.9% of control; P = 1; Figure 3-25). Sighs, larger breaths generated periodically to hyperinflate the lungs, had greater amplitudes and durations than the augmented breaths generated from photoinhibition. Sighs had a peak inspiratory airflow that was 173 ± 14.5% of control ($P = 10^{-5}$) which was also statistically different from photoinhibition-induced augmented breaths (P = 0.02). On average, sighs did not have a significant difference in inspiratory duration (113.9 ± 11.8% of control; P = 0.13). Although there were individual instances where breaths larger enough to qualify as sighs were generated (see Figure 3-22), most affected breaths did not reach comparable amplitudes or durations to sighs.

There was a photoinhibition-induced shift in respiratory phase (Figure 3-26). Stimulation during expiration advanced the onset of the next breath with a -52.3 ± 6.2° phase shift ($P = 10^{-5}$), that was significant for pulses delivered between 150 - 240°, with a maximal effect between 210 - 240°. Photoinhibition during early inspiration (0 - 30°) did not significantly alter the respiratory phase (P = 1). Prolonged photoinhibition (5 s continuous pulse) increased respiratory frequency but the effect was transient and did not last for the full duration of the laser pulse (Figure 3-27).

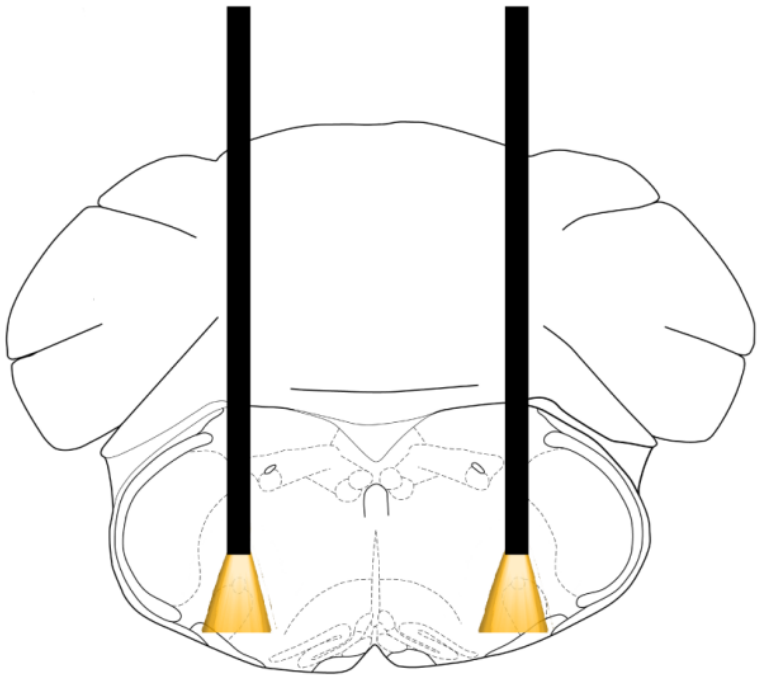

Figure 3-21 Schematic representation depicting bilateral placement of optical cannulae targeting preBötC for directing orange light into the brain.

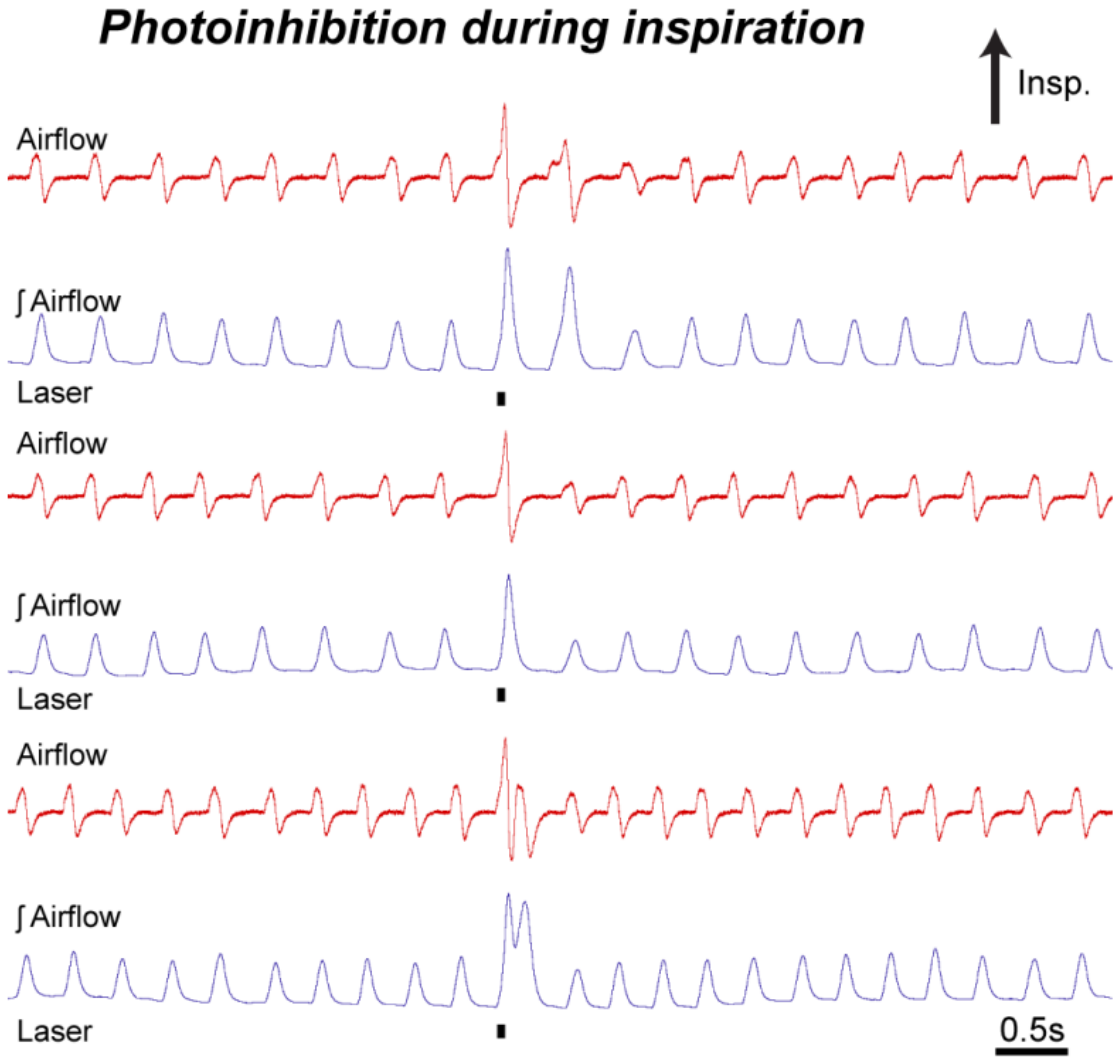

Figure 3-22 Brief photoinhibition of Arch-expressing GlyT2 preBötC neurons during inspiration augments peak inspiratory airflow. Several representative airflow and tidal volume traces from anesthetized GlyT2-Cre+ mice receiving photoinhibition during inspiration. Laser indicated with a black line underneath trace. Scale bar: 0.5 s.

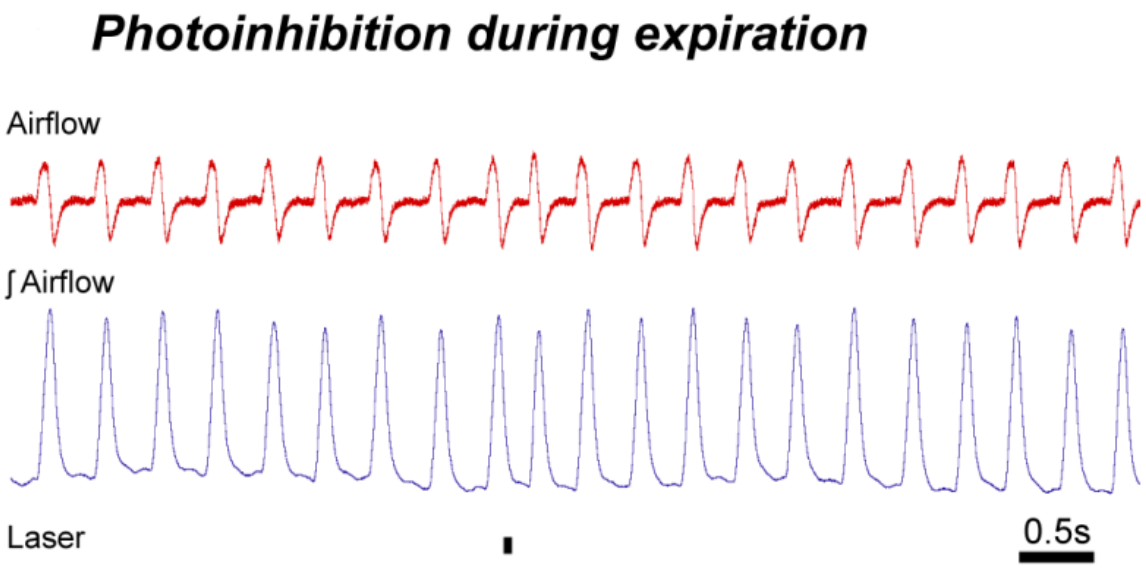

Figure 3-23 Brief photoinhibition of Arch-expressing GlyT2 preBötC neurons during expiration shortens delay until the onset of the next breath. Representative airflow and tidal volume trace from an anesthetized GlyT2-Cre^{+} mouse receiving photoinhibition during expiration. Laser indicated with a black line. Scale bar: 0.5 s.

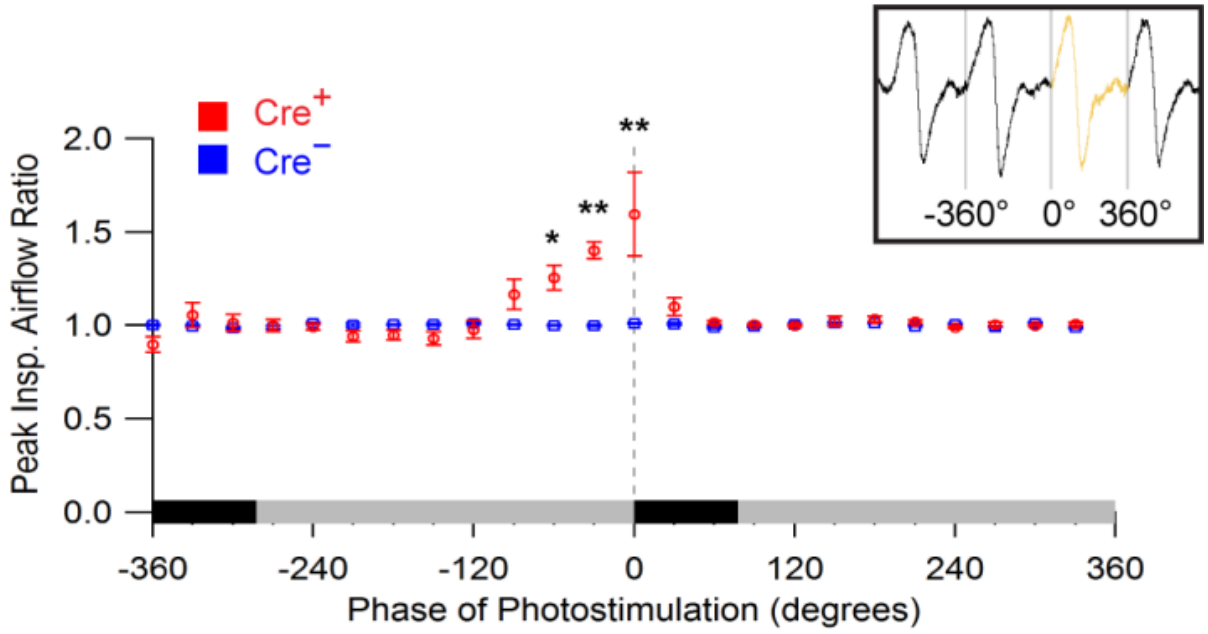

Figure 3-24 Comparison of photoinhibited cycle to prior control cycle for ratio of peak inspiratory airflow in Cre^{+} and Cre^{-} anesthetized mice. Respiratory phase is depicted on the x axis, with inspiration (black) defined from 0 to 77.9° and expiration (gray) defined from 77.9° to 360°. The dotted vertical line at 0° indicates onset of inspiration. Error bars, mean ± s.e.m. * $P < 0.05$; ** $P < 0.001$; † $P < 10^{-8}$. Inset: respiratory phases as defined in degrees.

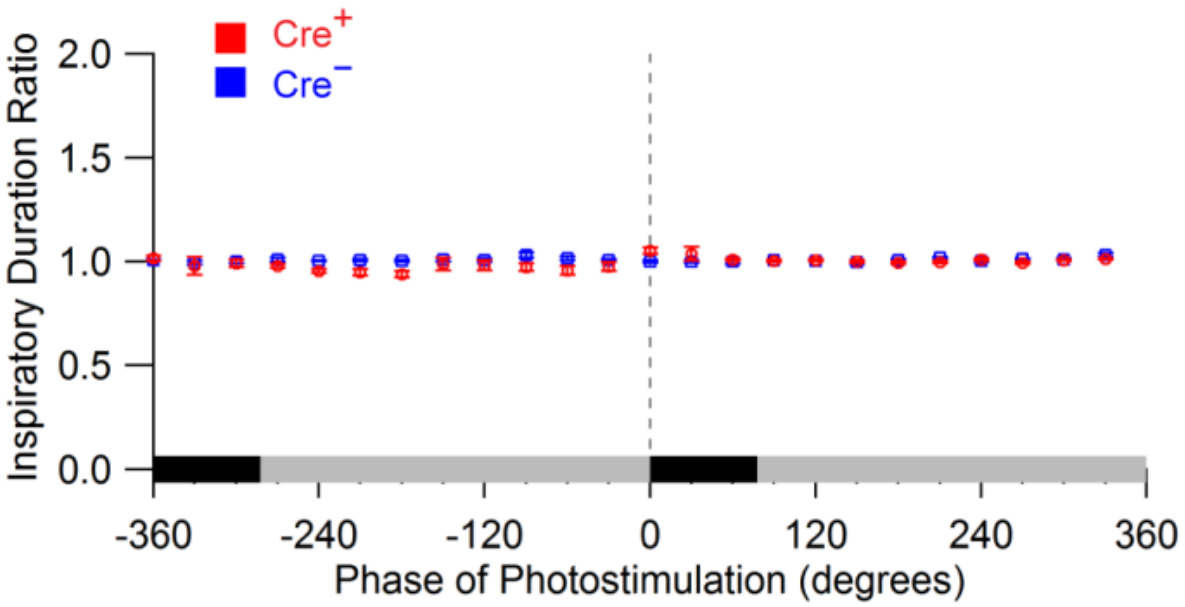

Figure 3-25 Comparison of photoinhibited cycle to prior control cycle for ratio of inspiratory duration in Cre^{+} and Cre^{-} anesthetized mice. Respiratory phase is depicted on the x axis, with inspiration (black) defined from 0 to 77.9° and expiration (gray) defined from 77.9° to 360°. The dotted vertical line at 0° indicates onset of inspiration. Error bars, mean ± s.e.m. * $P < 0.05$; ** $P < 0.001$; † $P < 10^{-8}$.

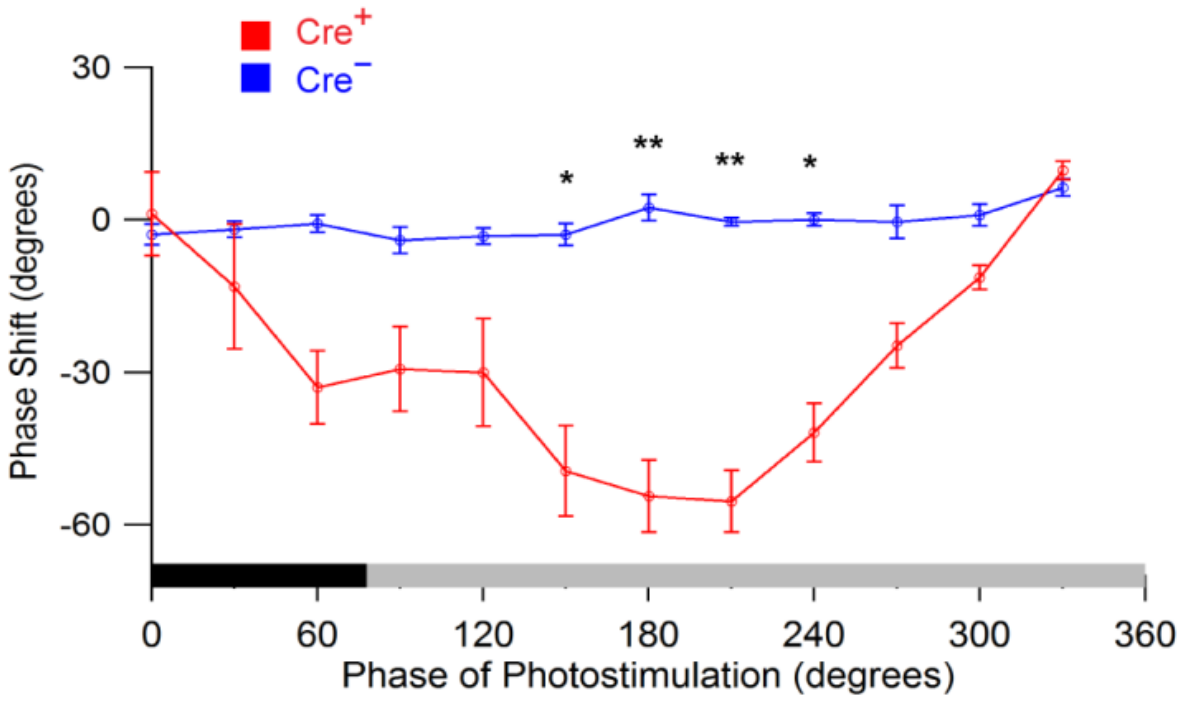

Figure 3-26 Phase response curve in response to brief photoinhibition of Arch-expressing GlyT2 preBötC neurons. Respiratory phase is depicted on the x axis, with inspiration (black) defined from 0 to 77.9° and expiration (gray) defined from 77.9° to 360°. Error bars, mean ± s.e.m. * $P < 0.05$; ** $P < 0.001$; † $P < 10^{-8}$.

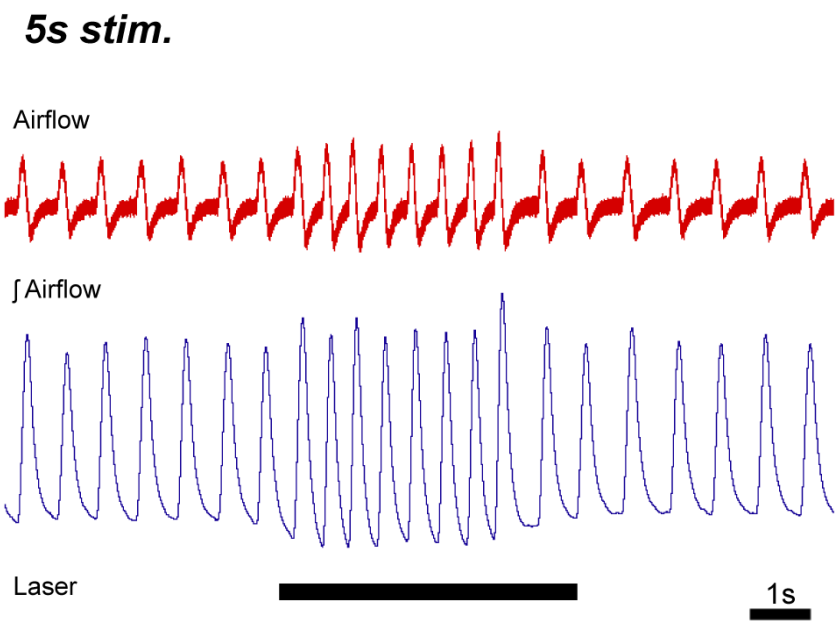

Figure 3-27 Prolonged photoinhibition increases respiratory frequency**.** A 5 s pulse of orange light produces an increase in ventilation shown on airflow and tidal volume traces. The laser is shown as a black line underneath the trace. Scale bar: 1 s.

Arch activation in GlyT2 preBötC neurons rescues breathing during a reflex apnea

We hypothesized that a critical role of inhibition in controlling respiratory pattern is in the production of apneas[20], such as during swallowing or breath holding. To determine whether GlyT2 preBötC neurons participate in generating central apneas, we photoinhibited these neurons during apneas that resulted from lung inflation, i.e., the Breuer-Hering lung inflation reflex[20]. The lungs were inflated with sufficient continuous positive airway pressure (CPAP) to produce apneas that lasted ~12 s (~4 cm H_2O; n = 3) during unstimulated control conditions. Photoinhibiting Arch-transfected GlyT2 preBötC neurons (1 s pulse) broke the apnea for the pulse duration with either one or two breaths (Figure 3-28a). Laser onset at 5.45 ± 0.5 s during an inflation-induced apnea (CPAP + Laser) induced a breath with only a 350 ms delay from laser onset, i.e., 5.8 ± 0.5 s after the start of CPAP (Figure 3-28b) versus an expected first breath with CPAP only of 11.8 ± 1.4 s (ANOVA; $P = 10^{-6}$).

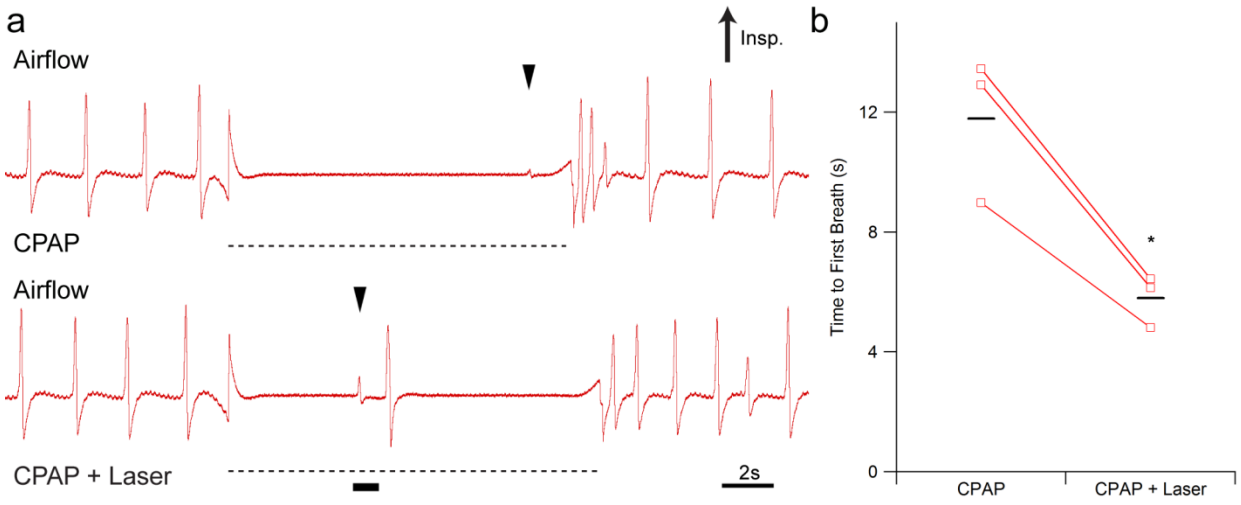

Figure 3-28 Photoinhibition of GlyT2 preBötC neurons during a reflex apnea rescues breathing. (**a**) Breuer-Hering lung inflation reflex triggered by applying continuous positive airway pressure (CPAP; ~4 cmH_2O; dotted black line) to a tracheotomized, anesthetized Arch-transfected mouse in control (top) and photoinhibition (bottom) conditions. During bilateral photoinhibition, a 1s pulse was applied ~5 s into the apnea and CPAP was sustained until the next breath "broke" through the apnea (black arrow). (**b**) Duration of induced apnea, measured from the onset of BHIR to the onset of the next inspiration, in BHIR alone and BHIR + laser conditions. Means are indicated with black horizontal lines. * $P < 10^{-5}$.

Single-unit recording in ChR2- and Arch-transfected mice

In ChR2-transfected mice, we unilaterally photostimulated (Figure 3-29a; n = 18) and recorded from preBötC neurons within the cone of light. Unilateral ChR2 photostimulation of GlyT2 preBötC neurons was sufficiently strong to recreate the effects observed from bilateral photostimulation, i.e., a consistent apnea for the duration of light. In total, we recorded 18 neurons, of which 8 were respiratory-modulated (5 neurons fired in a typical pre-I pattern, 2 were inspiratory, and 1 was expiratory; Figure 3-29b) and 10 neurons exhibited tonic firing. All of the recorded respiratory-modulated neurons and all but two of the tonically firing neurons were silenced during photostimulation. Several of the neurons exhibited a rebound effect, firing at an increased rate during the burst following the laser stimulus. Pre-I neurons could be silenced at any point in their firing, including early enough in the preinspiratory phase to preclude initial preBötC activity from translating into motor output (Figure 3-29b, black arrow), despite the typical pre-I firing that normally preceded an inspiratory burst. During such instances, pre-inspiratory activity did not lead to burst firing in the preBötC and no change was elicited on the airflow trace. The delay between the laser shutting off and the onset of the next breath described above (see Fig. 3-18) was also found at the neuron level.

In Arch-transfected mice, we recorded from preBötC neurons during unilateral photoinhibition (Figure 3-30a; n = 12), finding 7 respiratory-modulated neurons (2 pre-I neurons, 2 inspiratory neurons, 1 post-I (or early-E) neuron, and 1 expiratory neuron) (Figure 6d) and 5 tonic neurons. Unilateral photoinhibition generated shifts in the respiratory cycle, comparable to that observed during bilateral photoinhibition, although unilateral light did not alter peak inspiratory airflow. During photoinhibition, preBötC neurons, and consequently the preBötC network, exhibit a shorter interburst interval between inspiratory bursts. We did not find any neurons that increased their firing during delivery of light pulses and in particular, pre-inspiratory and inspiratory-modulated neurons did not show any alterations in their firing patterns that might

account for the augmented inspirations. We also found 2 tonic neurons that were silenced in response to light from a baseline firing rate of ~16 Hz (Figure 3-30b, top). Following a 1 s light pulse, this neuron exhibited a characteristic rebound firing rate lasting approximately 250 ms. The remaining neurons did not change their firing pattern or phase relationship to breathing during photoinhibition.

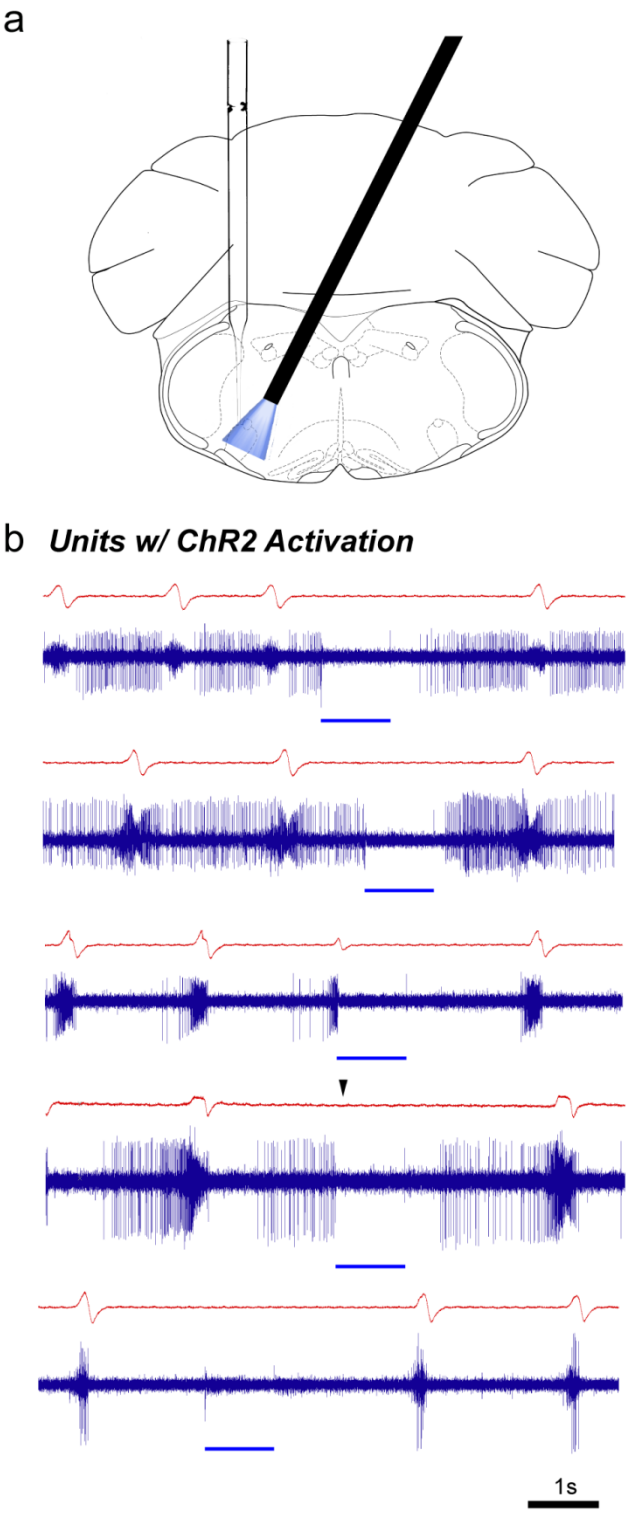

Figure 3-29 Unit recording during photostimulation of ChR2-expressing GlyT2 preBötC neurons reveals direct actions on preBötC rhythm generator. (**a**) Schematic representation

showing cannulae implantation at a 27° angle and recording electrode placement to record from units within the cone of blue (473 nm) light. (**b**) During 1s continuous laser pulse, photostimulation of ChR2-expressing GlyT2 preBötC neurons strongly inhibits respiratory-modulated neurons. Laser pulses indicated with a blue line. Scale bar: 1s.

a

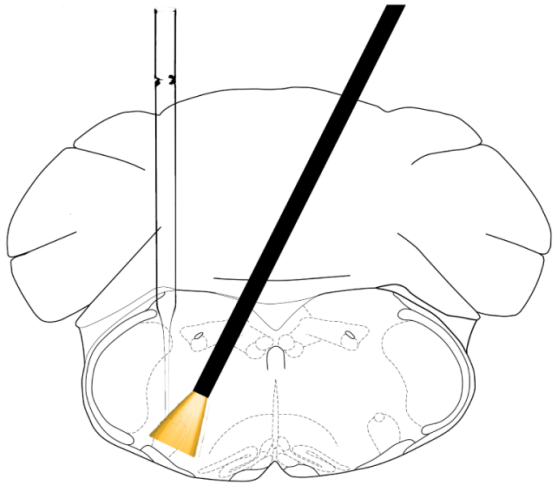

b ***Units w/ Arch Activation***

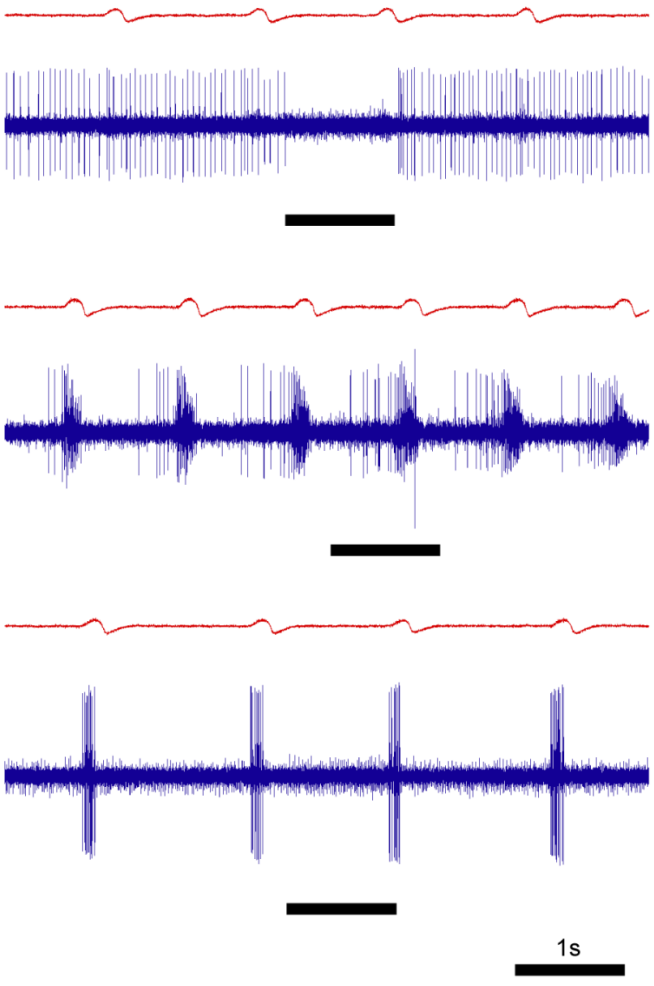

Figure 3-30 Unit recording during photoinhibition of Arch-expressing GlyT2 preBötC neurons. (**a**) Schematic representation showing cannulae implantation at a 27° angle and recording electrode placement to record from units within the cone of orange (593 nm) light. (**b**) Response of preBötC neurons to photoinhibition of Arch-expressing GlyT2 preBötC neurons with 1 s continuous laser pulse. Laser pulses indicated with a blue line. Scale bar: 1 s.

DISCUSSION

Inhibition is an essential element of most neural circuits in the mammalian nervous system. While inhibitory neurons are present in the preBötC and can fire in phase with inspiration[3, 9], their functional role in the generation of respiratory rhythm and pattern is not well understood. While at least a subset of preBötC excitatory neurons are critical for rhythmogenesis[1, 20], there are differing opinions as to the contribution of inhibitory neurons to rhythmogenesis, if any, and/or regulation of breathing pattern[8, 21]. Strong post-inspiratory inhibitory currents are observed in intracellular recordings of preBötC neurons[22], which suggests that inhibition within the respiratory network may contribute to inspiratory burst termination. While the preBötC may function in the absence of inhibition[8, 23], a growing body of evidence suggests inhibitory modulation plays important roles in the dynamics of the preBötC[22]. By making temporally-precise brief bilateral perturbations of GlyT2 preBötC neurons, we probed their role in generation of respiratory pattern in spontaneously breathing adult mice.

Our injection sites were centered on the preBötC with a few GlyT2 neuronal somas transfected rostrally including in the BötC, which also contains substantial numbers of respiratory-modulated inhibitory neurons[24-26], and dorsally in the adjacent reticular formation. Peak densities of transfected neurons overlapped with the distribution of SST neurons relative to the caudal boundary of the facial nucleus, indicating that we successfully hit the preBötC. Optical cannulae were placed 200 – 400 µm dorsal to the caudal end of the preBötC to limit the light path to mainly target the preBötC and avoid the few transfected neurons in the more rostral BötC. We assert that the combined spatial specificity from the virus injection and the cannulae placement ensured that the pool of transfected neurons able to affect the burst in response to light was predominantly GlyT2 preBötC neurons.

We utilized a genetics-based strategy for restricting protein expression to inhibitory preBötC neurons. This approach combined injections of cre-dependent viruses into transgenic

mice having the gene Cre recombinase under the regulation of the GlyT2 promoter, which resulted in cell-specific expression via a cre-mediated recombination occurring only in $GlyT2^{+}$, i.e., glycinergic, neurons. To verify this, we examined the overlap of transfected neurons with known markers of excitatory or inhibitory neurons. We found that transfected neurons rarely colocalize SST, which demarcates a subset of excitatory preBötC neurons and strongly colocalize with glycine immunoreactivity, which identifies glycinergic neurons.

Opsins are not localized to any one domain of the neuron (including expression in its synaptic terminals), so there is the possibility that light affected some synaptic terminals in the preBötC that originated from transfected somas located outside of its boundaries. We decided to utilize a virus-mediated recombination, as opposed to a transgenic, and consequently global, approach, since this greatly reduced this complication by limiting cre recombination to the local injection site. By aiming caudal of the preBötC with our injection, we avoided most BötC neurons, which would be the most likely source of non-preBötC inhibitory terminals within the vicinity of the virus injection. To an extent, the possibility of affecting non-preBötC opsin-expressing terminals reflects a limitation of the GlyT2 promoter that cannot be overcome without the identification of better, i.e., exclusive to GlyT2 preBötC neurons, cellular markers and more advanced intersectional targeting strategies to better restrict expression. Thus, within the limits of present technology, we have targeted GlyT2 preBötC neurons and expect that behavioral changes resulting from photostimulation or photoinhibition reflect alterations in the firing of these neurons and/or in stimulating/inhibiting direct release from their terminals.

Brief photoinhibition of Arch-expressing GlyT2 preBötC neurons, when delivered during the preinspiratory or inspiratory phases, produced significantly larger breaths. Thus, at least a subset of transfected GlyT2 neurons is endogenously active during (pre-)inspiration and can affect respiratory pattern. In support of this, we found units that were spontaneously active and were silenced during photoinhibition. When photoinhibition occurred during the preinspiratory

phase, there was an advancement of the respiratory cycle, i.e., expiratory duration shortened, indicating that silencing these neurons can alter respiratory timing. We expect that the withdrawal of inhibition allows preBötC activity to initiate earlier and/or spread through the network more rapidly, resulting in an inspiratory burst being triggered sooner than it otherwise would be.

Brief photostimulation of ChR2-expressing GlyT2 preBötC neurons when delivered during the inspiratory phase prematurely terminated inspiration, i.e., shorter inspiratory durations and smaller peak inspiratory airflows. Photostimulation during expiration, including the preinspiratory phase, significantly delayed the subsequent inspiration. In response to longer stimuli, this effect was sufficiently strong to produce apnea in anesthetized or awake behaving mice, as well as during hypoxic and hypercapnic challenges. We found that respiration resumed with a consistent latency after the laser shut off regardless of the phase of photostimulation, which indicates that activation of GlyT2 preBötC neurons can reset the respiratory cycle. At the neuron level, activation of GlyT2 preBötC neurons inhibits other respiratory-modulated preBötC neurons. We found 7 (pre-)inspiratory-modulated neurons in total and all were silenced by ChR2 activation, at any point in the respiratory cycle. Silencing preinspiratory neurons prior to the start of inspiration resulted in typical preinspiratory spiking activity that was not followed by an inspiratory burst. This data demonstrate that GlyT2 preBötC neurons can exert profound influence over rhythmogenic preBötC neurons and, when activated, can prematurely terminate an inspiratory burst.

We suggest, based on these observations, that one essential role of preBötC GLYT2 inhibitory neurons is to modulate basic breathing parameters such as peak inspiratory flow, tidal volume, expiratory duration, and respiratory frequency, irrespective of any role in rhythmogenesis *per se*.

Numerous models of central pattern generation focus on inhibition as a key component in the formation of rhythmic behaviors[27-30]; for breathing, inspiratory burst termination and/or phase transitions are often postulated to be mediated by postsynaptic actions of inhibitory neurons[31-33]. The most recent models, molded by a slightly more refined but nonetheless coarse understanding of the underlying neuroanatomy, theorize that interactions between excitatory preBötC neurons and inhibitory subpopulations within the preBötC and BötC generate respiratory rhythm[21]. However, while profound changes in breathing result from slow or relatively rapid onset perturbations to excitatory preBötC subpopulations[1, 5],a normal respiratory rhythm persists in anesthetized adult rats after substantial blockade of inhibitory neurotransmission in preBötC and BötC by local injection of inhibitory antagonists[8]. Here, we further refine our understanding of the role of inhibitory neurons in the preBötC by using fast onset and relatively brief perturbations, sufficient to construct phase-response curves and see effects on respiratory output within milliseconds of the stimulus onset.

Photoinhibition of GlyT2 preBötC neurons increased respiratory drive, producing larger breaths at a higher frequency. Thus, the preBötC *in vivo* with significantly diminished GlyT2 preBötC neuronal activity but otherwise fully intact, continued to generate a eupneic breathing rhythm. In Arch-transfected mice, photoinhibition produced no change in (pre)inspiratory-modulated preBötC neurons activity, indicative of an absence of Arch expression in these presumptively excitatory neurons, and a powerful effect of preinspiratory glycinergic inhibition. Since we did not observe increased activity in (pre)inspiratory neurons, we suggest that the increased respiratory drive results from an increase in the total number of active neurons, not the number of spikes *per se*.

We did not observe any breakdown in eupneic breathing when silencing a substantial subset of the GlyT2 preBötC neurons, though we clearly reduced ongoing activity in GlyT2 neurons. From this experiment alone, we recognize the possibility that we did not affect enough

of the inhibitory preBötC population to disrupt rhythmogenesis. However, rhythm persists after blocking all inhibitory neurotransmission within the preBötC in adult rats regardless of whether the source was preBötC GlyT2 neurons and/or other inhibitory neurons with terminals in the preBötC[8]. Our data are consistent with this result. Taken together, the failure to stop or destabilize respiratory rhythm after silencing GlyT2 preBötC neurons reflects a modulatory, but non-rhythmogenic, role for these neurons.

Many vital, complex oropharyngeal movements require precisely timed apneas, e.g., swallowing, vocalization, suckling, and chewing, and there are many powerful reflex apneas, such as the Breuer-Hering inflation reflex or following superior laryngeal nerve activation[34-36] that can be triggered by tracheal obstruction. We hypothesized that inhibitory neurons play an important role in the generation of central apneas[8]. In support of this hypothesis and refining the experimental protocol to exclusively target preBötC inhibitory neurons, we found that photostimulation of preBötC GlyT2 neurons at any point in the respiratory cycle can produce apnea. Moreover, photoinhibition can counteract a reflex-induced apnea generated by the Breuer-Hering lung inflation reflex. That breathing was rescued from an apneic state by silencing GlyT2 preBötC neurons is consistent with prior work showing the respiratory rhythm persists after blockade of inhibitory neurotransmission.

CHAPTER IV

Methods

Methods for Identification of Reelin as a preBötC Marker

Medullary slice preparation

All experiments on animals were carried out with the approval of the UCLA Institutional Animal Care and Use Committee. The preparation of a medullary slice that retains functional respiratory networks and generates respiratory rhythm has been described previously[1]. Briefly, C57Bl6 neonatal mice of either sex aged P1–P5 were anesthetized, and the brainstem was isolated with care to preserve the XII nerve roots, followed by removal of the cerebellum. The brainstem was pinned down on a paraffin-coated block with the ventral surface upward, and the block was mounted in a Vibratome (VT1000S; Technical Products International, St. Louis, MO). The brainstem was sectioned (slice thickness 500–600 µm) serially in the transverse plane starting from the rostral medulla to the rostral boundary of the preBötC. One transverse slice, in which XII was included, was transferred to a recording chamber. The slice was perfused in an artificial cerebrospinal fluid (ACSF) containing (in mM) 128 NaCl, 3.0 KCl, 1.5 $CaCl_2$, 1.0 $MgSO_4$, 23.5 $NaHCO_3$, 0.5 NaH_2PO_4, and 30 glucose, with increased KCl (9 mM) to stimulate the spontaneous rhythmic respiratory motor discharge.

Electrophysiological recording and intracellular mRNA aspiration

Respiratory-related nerve activity was recorded from XII nerve roots with a suction electrode. Patch electrodes were pulled from thick-wall borosilicate glass with a tip size of 1–1.5 µm (resistance 4–6.5 MΩ). The electrode filling solution was prepared with DEPC-treated water and contained (in mM) 140 potassium gluconate, 5.0 NaCl, 0.1 $CaCl_2$, 1.1 EGTA, 2.0 ATP (Mg^{2+} salt), and 1 U/µl RNasin (Ambion, Austin, TX). The whole-cell patch recordings were obtained from the inspiratory neurons that fired in phase with the inspiratory burst from the XII nerve and localized ventrolaterally to the nucleus ambiguous. The intracellular components of

inspiratory neurons were carefully aspirated into the tip of electrode pipette via gently applying a suitable negative pressure under Gigaohm seal condition and were visualized with infrared-differential interference contrast (IR-DIC) microscopy (×400, Axioskop; Carl Zeiss, Heidenheim, Germany). The mRNAs obtained from nucleus ambiguous neurons in the same way as described above were used to synthesize the control cDNAs for subtractive hybridization.

cDNA amplification and single-cell subtractive library construction

Single-cell cDNA amplification was based on methods previously reported.[98] Briefly, the glass pipette tips were immediately broken in 4 µl of ice-cold cell lysis buffer (in mM: 50 Tris-HCl, pH 8.3, 75 KCl, 3 $MgCl_2$, 0.5% NP-40) containing 80 ng/ml oligo-d(T) 12– 16 (Promega, Madison, WI), 1 U/µl RNasin (Ambion, Austin, TX), and 10 µM each of dATP, dCTP, dGTP, and dTTP (Promega, Madison, WI). The lysis buffer with pipette tips was incubated at 65°C for 1 min, followed by addition of 10 U transcriptase (Qiagen, Valencia, CA) and incubation at 37°C for 30 min. The samples were heated at 65°C for 10 min. Poly(A) was tailed to the first-strand cDNA product by adding 4 µl of tailing solution containing 10 U terminal transferase (Promega, Madison, WI), 200 mM potassium cacodylate (pH 7.2), 4 mM $CoCl_2$, 0.4 mM DTT, and 200 µM dATP at 37°C for 15 min. Samples were heat inactivated again at 65°C for 10 min.

The cDNAs were amplified by a specific anchor primer (5′-TTTTTTTTTTTTTTT-3′) via PCR. PCR was carried out using 0.5 U Pfx and 0.25 U Taq (Invitrogen, Carlsbad, CA) DNA polymerase. Biotin-dCTP was incorporated into PCR during the amplification of cDNAs from ambiguous neurons. The cDNA fragments were used to construct a subtractive library after removal of those of length less than 500 base pairs and subtraction from ambiguous neuronal cDNAs. The remaining cDNAs were used to construct a cDNA library using SMART cDNA library construction kit based on the manufacturer's instruction (Clontech, Mountain View, CA). About 3,500 individual colonies were obtained, and most of them contained inspiratory neuronal cDNA fragments of over 500 base pairs (data not shown). The second round of hybridization

was performed using biotin-labeled ambiguous neuron cDNAs prepared as described above as probes to decrease the background further. The negative clones were picked up and identified by sequencing.

Immunohistochemistry and antibody characterization

The expression patterns of the candidates (Table 1) in the preBötC area were confirmed by immunohistochemistry in adult male Sprague Dawley rats, when an antibody was available, or in situ hybridization in adult mouse brainstem. Table 2 provides a list of all antibodies used in the present study.

Table 2. Antibodies Used for Immunohistochemistry in Reelin study

Antibody	Source	Immunogen	Dilution
Choline acetyltransferase (ChAT)	Chemicon, AB144 goat polyclonal	Human placental ChAT	1:500
Neurokinin 1 receptor (NK1R)	Advanced Targeting Systems, AB-N04, rabbit polyclonal	synthetic peptide corresponding to 393-407 amino acid sequence of NK1R sequence at the C-terminus of dog NK-1 receptor	1:500
Reelin	Millipore, MAB5364, mouse monoclonal	Recombinant *reelin* amino acids 164-496	1:500
Somatostatin (SST)	Peninsula Labs, T4103, rabbit polyclonal	H-Ala-Gly-Cys-Lys-Asn-Phe-Phe-Trp-Lys-Thr-Phe-Thr-Ser-Cys-OH	1:500
Tyrosine Hydroxylase (TH)	Aves, F1005, chicken polyclonal	synthetic peptides corresponding to different regions of the Tyrosine Hydroxylase gene product, but were shared between the human (P07101, NCBI) and mouse (P24529, NCBI) sequences	1:500

Antibodies Used in the Present Study

The rabbit polyclonal NK1R antibody was raised in rabbit using a synthetic peptide corresponding to the 393–407- amino-acid sequence of NK1R. The antiserum recognizes the NK1R in rat, mouse, and guinea pig (technical information provided by Advanced Targeting Systems, San Diego, CA). The specificity of the antibody has been previously demonstrated;[99] the antibody labeled exclusively rat kidney epithelial cells, neurons in the dorsal horn of the spinal cord in the regions corresponding to SP inputs (substantia gelatinosa), and neurons and muscle cells in the ileum; Western blot analysis of proteins obtained from rat kidney epithelial cells that expressed functional NK1Rs showed a broad immunoreactive band corresponding to the NK1R (70 to over 150 kDa). The specificity of the antibody has been further confirmed by demonstrating that it colabels exclusively neurons that have internalized fluorescent SP and thus express the NK1R.[100] Labeling with this antibody was abolished following preadsorption of diluted antiserum with the immunogenic amino acid sequence (NK1R 393- 407)[99] and by lack of staining in tissue in which neurons expressing the NK1R were killed using saporin- conjugated SP[101].

The goat polyclonal choline acetyltransferase (ChAT) antibody was prepared against the human placental enzyme. In an immunoblot in mouse NIH/3T3 cell lysates, a single band of the correct molecular weight was identified (manufacturer's technical information). In the brainstem, it stains a pattern that is consistent with previous reports[37].

The rabbit polyclonal somatostatin (SST) antibody was prepared against the first 14 aa of the synthetic peptide SST. The antibody is specific for SST; no cross-reactivity of the antibody with other peptides such as SP, amylin, glucagon, insulin, neuropeptide Y (NPY), or vasoactive intestinal peptide has been reported from immunoblotting according to the manufacturer's instructions.

The mouse monoclonal reelin antibody (IgG1, clone G10) was prepared against the recombinant reelin residues 164–496 derived from mouse E15–E17 embryonic brain[102]. On immunoblots from mouse and rat brain lysates, it recognizes a band representing the reelin peptide at ~388 kDa; it stains the Cajal-Retzius cell layer in the marginal zone in embryonic cerebral cortex at 15 days in utero (manufacturer's technical information).

The chicken polyclonal TH antibody (F1005; Aves Labs, Tigard, OR) was prepared against residues 37–50 (RRQ SLI EDA RKE RE) and against residues 439–454 (SDA KDK LR[N/S] YAS RIQ R) of the human gene product (P07101; NCBI). In the second peptide, there was a mixture of asparagine and serine at position 9 to ensure that the antibodies would recognize both human (serine) and mouse (asparagine) gene products. Immunostaining with this antibody yields staining in the brainstem identical to that with the mouse monoclonal antiserum TH (Millipore, Bedford, MA; MAB5280)[2] in our antibody characterization experiments (data not shown).

For all secondary antibody immunohistochemical controls, the primary antibodies were omitted, and the tissue showed no immunoreactivity above background.

The procedures for immunohistochemistry were described previously[2]. Rats were anesthetized with Nembutal (100 mg kg^{-1}, i.p.; Lundbeck Inc., Deerfield, IL) and perfused transcardially with 4% paraformadehyde in phosphate-buffered saline (PBS; 137 mM NaCl, 2.7 mM KCl, 8.1 mM $Na_2HPO_4 \cdot 2H_2O$, 1.76 mM KH_2PO_4, pH7.4). The brainstem was removed and postfixed in 4% paraformadehyde/PBS overnight at 4°C, followed by cryoprotection overnight in 30% sucrose in PBS. Forty-micrometer-thick transverse or sagittal sections were cut using a cryostat and incubated in the primary antibodies described above, with 10% normal donkey serum for 24 or 48 hours at 4°C. After a series of washes, the primary antibodies were detected by using the specific secondary antibodies (dilution 1:250): rhodamine-conjugated donkey anti-rabbit and rhodamine-conjugated donkey anti-chicken (Jackson Immunoresearch, West Grove,

PA) and Alexa 488-conjugated donkey anti-mouse secondary antibodies (Invitrogen, Calsbad, CA). Sections were then washed, mounted on gelatin-coated slides, and coverslipped.

For reelin DAB staining, the sections were washed in PBS briefly, followed by blocking with 10% donkey serum in PBS with 0.3% triton 100 for 1 hour at room temperature. The primary antibody G10 was incubated with sections overnight at room temperature. The secondary biotinylated donkey anti-mouse (1:1,000; Jackson Immunoresearch) was added to the sections for 2 hours at room temperature after three washes by PBS/Triton 100 solution. The Vectastain ABC reagent (Vector, Burlingame, CA) was added and incubated for 1 hour, and the color was developed using DAB reagent (Vector, Burlingame, CA) after three washes. The sections were stained brown with DAB only or black by adding 0.05% cobalt chloride and 0.01% nickel ammonium sulfate to the DAB solution. The tissue was mounted on gelatin-coated slides, dehydrated in graded ethanols, cleared in xylenes, and coverslipped.

Brainstem sections were grouped as one-in-six of sequential series of 40-µm transverse sections; six groups of brainstem sections were collected from each rat, and immunohistochemistry was performed using the following three groups of primary antibodies: SST/reelin, NK1R/reelin, TH/reelin. Images were acquired by confocal laser scanning microscopy (LSM510 Meta; Carl Zeiss, Heidenheim, Germany). For Alexa 488, excitation (argon, 1 mV) was set to 488 nm, and emissions were gathered with a 500–530-nm bandpass filter. For rhodamine fluorescence, excitation (HeNe, 1 mV) was set to 543 nm, and emissions were gathered with a 560–615-nm bandpass filter. For experiments involving FG, images were taken with an epifluorescence microscope using a mercury arc lamp (Axioplan 2; Carl Zeiss, Heidenheim, Germany). Z-stack images were acquired at ×20 or ×40 magnification, and images were exported to Adobe Illustrator (Adobe, San Jose, CA) for figure composition. The images were cropped into suitable sizes without any other type of modification, such as contrast or brightness. Three different ages of rats, 4 weeks (n = 4), 8 weeks (n = 5), and 24 weeks (n = 4),

were used for cell counting experiments. Briefly, sagittal sections from one hemisphere of brainstem of each rat were obtained and incubated with reelin G10 antibody, followed by the diaminobenzidine (DAB) staining procedure as described above. Sagittal sections containing preBötC area (usually three sections) from one hemisphere of the brainstem were set as one group. Mosaic images of whole sagittal sections were acquired by brightfield light microscopy (Axioplan 2; Carl Zeiss, Heidenheim, Germany) using AxioVision software (Carl Zeiss, Heidenheim, Germany). During cell counting, each image of one sagittal section was divided along the rostral–caudal axis into an array of columns running dorsal to ventral with exactly 100 μm spanning width. Each column's position relative to Bregma was determined by its distance to the caudal edge of the VII motor nucleus, e.g., Bregma −11.7 mm based on the rat atlas of Paxinos and Watson. Reelin-positive neurons in the DFG and ventrolateral medulla in every column of the section were counted. The reelin neurons from all columns in the same Bregma level were set as one group, and data are presented as mean ± SD.

In situ hybridization

Male mice aged 6–8 weeks were used for the experiments. The mice were anesthetized by isoflurane and decapitated. The brainstems were rapidly removed and frozen in methybulton in dry ice. Brainstems were stored at −80°C until sectioning. The coronal sections were cut at 12 μm thickness, mounted on gelatin-coated slides, and kept at −80°C until the day of the experiment.

The PCR fragments with 5′ flanking T7 promoter sequence and 3′ flanking T3 promoter sequence were used to synthesize ^{35}S-radiolabeled RNA probes. The RNA probes were transcribed following standard protocols[103]. Briefly, 400 ng of PCR fragments was used for 20 μl synthesis mixture containing 10 μM UTP; 2.5 μM ^{35}S-UTP (1,000 Ci/mmol); 10 μM each of ATP, CTP, and GTP; 5 mM of dithiothreitol; 20 U superRNAsin (Ambion, Austin, TX); and 10 U T7 or

T3 RNA polymerase (Promega, Madison, WI). The probes were extracted in phenol/ chloroform/isoamyl alcohol and precipitated overnight in ethanol at −80°C. All the solutions and buffers were prepared with 0.1% diethylpyrocarbonate (DEPC)-treated distilled water. Sections were removed from −80°C and completely dried on dry ice under a stream of cool air. Sections were postfixed by 3% paraformaldehyde containing 0.02% DEPC, acetylated, and dehydrated. Then, 3–6 ng of probe (4 million dpm/ng) in hybridization mixture was applied to each section. Hybridizations were carried out at 50°C for 12–14 hours in humid chambers. Posthybridization washes included three times in 50% formamide in 2× SSC (0.3 M NaCl/0.03 M sodium citrate) at 52°C for 30 min, followed by a 30-min incubation of RNase A (100 µg /ml; Promega, Madison, WI) at 37°C and an overnight rinse in 2× SSC with 0.05% Triton X-100. The sections were then dehydrated through graded ethanols and xylenes and dried in the air. The sections were first exposed to BioMax X-film (Kodak, Rochester, NY) for 1 week and subsequently dipped into Kodak NTB3 emulsion (Kodak, Rochester, NY) and exposed for 10–30 days. Sections were developed in D19 (3.5 minutes) fixed in Kodak fixative (5 minutes), counterstained by hemotoxylin-eosin, and mounted with Eukitt (Electron Microscopy Sciences, Hatfield, PA). The sections were examined under light- and darkfield microscopy.

Plethysmograph recording and data analysis

Reeler mice and their littermates were kindly provided by Prof. P. Phelps of the University of California, Los Angeles. Adult male mice aged 6–8 weeks were recorded using a whole-body mouse plethysmograph (Buxco Research Systems, Sharon, CT). The signal from the plethysmograph corresponds to changes in tidal volume. While in the plethysmograph, the mouse could move freely, with access to water and chow. Reeler mice and their littermates were studied for 4 hours in the plethysmograph. For hypoxia and hypercapnia challenges, the

mice were challenged for 5 min with 8% O_2 or 5% CO_2, respectively, and data were collected from the final 30 seconds of the challenge.

Surgical procedure for tracing bulbospinal neurons

For spinal injections under ketamine anesthesia (50 mg/kg, Ketaject; Phoenix Pharmaceuticals, St. Joseph, MO), a hole was drilled into the C4 vertebrae and a fine glass pipette containing FG (5%; Fluorochrome, Denver, CO) was lowered into the ventral horn based on the rat atlas of Paxinos and Watson. A 100-nl solution containing the tracer was injected by an air pressure system. After 5 additional minutes, the pipette was slowly withdrawn, and the incision was sutured with absorbable sutures for inner muscles and nonabsorbable nylon sutures for the skin. Animals survived for 7 days.

Methods for Optogenetic Targeting and Recording

Animals

Animal use was in accordance with the guidelines approved by the UCLA Institutional Animal Care and Use Committee. All experiments were done on adult male GlyT2-Cre mice (24-30 g; average post-surgery duration of ~30 days) that were 10-14 weeks of age at the time of AAV injection. The GlyT2-Cre mice were kindly provided by H.U. Zeilhofer, University of Zurich, Switzerland. Preliminary studies were conducted in transgenic GlyT2-ChR2 and GlyT2-Arch mice, generated by crossing GlyT2-Cre mice with transgenic lines containing a floxed conditional expression cassette containing either ChR2-tdTomato or Arch-GFP.

Viral vector design

The viral constructs *AAV2/1-Ef1α-DIO-ChR2-eYFP* (Addgene plasmid 20298; provided by K. Deisseroth, Stanford University, Palo Alto, CA)[87] and *AAV2/1-flex-CBA-Arch-GFP* (Penn Vector P2432; provided by E. Boyden, Massachusetts Institute of Technology, Cambridge, MA)[47] were produced by the University of Pennsylvania Gene Therapy Program Vector Core. We used a ChR2 variant with the H134R mutation, which produces a twofold increase in the steady-state current as compared to the wildtype variant of ChR2[104, 105].

Microinjection

Mice were anesthetized with isoflurane (4% for induction and 2% for maintenance) and placed in a stereotaxic apparatus (David Kopf Instruments) with Bregma and Lambda skull landmarks level. Two holes were drilled in the skull at predefined coordinates relative to Bregma, and then 50-100 nl of virus solution (ChR2: 5-10 x 10^{12} GC/ml; Arch: 6-10 x 10^{12} GC/ml) per side was injected into the preBötC through a glass pipette connected to a pressure

ejection system (Picospritzer II; Parker Hannafin). Injections were made 6.80 mm caudal to Bregma, 1.2 mm lateral to the midline, and 4.65 mm ventral from the dorsal surface of the brain. Coordinates were determined from microinjections (n = 7) of red fluorescent microspheres (1.0 µm diameter, 5% solution; Invitrogen) into calculated coordinates based on a mouse brain atlas[106] and adjusted based on the distance from preBötC, as determined by the location of SST immunoreactive neurons[3]. The pipette was left in place for 5 min after injection to minimize backflow. The wound was closed with 5-0 non-absorbable sutures. The mice were returned to their home cage and allowed 2-3 weeks to recover that allowed for sufficient levels of protein to express. For controls, negative littermates (those not expressing Cre recombinase) received virus injections as described above; as expected, there was no virus expression.

Implantation of fiber optics

Mice were placed into the stereotaxic frame and fiber-optic cannulae with a 1.25 mm stainless steel ferrule (200 µm fiber; Doric Lenses), held by a stereotaxic adaptor (Doric Lenses), were implanted bilaterally to a depth 200-400 µm dorsal to the preBötC, based on predetermined coordinates. The cannulae were glued to the skull using Metabond™ (Parkell) and the wound was sealed by applying a layer of clear dental acrylic (Lang Dental).

Photostimulation and photoinhibition

Branching optical fibers (200 µm fiber; Doric Lenses) with 1.25 mm stainless steel ferrules as ends were connected to the implanted cannulae via plastic sleeves. The back end of the fiber was connected to a 473nm/593nm double wavelength laser (OptoDuet Laser; IkeCool) via an optical rotary joint (Doric Lenses). Light pulses were controlled by a pulse generator (Pulsemaster A300 Generator; WPI). Anesthetized mice were placed on a heating pad in front of a nose cone connected to a flowmeter (GM Instruments) to record airflow measurements

during photostimulation. Awake mice were placed in a plethysmograph chamber (Buxco) connected to a pressure transducer (F.W. Kirk Company) with the optical fibers exiting the chamber through a small hole.

Breuer-Hering inflation reflex (BHIR)

The BHIR was induced in anesthetized Arch transfected mice (FLEX-Arch) by inflating the lungs with continuous positive airway pressure (CPAP). The pressure was adjusted to yield an apnea that lasted for ~10 - 15s (~4 cm H_2O) before being "broken" by breaths reappearing despite the CPAP. We applied one control period of CPAP, waited for 30-60s, and then applied a second period of CPAP combined with a 1s pulse of light (593nm) delivered bilaterally into the preBötC. We measured both the amount of time it took for breathing to resume relative to the start of the reflex and the onset of the laser pulse.

Single-unit recording

To record neuronal activity, transfected mice were placed in the stereotaxic frame as described above. An optical cannula was implanted at a 27° angle from vertical, tilted across the midline from right to left, down to preBötC and glued to the skull with Metabond (Parkell). A window was drilled through the skull of sufficient size to allow the recording electrode free range of movement to record on the left side of the brain. Respiratory-modulated units were found 4.6 to 4.9 mm below the cerebellar surface and 1.1 to 1.3 mm lateral to the midline. A glass electrode (~3 µm inner tip diameter; filled with aCSF containing (in mM) 124 NaCl, 3 KCl, 1.5 $CaCl_2$, 1 $MgSO_4$, 25 $NaHCO_3$, 0.5 NaH_2PO_4, and 30 D-glucose) was connected to a headstage (Siskiyou) and the signal amplified (Grass Model P511; Grass Instruments) and sampled at 20 kHz (PowerLab 16SP; ADInstruments). Due to a laser artifact apparent at the start and end of

laser pulses, we used a single 1 s pulse for photostimulation to reduce noise. Most neural recordings were stable for 5 - 10 min.

Immunohistochemistry

After the completion of the experiment, mice were deeply anesthetized with pentobarbital and perfused transcardially with saline followed by 4% paraformaldehyde in phosphate-buffered saline (PBS). Brains were removed, postfixed overnight at 4°C, and cryoprotected in 30% sucrose in PBS for 24-48 h before sectioning. Free-floating coronal or sagittal sections (40 µm) were cut using a cryostat (CryoStar NX70, Leica Microsystems) in two series and stored at 4°C until further processing. Sections were incubated with primary antibodies in PBS containing 0.3% Triton X-100 (PBT) overnight at room temperature. After 3 washes, sections were incubated in species-appropriate secondary antibodies in PBS for 4h at room temperature. After 3 washes, sections were mounted onto gelatin-coated glass slides, dehydrated in graded alcohols, cleared in Xylenes, and coverslipped. Fluorescence was visualized with a confocal laser scanning microscope (LSM710; Carl Zeiss). Images were acquired with Zen software (Carl Zeiss), exported as TIFF files, and arranged to prepare figures in Adobe Photoshop and Illustrator (Adobe).

We used the following primary antibodies: rabbit polyclonal anti-somatostatin-14 (1:500; Peninsula Laboratories), mouse monoclonal anti-NeuN (1:500; Millipore), chicken polyclonal anti-GFP (1:500; Aves Labs), and rabbit polyclonal anti-glycine (low-glutaraldehyde; 1:167; Millipore). Rhodamine Red-X donkey anti-rabbit, DyLight488 donkey anti-chicken, and Cy5 donkey anti-mouse conjugated secondary antibodies (1:250; Jackson ImmunoResearch) were used to detect primary antibodies.

Table 3. Antibodies Used for Immunohistochemistry in Optogenetics study

Antibody	Source	Immunogen	Dilution
Green Fluorescent Protein (GFP)	Millipore, GFP-1020 chicken polyclonal	Recombinant GFP protein	1:500
Glycine (low glutaraldehyde)	Millipore, AB5020, rabbit polyclonal	Glycine-glutaraldehyde-BSA	1:167
Neuronal Nuclei (NeuN)	Millipore, MAB377, mouse monoclonal	Purified cell nuclei from mouse brain	1:500
Somatostatin (SST)	Peninsula Labs, T4103, rabbit polyclonal	H-Ala-Gly-Cys-Lys-Asn-Phe-Phe-Trp-Lys-Thr-Phe-Thr-Ser-Cys-OH	1:500

Data analysis and statistics

Traces were recorded on a 64-bit computer using LabChart 7 Pro (ADInstruments). The airflow signal was high-pass filtered (>0.1 Hz) to eliminate DC shifts and slow drifts, and used to calculate respiratory frequency, period, inspiratory (T_I) and expiratory (T_E) durations. The airflow signal was integrated to compute tidal volume (V_T).

Cell counts were performed on 3 sequential sagittal sections as defined by the localization of SST-immunoreactive neurons and soma distances relative to the caudal boundary of the facial motor nucleus were calculated. Counts were performed with ImageJ (http://rsb.info.nih.gov/ij/) and exported to Igor (Wavemetrics) for analysis with custom software.

All statistics were performed in Igor (Wavemetrics). Statistical significance was set at $P < 0.05$. Unpaired t-tests and one way ANOVAs were used as required. Pair-wise comparisons were performed using a Tukey's HSD test. All values are presented as mean ± SEM.

Phase response analysis

The photostimulation-evoked reset of the respiratory rhythm was studied by applying a single 100 ms light pulse at various times spanning the respiratory cycle. The control respiratory period for each photostimulation-affected breath was defined as spanning 0-360°, calculated based on the duration of the previous cycle. Across experiments, inspiration (defined as the period of inward airflow) lasted from onset at 0° until 71.8 ± 11.6° (n = 5) in ChR2 experiments and until 77.9 ± 7.1° (n = 7) for Arch experiments; expiration was defined as the remainder of the cycle. Thus, the phase of any event could be calculated based on the time at which it occurred relative to the preceding inspiratory onset and referenced to the preceding control period. More specifically, phase values were obtained by calculating the ratio of the event onset time to the respiratory period and multiplying by 360°.

Stimulus phase, induced phase, and the expected phase of respiration were computed[37, 107] and plotted using software written in Igor (Wavemetrics). Stimulus phase, i.e., the time at which stimulation was delivered during the ongoing respiratory cycle, was calculated based on the delay from the beginning of the previous inspiration to the onset of stimulus delivery.

GENERAL SUMMARY

(1) AAV-mediated in vivo gene delivery. We found AAV2/1 efficiently delivers genes into the preBötC in adult mice with low cytotoxicity. We employed an intersectional strategy whereby a cre-dependent recombination was required in order for protein expression to occur. By making microinjections of cre-dependent viral vectors into transgenic mice that expressed cre recombinase under the GlyT2 promoter, we can ensure that expression was truly restricted to our target neuron type, i.e., those neurons defined by an active GlyT2 promoter and presumed glycinergic. After recombination, constitutive promoters encoded in either virus – Ef1α or CBA – provided high levels of protein expression in transfected neurons, which was readily visualized *post hoc* by a fluorescent protein tag. In both sets of experiments, transfected neurons colocalized with glycine immunoreactivity and largely overlapped with the preBötC region, as defined by the distribution of SST^+ preBötC neurons. There were some transfected neurons rostrally in the Bötzinger Complex and some dorsally spreading into the reticular formation; however, based on the distribution of transfected neurons and placement of fiber optics, the pool of light-responsive neurons available to affect a given breath was largely GlyT2 preBötC neurons.

(2) *Perturbing glycinergic preBötC neuronal activity alters inspiratory pattern in vivo.* In this study, we employed optogenetics to rapidly alter the excitability of GlyT2 preBötC neurons, using Channelrhodopsin-2 (ChR2) expression to activate GlyT2 neurons and Archaerhodopsin (Arch) to silence GlyT2 neurons. We express either ChR2 or Arch in GlyT2 preBötC neurons so that by delivering light into the brainstem via chronically implanted, bilateral fiber optics, we were able to rapidly alter the state of the respiratory network and measure changes in respiration. In anesthetized mice, brief photostimulation of ChR2-expressing preBötC neurons truncated inspiratory airflow and shortened inspiratory duration when applied during inspiration and delayed the onset of the subsequent breath when applied during the expiratory period. Longer

photostimulations resulted in apneas that persisted until after the laser had turned off. Interestingly, we observed that post-apnea, breathing rebounded with a constant delay, indicative of a phase reset in the rhythm generator. Awake, behaving mice exhibited similar apneas in response to photostimulation when breathing room air, or during hypoxic or hypercapnic respiratory challenges. Unit recordings of preBötC neurons confirm that these apneas are manifesting directly in the preBötC. Activating ChR2-expressing GlyT2 preBötC neurons with 1 s photostimulation rapidly silences neuronal firing in recorded pre-I neurons at any stage of the respiratory cycle.

Brief photoinhibition of Arch-expressing GlyT2 preBötC neurons resulted in augmented peak inspiratory airflows when delivered during inspiration and shortened latencies until the next inspiration when delivered during expiration. As this loss-of-function test eliminates an endogenous, and active, component of the respiratory network, this experiment more closely tests the network in its normal physiological state. There was no observed change in the duration of inspiration which makes it unlikely that these neurons are contributing to burst termination. We found alterations in the neuronal firing of the preBötC during light-induced shifts in the rhythm that could underlie this change in behavioral phenotype. Due to its light-responsiveness, one of the recorded neuron is presumed to be glycinergic and its silencing during photoinhibition confirms the effectiveness of Arch as a tool in the study of this microcircuit. In addition, the complete cessation of activity from Arch-expressing preBötC neurons suggests that the network can truly operate to produce eupneic breathing without these neurons functioning.

While *post hoc* examination of the brains shows injection sites hitting the preBötC and transfected neurons tagged with a fluorescent protein, we cannot know with certainty which transfected neurons were active and positioned to affect the growth of preBötC activity. Although we may not be affecting 100% of the GlyT2 preBötC population, the virus injections

broadly cover the preBötC and the chosen AAV serotype (AAV2/1) has a high transfection efficiency making it likely that our targeting and coverage of the GlyT2 population was sufficient to see a behavioral phenotype. Contrary to several models claiming that inhibitory neurons are obligatory for rhythmogenesis, silencing these neurons in the intact animal did not produce apneas, as was found in prior studies when other subsets of preBötC neurons, i.e., SST-expressing preBötC neurons, are silenced in adult rats[2]. During prolonged photoinhibition, there was actually an increase in breathing frequency. In fact, when we induced apneas by triggering a Breuer-Hering lung inflation reflex, photoinhibition of GlyT2 preBötC neurons during the apnea rescued breathing. Our results suggest that these neurons play an active, but largely modulatory, role in rhythm generation. This corroborates prior *in vitro* and *in vivo* work that demonstrated blockade of inhibitory neurotransmitters does not abolish the respiratory rhythm[20, 21]. However, our present study with Arch furthers this result by specifically showing that the absence of neurotransmission from GlyT2 preBötC neurons alone, excluding non-preBötC sources of inhibition, is still permissive for a eupneic breathing pattern. Evidence is lacking to support the idea that GlyT2 preBötC neurons are critical for breathing and models reliant on such neurons may need revisiting in light of this work. Though we cannot exclude the possibility that under different conditions, particularly reduced, i.e., slice or *en bloc*, preparations, these neurons may play a more substantial role in shaping respiratory output, our results indicate that in the spontaneously breathing, intact mouse, these neurons are not obligatory for generating respiratory rhythm.

(3) *Identification of novel marker for preBötC neurons.* We identified a novel marker, the reelin protein that labels a subset of preBötC neurons partially overlapping with known $NK1R^+$ and SST^+ subpopulations. We conducted a subtractive genetic screen of inspiratory-modulated preBötC neurons by single-cell cDNA amplification from the aspirated contents of recorded inspiratory-modulated neurons *in vitro*. Within the respiratory network, we found that reelin

demarcates the preBötC as well as the premotor neurons of the rostral ventral respiratory group (rVRG). While we did not determine whether all reelin neurons are respiratory-related, their strong overlap with known markers and localization to the respiratory network suggests a close relationship with rhythmogenesis. Reelin neurons are also found in several areas adjacent to motoneuron pools, i.e. ventrolateral to the hypoglossal nucleus (parahypoglossal), dorsal to the facial nucleus (parafacial), and dorsal to the trigeminal nucleus (paratrigeminal). Although reelin is found in premotor neurons within the spinal cord, we do know whether these brainstem reelin populations are premotor neurons or whether they are respiratory-related. Although we do not know how reelin functions within the preBötC, the presence of this marker confined to only a few areas that are all linked to respiratory (and autonomic) function is interesting and warrants further investigation.

BIBLIOGRAPHY

1. Smith, J.C., Ellenberger, H.H., Ballanyi, K., Richter, D.W. & Feldman, J.L. Pre-Botzinger complex: a brainstem region that may generate respiratory rhythm in mammals. *Science (New York, N.Y* **254**, 726-729 (1991).
2. Tan, W.*, et al.* Silencing preBotzinger complex somatostatin-expressing neurons induces persistent apnea in awake rat. *Nat Neurosci* **11**, 538-540 (2008).
3. Stornetta, R.L.*, et al.* A group of glutamatergic interneurons expressing high levels of both neurokinin-1 receptors and somatostatin identifies the region of the pre-Botzinger complex. *J Comp Neurol* **455**, 499-512 (2003).
4. Winter, S.M.*, et al.* Glycinergic interneurons are functionally integrated into the inspiratory network of mouse medullary slices. *Pflugers Arch* **458**, 459-469 (2009).
5. Feldman, J.L. & Del Negro, C.A. Looking for inspiration: new perspectives on respiratory rhythm. *Nat Rev Neurosci* **7**, 232-241 (2006).
6. Feldman, J.L., Mitchell, G.S. & Nattie, E.E. BREATHING: Rhythmicity, Plasticity, Chemosensitivity. *Annual Review of Neuroscience* **26**, 239-266 (2003).
7. Del Negro, C.A.*, et al.* Sodium and calcium current-mediated pacemaker neurons and respiratory rhythm generation. *J Neurosci* **25**, 446-453 (2005).
8. Del Negro, C.A., Koshiya, N., Butera, R.J., Jr. & Smith, J.C. Persistent sodium current, membrane properties and bursting behavior of pre-botzinger complex inspiratory neurons in vitro. *J Neurophysiol* **88**, 2242-2250 (2002).
9. Rybak, I.A., Ptak, K., Shevtsova, N.A. & McCrimmon, D.R. Sodium currents in neurons from the rostroventrolateral medulla of the rat. *J Neurophysiol* **90**, 1635-1642 (2003).

10. Pena, F., Parkis, M.A., Tryba, A.K. & Ramirez, J.M. Differential contribution of pacemaker properties to the generation of respiratory rhythms during normoxia and hypoxia. *Neuron* **43**, 105-117 (2004).

11. Johnson, S.M., Smith, J.C., Funk, G.D. & Feldman, J.L. Pacemaker behavior of respiratory neurons in medullary slices from neonatal rat. *J Neurophysiol* **72**, 2598-2608 (1994).

12. McKay, L.C. & Feldman, J.L. Unilateral Ablation of Pre-Bötzinger Complex Disrupts Breathing during Sleep but Not Wakefulness. *American Journal of Respiratory and Critical Care Medicine* **178**, 89-95 (2008).

13. Tan, E.M.*, et al.* Selective and quickly reversible inactivation of mammalian neurons in vivo using the Drosophila allatostatin receptor. *Neuron* **51**, 157-170 (2006).

14. Wehr, M.*, et al.* Transgenic silencing of neurons in the mammalian brain by expression of the allatostatin receptor (AlstR). *J Neurophysiol* **102**, 2554-2562 (2009).

15. Kam, K., Worrell, J.W., Ventalon, C., Emiliani, V. & Feldman, J.L. Emergence of Population Bursts from Simultaneous Activation of Small Subsets of preBötzinger Complex Inspiratory Neurons. *The Journal of Neuroscience* **33**, 3332-3338 (2013).

16. Morgado-Valle, C., Baca, S.M. & Feldman, J.L. Glycinergic pacemaker neurons in preBotzinger complex of neonatal mouse. *J Neurosci* **30**, 3634-3639 (2010).

17. Richter, D.W. Neural Regulation of Respiration: Rhythmogenesis and Afferent Control. in *Comprehensive Human Physiology* (ed. R. Greger & U. Windhorst) 2079-2095 (Springer Berlin Heidelberg, 1996).

18. Richter, D.W., Ballanyi, K. & Schwarzacher, S. Mechanisms of respiratory rhythm generation. *Curr Opin Neurobiol* **2**, 788-793 (1992).

19. Richter, D.W. & Spyer, K.M. Studying rhythmogenesis of breathing: comparison of in vivo and in vitro models. *Trends Neurosci* **24**, 464-472 (2001).

20. Janczewski, W.A., Tashima, A., Hsu, P., Cui, Y. & Feldman, J.L. Role of inhibition in respiratory pattern generation. *J Neurosci* **33**, 5454-5465 (2013).

21. Shao, X.M. & Feldman, J.L. Respiratory rhythm generation and synaptic inhibition of expiratory neurons in pre-Botzinger complex: differential roles of glycinergic and GABAergic neural transmission. *J Neurophysiol* **77**, 1853-1860 (1997).

22. Smith, J.C., Abdala, A.P., Koizumi, H., Rybak, I.A. & Paton, J.F. Spatial and functional architecture of the mammalian brain stem respiratory network: a hierarchy of three oscillatory mechanisms. *Journal of neurophysiology* **98**, 3370-3387 (2007).

23. Rybak, I.A., St. John, W.M. & Paton, J.F.R. Models of neuronal bursting behavior: implications for in vivo versus in vitro respiratory rhythmogenesis. in *Frontiers in modeling and control of breathing: integration at molecular, cellular and syatems levels* (ed. H. Kazemi) 159-164 (Kluwer Academic/Pleanum, New York, 2001).

24. Maria, B.*, et al.* Sleep breathing disorders in patients with idiopathic Parkinson's disease. *Respir Med* **97**, 1151-1157 (2003).

25. Stocchi, F., Barbato, L., Nordera, G., Berardelli, A. & Ruggieri, S. Sleep disorders in Parkinson's disease. *J Neurol* **245 Suppl 1**, S15-18 (1998).

26. Vetrugno, R.*, et al.* Sleep disorders in multiple system atrophy: a correlative video-polysomnographic study. *Sleep Med* **5**, 21-30 (2004).

27. Munschauer, F.E., Loh, L., Bannister, R. & Newsom-Davis, J. Abnormal respiration and sudden death during sleep in multiple system atrophy with autonomic failure. *Neurology* **40**, 677-679 (1990).

28. Barthlen, G.M. & Lange, D.J. Unexpectedly severe sleep and respiratory pathology in patients with amyotrophic lateral sclerosis. *Eur J Neurol* **7**, 299-302 (2000).

29. Arnulf, I.*, et al.* Improvement of sleep architecture in PD with subthalamic nucleus stimulation. *Neurology* **55**, 1732-1734 (2000).

30. Gray, P.A., Rekling, J.C., Bocchiaro, C.M. & Feldman, J.L. Modulation of respiratory frequency by peptidergic input to rhythmogenic neurons in the preBotzinger complex. *Science (New York, N.Y* **286**, 1566-1568 (1999).

31. Guyenet, P.G., Sevigny, C.P., Weston, M.C. & Stornetta, R.L. Neurokinin-1 receptor-expressing cells of the ventral respiratory group are functionally heterogeneous and predominantly glutamatergic. *J Neurosci* **22**, 3806-3816 (2002).

32. Bouvier, J.*, et al.* Hindbrain interneurons and axon guidance signaling critical for breathing. *Nat Neurosci* **13**, 1066-1074 (2010).

33. Gray, P.A.*, et al.* Developmental origin of preBotzinger complex respiratory neurons. *J Neurosci* **30**, 14883-14895 (2010).

34. Jiang, C. & Lipski, J. Extensive monosynaptic inhibition of ventral respiratory group neurons by augmenting neurons in the Botzinger complex in the cat. *Exp Brain Res* **81**, 639-648 (1990).

35. Merrill, E.G. & Fedorko, L. Monosynaptic inhibition of phrenic motoneurons: a long descending projection from Botzinger neurons. *J Neurosci* **4**, 2350-2353 (1984).

36. Fedorko, L. & Merrill, E.G. Axonal projections from the rostral expiratory neurones of the Botzinger complex to medulla and spinal cord in the cat. *J Physiol* **350**, 487-496 (1984).

37. Pagliardini, S.*, et al.* Active expiration induced by excitation of ventral medulla in adult anesthetized rats. *J Neurosci* **31**, 2895-2905 (2011).

38. Janczewski, W.A. & Feldman, J.L. Novel data supporting the two respiratory rhythm oscillator hypothesis. Focus on "respiration-related rhythmic activity in the rostral medulla of newborn rats". *J Neurophysiol* **96**, 1-2 (2006).

39. Janczewski, W.A. & Feldman, J.L. Distinct rhythm generators for inspiration and expiration in the juvenile rat. *J Physiol* **570**, 407-420 (2006).

40. Chan, R.K. & Sawchenko, P.E. Organization and transmitter specificity of medullary neurons activated by sustained hypertension: implications for understanding baroreceptor reflex circuitry. *J Neurosci* **18**, 371-387 (1998).

41. Bianchi, A.L., Denavit-Saubie, M. & Champagnat, J. Central control of breathing in mammals: neuronal circuitry, membrane properties, and neurotransmitters. *Physiol Rev* **75**, 1-45 (1995).

42. Guyenet, P.G. Neural structures that mediate sympathoexcitation during hypoxia. *Respir Physiol* **121**, 147-162 (2000).

43. Standish, A., Enquist, L.W. & Schwaber, J.S. Innervation of the heart and its central medullary origin defined by viral tracing. *Science (New York, N.Y* **263**, 232-234 (1994).

44. Crick, F. The impact of molecular biology on neuroscience. *Philos Trans R Soc Lond B Biol Sci* **354**, 2021-2025 (1999).

45. Deisseroth, K.*, et al.* Next-generation optical technologies for illuminating genetically targeted brain circuits. *J Neurosci* **26**, 10380-10386 (2006).

46. Deisseroth, K. Controlling the brain with light. *Sci Am* **303**, 48-55 (2010).

47. Chow, B.Y.*, et al.* High-performance genetically targetable optical neural silencing by light-driven proton pumps. *Nature* **463**, 98-102 (2010).

48. Zhang, F., Wang, L.P., Boyden, E.S. & Deisseroth, K. Channelrhodopsin-2 and optical control of excitable cells. *Nature methods* **3**, 785-792 (2006).

49. Nagel, G.*, et al.* Channelrhodopsin-2, a directly light-gated cation-selective membrane channel. *Proceedings of the National Academy of Sciences* **100**, 13940-13945 (2003).

50. Chalphin, A.V. & Saha, M.S. The specification of glycinergic neurons and the role of glycinergic transmission in development. *Frontiers in molecular neuroscience* **3**, 11 (2010).

51. Gray, P.A., Janczewski, W.A., Mellen, N., McCrimmon, D.R. & Feldman, J.L. Normal breathing requires preBotzinger complex neurokinin-1 receptor-expressing neurons. *Nat Neurosci* **4**, 927-930 (2001).

52. Guyenet, P.G. & Wang, H. Pre-Botzinger neurons with preinspiratory discharges "in vivo" express NK1 receptors in the rat. *J Neurophysiol* **86**, 438-446 (2001).

53. Schwarzacher, S.W., Smith, J.C. & Richter, D.W. Pre-Botzinger complex in the cat. *J Neurophysiol* **73**, 1452-1461 (1995).

54. Tan, W., Pagliardini, S., Yang, P., Janczewski, W.A. & Feldman, J.L. Projections of preBotzinger complex neurons in adult rats. *J Comp Neurol* **518**, 1862-1878 (2010).

55. Lu, T.*, et al.* Gene regulation and DNA damage in the ageing human brain. *Nature* **429**, 883-891 (2004).

56. Hayashi, M., Yamashita, A. & Shimizu, K. Somatostatin and brain-derived neurotrophic factor mRNA expression in the primate brain: decreased levels of mRNAs during aging. *Brain Res* **749**, 283-289 (1997).

57. Dixon-Salazar, T.*, et al.* Mutations in the AHI1 gene, encoding jouberin, cause Joubert syndrome with cortical polymicrogyria. *Am J Hum Genet* **75**, 979-987 (2004).

58. Ferland, R.J.*, et al.* Abnormal cerebellar development and axonal decussation due to mutations in AHI1 in Joubert syndrome. *Nat Genet* **36**, 1008-1013 (2004).

59. D'Arcangelo, G. The role of the Reelin pathway in cortical development. *Symp Soc Exp Biol*, 59-73 (2001).

60. D'Arcangelo, G.*, et al.* A protein related to extracellular matrix proteins deleted in the mouse mutant reeler. *Nature* **374**, 719-723 (1995).

61. Miao, G.G.*, et al.* Isolation of an allele of reeler by insertional mutagenesis. *Proc Natl Acad Sci U S A* **91**, 11050-11054 (1994).

62. Molnar, Z., Adams, R., Goffinet, A.M. & Blakemore, C. The role of the first postmitotic cortical cells in the development of thalamocortical innervation in the reeler mouse. *J Neurosci* **18**, 5746-5765 (1998).

63. Falconer, D.S. Two new mutants, 'Trembler' and 'Reeler', with neurological actions in the house mouse (Mus Musculus L.). *Journal of Genetics* **50**, 192-205 (1951).

64. Alcantara, S.*, et al.* Regional and cellular patterns of reelin mRNA expression in the forebrain of the developing and adult mouse. *J Neurosci* **18**, 7779-7799 (1998).

65. Cooper, J.A. A mechanism for inside-out lamination in the neocortex. *Trends Neurosci* **31**, 113-119 (2008).

66. Rice, D.S. & Curran, T. Role of the reelin signaling pathway in central nervous system development. *Annu Rev Neurosci* **24**, 1005-1039 (2001).

67. Soriano, E. & Del Rio, J.A. The cells of cajal-retzius: still a mystery one century after. *Neuron* **46**, 389-394 (2005).

68. Alcantara, S., Pozas, E., Ibanez, C.F. & Soriano, E. BDNF-modulated spatial organization of Cajal-Retzius and GABAergic neurons in the marginal zone plays a role in the development of cortical organization. *Cereb Cortex* **16**, 487-499 (2006).

69. Beffert, U.*, et al.* Modulation of synaptic plasticity and memory by Reelin involves differential splicing of the lipoprotein receptor Apoer2. *Neuron* **47**, 567-579 (2005).

70. Groc, L.*, et al.* NMDA receptor surface trafficking and synaptic subunit composition are developmentally regulated by the extracellular matrix protein Reelin. *J Neurosci* **27**, 10165-10175 (2007).

71. Niu, S., Yabut, O. & D'Arcangelo, G. The Reelin signaling pathway promotes dendritic spine development in hippocampal neurons. *J Neurosci* **28**, 10339-10348 (2008).

72. Pesold, C.*, et al.* Reelin is preferentially expressed in neurons synthesizing gamma-aminobutyric acid in cortex and hippocampus of adult rats. *Proc Natl Acad Sci U S A* **95**, 3221-3226 (1998).

73. Pesold, C., Liu, W.S., Guidotti, A., Costa, E. & Caruncho, H.J. Cortical bitufted, horizontal, and Martinotti cells preferentially express and secrete reelin into perineuronal nets, nonsynaptically modulating gene expression. *Proc Natl Acad Sci U S A* **96**, 3217-3222 (1999).

74. Herz, J. & Chen, Y. Reelin, lipoprotein receptors and synaptic plasticity. *Nat Rev Neurosci* **7**, 850-859 (2006).

75. Pujadas, L.*, et al.* Reelin regulates postnatal neurogenesis and enhances spine hypertrophy and long-term potentiation. *J Neurosci* **30**, 4636-4649.

76. Guidotti, A.*, et al.* Decrease in reelin and glutamic acid decarboxylase67 (GAD67) expression in schizophrenia and bipolar disorder: a postmortem brain study. *Arch Gen Psychiatry* **57**, 1061-1069 (2000).

77. Impagnatiello, F.*, et al.* A decrease of reelin expression as a putative vulnerability factor in schizophrenia. *Proc Natl Acad Sci U S A* **95**, 15718-15723 (1998).

78. Knable, M.B., Torrey, E.F., Webster, M.J. & Bartko, J.J. Multivariate analysis of prefrontal cortical data from the Stanley Foundation Neuropathology Consortium. *Brain Res Bull* **55**, 651-659 (2001).

79. Veldic, M.*, et al.* Epigenetic mechanisms expressed in basal ganglia GABAergic neurons differentiate schizophrenia from bipolar disorder. *Schizophr Res* **91**, 51-61 (2007).

80. Botella-Lopez, A.*, et al.* Reelin expression and glycosylation patterns are altered in Alzheimer's disease. *Proc Natl Acad Sci U S A* **103**, 5573-5578 (2006).

81. Seripa, D.*, et al.* The RELN locus in Alzheimer's disease. *J Alzheimers Dis* **14**, 335-344 (2008).

82. Vetrivelan, R., Fuller, P.M., Tong, Q. & Lu, J. Medullary circuitry regulating rapid eye movement sleep and motor atonia. *J Neurosci* **29**, 9361-9369 (2009).

83. Lai, Y. & Siegel, J. Medullary regions mediating atonia. *J. Neurosci.* **8**, 4790-4796 (1988).

84. Hamburgh, M. Analysis of the Postnatal Developmental Effects of "Reeler," a Neurological Mutation in Mice. a Study in Developmental Genetics. *Dev Biol* **19**, 165-185 (1963).

85. Niu, S., Renfro, A., Quattrocchi, C.C., Sheldon, M. & D'Arcangelo, G. Reelin promotes hippocampal dendrite development through the VLDLR/ApoER2-Dab1 pathway. *Neuron* **41**, 71-84 (2004).

86. Koizumi, H.*, et al.* Structural-functional properties of identified excitatory and inhibitory interneurons within pre-Botzinger complex respiratory microcircuits. *J Neurosci* **33**, 2994-3009 (2013).

87. Cardin, J.A.*, et al.* Driving fast-spiking cells induces gamma rhythm and controls sensory responses. *Nature* **459**, 663-667 (2009).

88. Schreihofer, A.M., Stornetta, R.L. & Guyenet, P.G. Evidence for glycinergic respiratory neurons: Botzinger neurons express mRNA for glycinergic transporter 2. *J Comp Neurol* **407**, 583-597 (1999).

89. Ezure, K., Tanaka, I. & Kondo, M. Glycine is used as a transmitter by decrementing expiratory neurons of the ventrolateral medulla in the rat. *J Neurosci* **23**, 8941-8948 (2003).

90. Burns, B.D. The central control of respiratory movements. *British medical bulletin* **19**, 7-9 (1963).

91. Bradley, G.W., von Euler, C., Marttila, I. & Roos, B. A model of the central and reflex inhibition of inspiration in the cat. *Biological cybernetics* **19**, 105-116 (1975).

92. von Euler, C. On the central pattern generator for the basic breathing rhythmicity. *Journal of applied physiology: respiratory, environmental and exercise physiology* **55**, 1647-1659 (1983).

93. Feldman, J.L. & Cowan, J.D. Large-scale activity in neural nets II: A model for the brainstem respiratory oscillator. *Biol Cybern* **17**, 39-51 (1975).

94. Xia, L., Damon, T., Niblock, M.M., Bartlett, D. & Leiter, J.C. Unilateral microdialysis of gabazine in the dorsal medulla reverses thermal prolongation of the laryngeal chemoreflex in decerebrate piglets. *Journal of Applied Physiology* **103**, 1864-1872 (2007).

95. Curran, A.K., Xia, L., Leiter, J.C. & Bartlett, D., Jr. Elevated body temperature enhances the laryngeal chemoreflex in decerebrate piglets. *J Appl Physiol (1985)* **98**, 780-786 (2005).

96. Heman-Ackah, Y.D., Pernell, K.J. & Goding, G.S. The laryngeal chemoreflex: An evaluation of the normoxic response. *The Laryngoscope* **119**, 370-379 (2009).

97. Hultborn, H., Lindstrom, S. & Wigstrom, H. On the function of recurrent inhibition in the spinal cord. *Exp Brain Res* **37**, 399-403 (1979).

98. Tietjen, I.*, et al.* Single-cell transcriptional analysis of neuronal progenitors. *Neuron* **38**, 161-175 (2003).

99. Vigna, S.R.*, et al.* Characterization of antibodies to the rat substance P (NK-1) receptor and to a chimeric substance P receptor expressed in mammalian cells. *J Neurosci* **14**, 834-845 (1994).

100. Pagliardini, S., Adachi, T., Ren, J., Funk, G.D. & Greer, J.J. Fluorescent tagging of rhythmically active respiratory neurons within the pre-Botzinger complex of rat medullary slice preparations. *J Neurosci* **25**, 2591-2596 (2005).

101. Mantyh, P.W.*, et al.* Inhibition of hyperalgesia by ablation of lamina I spinal neurons expressing the substance P receptor [see comments]. *Science* **278**, 275-279 (1997).

102. Yip, Y.P., Mehta, N., Magdaleno, S., Curran, T. & Yip, J.W. Ectopic expression of reelin alters migration of sympathetic preganglionic neurons in the spinal cord. *J Comp Neurol* **515**, 260-268 (2009).

103. Chesselet, M.F. & Affolter, H.U. Preprotachykinin messenger RNA detected by in situ hybridization in striatal neurons of the human brain. *Brain Res* **410**, 83-88 (1987).

104. Adamantidis, A.R., Zhang, F., Aravanis, A.M., Deisseroth, K. & de Lecea, L. Neural substrates of awakening probed with optogenetic control of hypocretin neurons. *Nature* **450**, 420-424 (2007).

105. Gradinaru, V.*, et al.* Targeting and readout strategies for fast optical neural control in vitro and in vivo. *J Neurosci* **27**, 14231-14238 (2007).

106. Paxinos, G., Franklin, K.B.J. & Franklin, K.B.J. *The mouse brain in stereotaxic coordinates* (Academic Press, San Diego, 2001).

107. Lewis, J., Bachoo, M., Polosa, C. & Glass, L. The effects of superior laryngeal nerve stimulation on the respiratory rhythm: phase-resetting and aftereffects. *Brain Research* **517**, 44-50 (1990).